INCORPORATING PROCESS SAFETY INTO HEAT EXCHANGER NETWORK SYNTHESIS

A Dissertation

by

AHMED HARHARA

Submitted to the Graduate and Professional School of
Texas A&M University
in partial fulfillment of the requirements for the degree of

DOCTOR OF PHILOSOPHY

Chair of Committee,	M. M. Faruque Hasan
Committee Members,	Ahmad Hilaly
	Qingsheng Wang
	Abu Rashid Hasan
Head of Department,	Arul Jayaraman

May 2022

Major Subject: Chemical Engineering

ABSTRACT

Process safety of inter-connected equipment, such as heat exchanger networks (HEN), is paramount to the operation of chemical plants. While there exists considerable research on further improving HEN, little attention has been paid to incorporating the safety of HEN at the conceptual design stage. In this work, we extend the optimization-based HEN synthesis to incorporate safety using a Safety Rating (SR) based on dynamic tube rupture scenarios for all plausible heat exchanger matches. In developing the SR, we describe a model-based step-by-step methodology to predict dynamic pressure profiles during tube rupture for liquid-liquid, vapor-liquid, and flashing liquid-liquid systems. The transient effects of the relief valve are considered. The effects of choked flow are also be considered for accurate maximum pressure predictions. This SR metric allows plants to assess the risk of overpressure resulting in failure of the equipment. Specifically, imposing a minimum SR ensures compliance with overpressure standards. We obtain HEN configurations with lowest costs that can safely handle tube rupture overpressure events for the entire network. The results obtained indicate a Pareto-like curve relating the safety of an exchanger with its cost. Furthermore, we show that pressure safety valves are a low cost form of overpressure protection.

ACKNOWLEDGMENTS

First and foremost, I would like to express my sincere gratitude to my advisor Dr. Faruque Hasan for his advice, mentorship, and support over the years. I also want to thank my dissertation committee members for their review and feedback of my work. I am also grateful to the staff at the Artie McFerrin Department of Chemical Engineering for their assistance in my PhD program. Last but not least, I would like to thank my parents, siblings, and friends for their tremendous support and encouragement.

CONTRIBUTORS AND FUNDING SOURCES

Contributors

This work was supported by a dissertation committee consisting of Professor Faruque Hasan, Professor Qingsheng Wang, Professor Abu Rashid Hasan, and Professor Ahmad Hilaly. Portions of this research were conducted with the advanced computing resources provided by Texas A&M High Performance Research Computing. All other work conducted for the dissertation was completed by the student independently.

Funding Sources

This work was funded by the Mary Kay O'Connor Process Safety Center, and the Artie McFerrin Department of Chemical Engineering at Texas A&M University.

TABLE OF CONTENTS

Page

LIST OF FIGURES

FIGURE Page

LIST OF TABLES

1. INTRODUCTION[1]

Chemical processes around the world are keen to meet environmental emission targets and to reduce the energy of their processes [1]. With the increasing cost of energy, and the need for sustainable processes, heat integration and heat recovery have gained popularity since the 1950s [2]. Conserving energy is critical to the future operation of plants. This increased focus has led to heat exchanger networks being one of the most studied topics in chemical engineering [3, 4, 5, 6, 7]. Since heat exchangers are one of the most widely used equipment in plants, heat exchanger networks can significantly affect the profitability of a plant [8]. As this is occurring, intensification is rapidly growing within the chemical engineering community [9, 10]. This technology allows an increase in production throughput using smaller equipment and fewer resources, increasing the profitability of a process [11]. However, at times, this higher throughput can require processes to use higher temperatures and pressures, which if left unchecked can jeopardize the safety of a process [12].

Heat exchangers are among the most common equipment found in chemical plants. In 2018 alone, the global heating and cooling market exceeded $1 trillion. It is predicted that by the year 2025, the heat exchanger market will surpass $26 billion annually. This increase is due to an increase in chemical process plants to meet global demands, an increase of offshore energy platform operations and installations, and an increase of small-scale, unconventional and distributed resources such as shale gas processing plants. As the demand for heat exchangers continues to increase, plants must be cognizant of the process conditions exchangers are subjected to. This includes, but is not limited to, corrosive fluid service, extreme temperatures, and high pressures. These conditions can serve as a point of failure for an exchanger. In fact, many plants nowadays

[1]This chapter was reprinted in whole or in part with permission from [1] "Incorporating Process Safety into Heat Exchanger Network Synthesis and Operation" by Harhara, A., & Hasan, M. M, 2019. *Computer Aided Chemical Engineering*, 47, 221-226, Copyright 2022 by Elsevier, [2] "Dynamic modeling of heat exchanger tube rupture" by Harhara, A., & Hasan, M. M, 2020. *BMC Chemical Engineering*, 2(1), 1-20, Copyright 2022 by Harhara, A., & Hasan, M. M, and [3] "Heat Exchanger Network Synthesis with Process Safety Compliance under Tube Rupture Scenarios" by Harhara, A., & Hasan, M. M, 2022. *Computers & Chemical Engineering*, 107817, Copyright 2022 by Elsevier.

operate at a hundred atmospheres or higher [13]. Thus, plants must exercise caution in selecting and sizing exchangers and their respective relief devices.

1.1 Heat exchanger safety

One way in which exchangers can fail is via a tube rupture [14]. During this incident, high pressure tube side fluid enters the low pressure shell side. If the shell side is inadequately sized to handle the influx of mass, the exchanger may catastrophically fail. This overpressure event is listed under API 521 as a credible overpressure scenario. This signifies that the specific reason that led to a tube failure is not considered. In practice, this is because a tube failure can occur due to a myriad of reasons including fatiguing tubes, tube vibration, or erosion [15]. API thus considers the process random. The assumption by API 521 is that this scenario may occur and should be mitigated properly [16]. However, one important caveat is that for most overpressure scenarios listed under API 521, a detailed approach for sizing their relief valves is given. With tube ruptures however, API 521 doesn't provide guidance on a specific methodology to use. As shall be detailed later, one must instead develop their own dynamic simulation [17].

Before modeling the tube rupture phenomena, it is helpful to understand its relevance to industry. Tube ruptures can occur in the chemical, oil, gas, offshore, and even the nuclear industry. Knowing where tube ruptures are more common allows one to scrutinize one set of systems over others. For reasons including the need to protect proprietary process information, reliability data on the failure of equipment in industry is hard to come by. However, there are efforts to counter this such as the Mary Kay O'Connor Process Safety Center's Instrument Reliability Network [18].

Because of this, it is often difficult to find statistics on the frequency of tube ruptures. Moreover, some failure rate databases may record a tube rupture failure under a different name, making it even harder to estimate the likelihood of this event. Fortunately, there are some databases that give us a clue as to where tube ruptures occur. The United Kingdom's Hydrocarbon Release Database collected data on offshore incidents [19]. By filtering out exchanger related releases, Table 1.1 shows an estimate of which areas in a plant experienced a tube rupture. From the table, it is evident that most offshore tube ruptures occur in gas compression systems. This is expected since

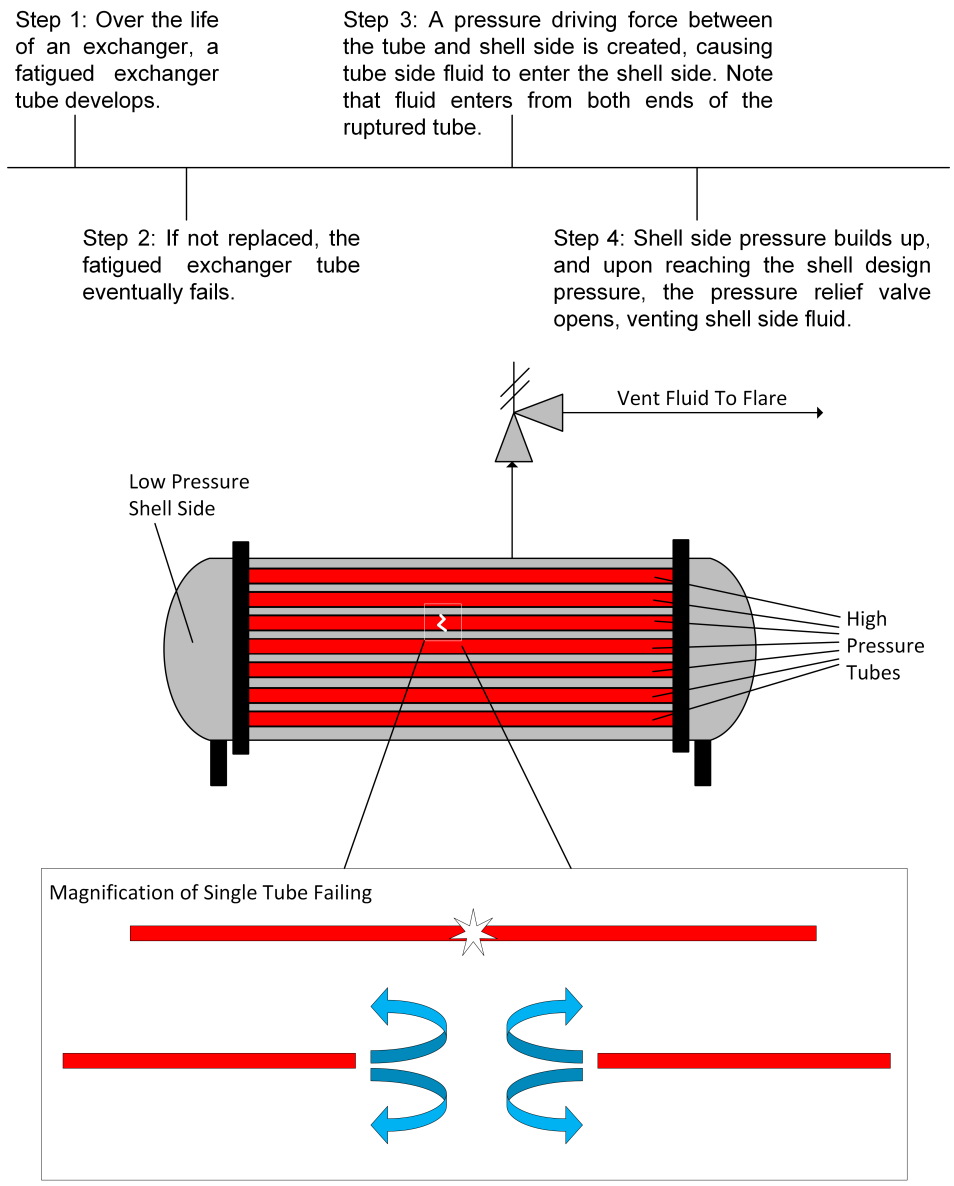

Figure 1.1: Sketch of heat exchanger tube rupture

gas compression systems contain a series of intercoolers, with high pressure gases on the tube-side, and low pressure cooling water on the shell-side.

Table 1.1: Recorded Offshore Systems Experiencing Tube Rupture Incidents.

	Severity			
System	Major	Significant	Minor	Total
Flare/HP		1		1
Gas compression	4	21	13	38
Processing/gas/dehydration		3	5	8
Processing/gas/LPG/condensate		1	2	3
Processing/gas/sour gas		1		1
Processing/oil/oil treatment		1		1
Separation/gas production	1			1
Utilities/gas/fuel gas			4	4
Utilities/oil/heat transfer oil			1	1
Total	5	28	25	58

The model by Fowler et al. was one of the earliest attempts to describe the tube rupture transient process [20]. A shell-average pressure model was developed to capture the pressure-time relationship. This was followed by a stress analysis to determine if shell failure was likely to occur. Simpson developed a different shell-average pressure model based on the assumption that a tube failure will result in an expanding translating spherical explosion [21]. The models by Fowler et al. and Simpson both accounted for the inertia of the shell-side fluid and relief line. They did not however simulate the sudden pressure increase following a tube break (commonly referred to as water-hammer). Sumaria et al. modeled the transient pressure surge by using a lumped parameter model to incorporate the compressibility of the shell-side fluid and relief line [22]. This model was applied to a high pressure gas entering a low pressure liquid. Ennis et al. extended this work

by considering the case of a tube-side flashing liquid and accounted for the spatial and temporal aspects of the attached piping system [23]. Furthermore, Botros addressed the importance of accounting for piping systems and specifying appropriate boundary conditions [24].

Cassata et al used commercial transient analysis software to model a tube rupture by performing a series of simulations with the burst occurring at the U bend [16]. Pressure profiles at various points along the exchanger were generated. Ewan et al calculated pressure profiles when varying the location of the tube burst [17]. For relief devices close to the tube burst, pulse widths were higher than bursts far from the relief device. Nagpal evaluated several tube rupture cases using dynamic simulations and provides a chart for when dynamic simulations are recommended [25]. The simulation results show that pressure relief devices can be used to protect liquid-filled exchangers. Aside from simulating the severity of this event through consequence modeling, Acosta and Siu examined the risk of this scenario through the use of dynamic event trees [26]. Lastly, a Joint Industry Project conducted a full-scale heat exchanger tube rupture [27]. These experimental results were compared against blind simulations performed by consultants. The results support using one dimensional dynamic models to model the pressure profiles during tube ruptures.

One technique on estimating the relief rate during a tube rupture is to apply a steady state calculation. This is done by first assuming a complete tube rupture has occurred (referred to in the literature as a guillotine rupture). A standard hydraulic orifice calculation is then performed to determine what is the rate of fluid entering the shell-side. This number is then doubled due to the fact that fluid is entering from both ends of the ruptured tube. Finally, this rate is then inputted into a relief valve calculation in order to determine what size valve is required for adequate protection of the heat exchanger. There are some issues that exist with this method however. The first is the concern that the shell-side of the exchanger can fail before the relief valve can open. The reasoning behind this is that tube rupture scenarios result in fast-acting transient shockwaves which can reach peak pressure in milliseconds [13]. This is especially the case for high pressure differences between the shell and tube-side.

Another concern with this technique is that the orifice calculation method ignores the shell-side

throughout the calculation. This is a problem because the tube rupture failure scenario is entirely focused on the shell-side failing since it is the low pressure side of the exchanger. Orifice-style calculations overlook how the shell-side pressure profile develops throughout the tube failure — the effects of mixing between the shell and tube-side fluids are ignored. Lastly, orifice calculations are more appropriate for tube rupture calculations that do not have a subcooled liquid on the tube-side. Subcooled liquids will flash once entering the low-pressure shell-side, further complicating the calculation of the required relief rate. For heat exchanger tube ruptures, the goal is to prevent the shell-side of the exchanger from failing. Thus, a dynamic simulation gives a more complete picture of the overpressure scenario, increasing a plant's confidence in its ability to withstand a tube rupture.

1.2 Heat exchanger network safety

Although we are interested in protecting individual heat exchangers from tube ruptures, heat exchanger networks present opportunities to design safe stream combinations for a minimal increase in cost. Traditional heat exchanger network synthesis is applied to a process to reduce energy costs. Hot and cold streams are identified and heat exchangers are proposed and configured in a network to minimize utility costs. The governing equations in heat exchanger network synthesis are the energy balance and heat transfer equations. The capital and operating costs of each exchanger are determined through well-established equipment sizing equations. Finally, for any remaining streams that have not reached their outlet temperature, hot and cold utilities are used [28]. Because heat exchanger network design includes an objective function that considers the capital and operating costs of the network, there is a built-in tradeoff between these variables. Currently, in heat exchanger network synthesis, there are two main approaches used to develop a network. The first is via pinch analysis [29, 30] and the second is via mathematical programming. Prior to these, less optimal methods such as trial and error were the only way of increasing the efficiency of a plant. Clearly, these lacked the advantages of a systematic approach.

Pinch analysis was developed in the late 1970s by Linnhoff and targets the pinch point, the minimum allowable temperature approach for a heat exchanger. This pinch point effectively decom-

poses the temperature range into a heat source and heat sink. Afterwards, hot and cold composite curves can be used to determine the minimum energy required for the process. This systematic design method for heat recovery has been widely applied across the chemical industry and variations of this work have been applied to mass transfer networks, carbon emissions, and supply chain planning, among others [31, 32, 33]. An added advantage of pinch analysis is its simplicity and that it employs graphical tools. Pinch analysis however does not guarantee an optimal solution.

The method by Yee & Grossmann uses mathematical programming to solve a stage-wise superstructure that allows for different possible stream matches [34, 35]. The objective function of the MINLP model minimizes the total annual cost of the network. While the objective function is nonlinear, all constraints are linear. A copy of the program can be found in the General Algebraic Modeling System (GAMS) library under the name SYNHEAT [36, 37]. Ponce-Ortega et al. (2008) build on this superstructure concept to propose an MINLP model for HEN synthesis that can accommodate streams with isothermal phase change [38]. In their work, constant sensible and latent heats for isothermal phase changes are assumed. Disjunctive programming is then used to model the temperature-enthalpy curve.

For our work, we modify Yee & Grossmann's SYNHEAT model for developing single phase tube-rupture safe heat exchanger networks. To account for streams with isothermal phase changes, we then modify the MINLP model proposed by Ponce-Ortega et al. For the latter model, we calculate a priori the safety rating for all possible PSV sizes and stream combinations across different temperature intervals. We then use an MINLP model by Rebennack and Kallrath to create a piecewise linear delta approximation that conservatively overestimates the severity of a tube rupture [39].

While tube ruptures can occur in single heat exchangers, their effects may be magnified in heat exchanger networks. With a shift in focus towards energy integration and sustainability in designing plants, these are all likely to increase a network complexity's, equipment interdependence, and the potential for overpressure. Heat exchanger networks, therefore, must also be designed to adequately protect against potential process safety events. While the traditional focus in HEN

synthesis has been on the annual cost of a network, novel process design and intensification may lead to new safety challenges.

The likelihood of process safety incidents such as overpressure increase with higher system pressures. One example of a hazard that can increase as a result of intensification is a heat exchanger tube rupture (shown in Figure 1.2), an event that is listed under API 521 as a credible overpressure scenario [40]. In the event of a tube rupture, the tube side can quickly overpressure the shell side. Upon the shell side pressure increasing beyond the hydrotest pressure, the shell material is prone to fail, potentially resulting in a catastrophic outcome. The severity of this pressurization increases with large differences in shell and tube side pressure [41]. Harhara and Hasan (2019) performed a dimensionless analysis on the effect that key thermodynamic parameters have on the severity of this scenario [42]. Their results show that the density ratio and pressure ratio play a significant role in the level of pressurization the shell side experiences. Mitigating this overpressure scenario, whether for a single heat exchanger or a network, via enhanced thermodynamic modeling and improved equipment design is of interest to the oil & gas, chemical, and power industry.

While there has been ample research in the field of HEN synthesis, in comparison, little work has been done to integrate safety concerns in HEN design. Here, we attempt to chronologically summarize some of the work that has been done. In our opinion, the first work to analyze safety in process systems engineering appeared in the 1980s by Saboo et al[43] and focused on resilient HEN synthesis via the use of a "Resilience Index (RI)". In their work, resilience solely refers to the ability to withstand inlet and outlet temperature disturbances. Accordingly, their Resilience Index metric was defined as the largest total disturbance a network is able to withstand without becoming infeasible. Saboo et al. demonstrated their disturbance-resistant HEN model in a case study for the energy management of two continuously stirred tank reactors (CSTR) in series. As one can probably guess, if instead, a non-temperature resilient HEN was put in service, any temperature disturbances would carry over to the two CSTRs, potentially compromising the plant's safety. One important feature of Saboo et al.'s model is that it can be applied in the design phase of HEN as

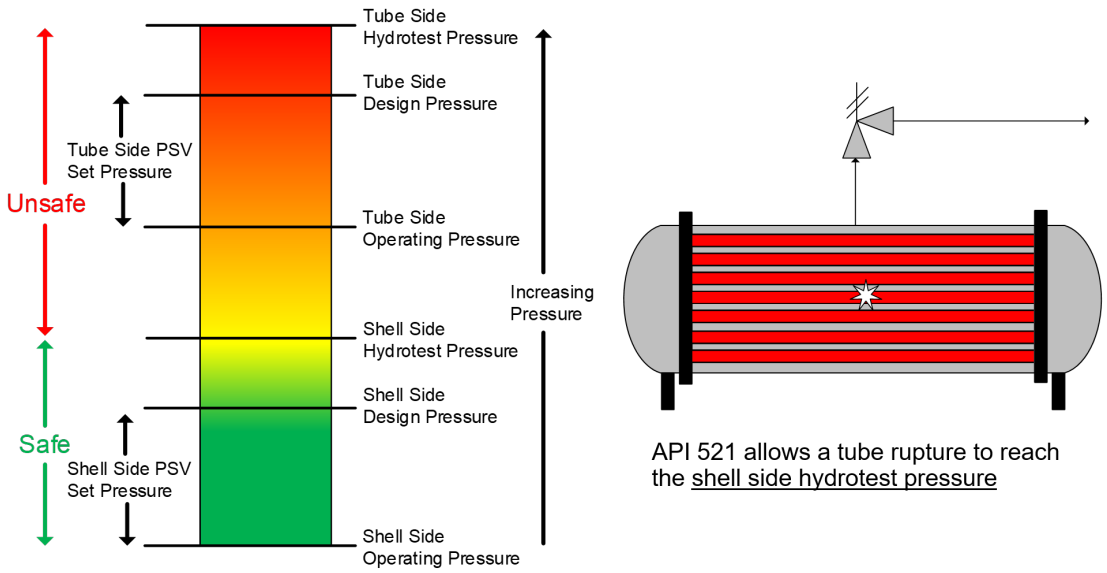

Figure 1.2: Heat exchangers are designed with relief valves limiting the tube and shell side pressures. During a tube rupture, API 521 permits the exchanger shell side to reach up to the shell side hydrotest pressure only if a dynamic simulation is performed. This threshold is shown as the boundary between a safe and an unsafe tube rupture.

well as detecting bottlenecks for existing HEN. This was later applied to RESHEX [44, 45].

Marselle et al. (1982) defined the resilient HENS problem[46]. In their problem, resilience is formally defined by three features. One, that a "disturbance range" captures all possible flow rate and temperature fluctuations of the network. Two, a "network structure" is resilient if it allows maximum energy recovery for a disturbance range. Three, a network is resilient if it is structurally resilient. At first glance, the previous two definitions may appear to be similar. However, the key distinction between the two is that a "network structure" signifies a single network configuration. Thus, the term "structurally resilient" corresponds to a network's ability to accommodate multiple network structures. Around the same time, Grossmann and Morari (1983) address operability in HENS as a network's ability to be flexible and resilient[47]. According to them, flexibility addresses steady state operation under different feed conditions, while resiliency is the ability to operate under process disturbances. Interestingly enough, Grossmann and Morari's work also listed a third definition of operability: the safe operation despite equipment failure. Note, however, that a solution to this problem was not addressed. As shall be demonstrated in this work, this third

definition overlaps quite a bit with this paper's contribution. To clarify, the heat exchanger tube rupture scenario is indeed a form of equipment failure. One important distinction, however, is that the third definition is not considered in our work. This definition assumes equipment failure. One example of such a failure is a tube rupture.

In a related approach, Nemet et al. (2017) proposed an MINLP model for HEN synthesis that accounts for toxicity, flammability, and explosiveness risk within the network [48]. The superstructure they use includes four different types of heat exchangers: double pipe, plate and frame, fixed plate shell and tube, and shell and tube with u-tubes. Their results indicate that plants can significantly increase their safety for a minimal increase in cost. Hafizan et al. (2016) proposed a pinch analysis framework for inherent safety and operability design in HENS [49]. Each stream's inherent safety is quantified based on data such as component properties such as temperature, flashpoint, and lower and upper explosive limits [50]. Flexibility is assessed using Bakar et al. (2013) [51]. The network is then assessed for controllability using Huang and Fan's framework [52]. The framework incorporates four types of disturbance propagation. These four disturbances are from the inlet of a stream, disturbances traveling through two, three, and more than three exchangers.

Traditional heat exchanger network synthesis is applied to a process to reduce energy costs. Hot and cold streams are identified and heat exchangers are proposed and configured in a network to minimize utility costs. The governing equations in heat exchanger network synthesis are the energy balance and heat transfer equations. The capital and operating costs of each exchanger are determined through well-established equipment sizing equations. Finally, for any remaining streams that have not reached their outlet temperature, hot and cold utilities are used [28]. Because heat exchanger network design includes an objective function that considers the capital and operating costs of the network, there is a built-in tradeoff between these variables. Currently, in heat exchanger network synthesis, there are two main approaches used to develop a network. The first is via pinch analysis [29, 30] and the second is via mathematical programming. Prior to these, less optimal methods such as trial and error were the only way of increasing the efficiency of a plant. Clearly, these lacked the advantages of a systematic approach.

Pinch analysis was developed in the late 1970s by Linnhoff and targets the pinch point, the minimum allowable temperature approach for a heat exchanger. This pinch point effectively decomposes the temperature range into a heat source and heat sink. Afterwards, hot and cold composite curves can be used to determine the minimum energy required for the process. This systematic design method for heat recovery has been widely applied across the chemical industry and variations of this work have been applied to mass transfer networks, carbon emissions, and supply chain planning, among others[31, 32, 33]. An added advantage of pinch analysis is its simplicity and that it employs graphical tools. Pinch analysis however does not guarantee an optimal solution. The second method by Yee & Grossman uses mathematical programming to solve a stage-wise superstructure that allows for different possible stream matches [34, 35]. The objective function of the MINLP model minimizes the total annual cost of the network. While the objective function is nonlinear, all constraints are linear. A copy of the program can be found in the General Algebraic Modeling System (GAMS) library under the name SYNHEAT [36, 37].

1.3 Safety via artificial neural networks

In the past, significant research has been devoted to monitoring the operations of plants [53, 54, 55, 56]. It comes as no surprise that monitoring industrial processes is key to improving product quality and plant economics [57]. However, while monitoring can be used to increase the economics of a plant, process safety incidents must be controlled as well. Perhaps the most known example of where this may be applicable is in runaway reactions. In here, the monitoring of temperature is key to avoiding a thermal runaway [58, 59, 60, 61].

For many other process safety incidents, it is less obvious how one should monitor a plant to avoid process safety incidents. This is because the way to protect a plant is evaluated through the use of consequence modeling. Over the years, high fidelity models have been developed for complex process safety scenarios including fire, overpressure, and dispersion modeling [62, 63, 64]. Although these models have a high accuracy, one disadvantage to them is the high computational resources required to perform them [65]. This problem is compounded by the fact that such problems can take significant amounts of time, making the possibility of real-time monitoring via con-

sequence modeling extremely difficult, if not impossible.

As will be demonstrated in this paper, artificial neural networks (ANN) have the potential to bridge this gap. Artificial neural networks have a wide range of applications in chemical engineering [66]. This includes fault detection, process modeling, and process design. Mannan et al. (2016) present an overview of major process safety incidents and the technologies they influenced [67]. Mannan et al. point out that ANN shows promise in its potential to contribute to reliability engineering. A brief timeline of other works related to ANN in safety include the following. Maki and Loparo (1997) proposed a detection system using a 2 stage ANN model [68]. Although a continuously stirred tank reaction was used as an example, their method can be broadly applicable to other unit operations. In their work, the detection of faults occurs during transient periods of the process. To train the network, they relied on the backpropagation algorithm. Kosinski and Kozlowski (1998) present a review of ANN in safety [69]. In their paper, ANN applications in safety should have the following requirements: system specification, implementation, verification and validation, and reliability of the system. Hussain (1999) reviewed ANN applications in chemical process control [70]. In Hussain's review, ANN's use up to 1999 was mostly limited to lab-scaled equipment. In another paper which tries to determine how to safely incorporate ANN, Kurd and Kelly (2003) define five safety criteria for ANN applications [71].

One thing to keep note of is that outliers in a data set are a real possibility. Clearly, this is problematic for ANN. El-Melegy et al. (2009) cover the topic of robustness of neural networks and as a solution propose training neural networks based on the least median of squares (LMeDs) [72]. Robustness in their work is defined as providing resistance to outliers. Their work found that training feedforward neural networks using the backpropagation method yields inaccurate results compared to LMeDs estimators. Honggui et al. (2014) proposed a fuzzy neural network framework for wastewater treatment, which is run in non-steady state conditions [73]. Because of wastewater's input data containing inaccuracy (sludge, waste, etc), fuzzy logic modeling was combined with ANN, yielding promising results. Lastly, in examining fault detection using ANN, Heo and Lee (2018) investigated the effects of number of hidden layers and number of neurons on

network performance [74]. They concluded that the network performance did not increase above a certain level.

1.4 Research gaps and key challenges

As discussed earlier, mitigating the impact of heat exchanger tube ruptures is necessary to the safe operation of plants. However, significant challenges arise due to the lack of a systematic method for quantifying these scenarios. An approach that addresses these concerns would form a basis for studying the scenario in further detail. In developing a systematic approach for sizing tube ruptures, one must first derive from first-principles a volumetric balance for the exchanger shell. This requires accounting for fluid entering from both ends of the ruptured tube and exiting the shell via a relief device. The shell and tube side fluids can vary in composition, phase, temperature, and pressure. Therefore, we must develop an approach to accurately "track" the tube side fluid as it pressurizes the low pressure shell side. This may subsequently give rise to a choked flow condition, which, if not modeled, risks severely misinterpreting the true mass flux entering the shell side. This highlights some of the challenges in systematically modeling tube ruptures. For a systematic and robust tube rupture dynamic model, the framework should be capable of handling the most common tube rupture scenarios. For niche scenarios where the model may not be appropriate, the framework can at least be used as the foundation for a more customized solution.

The other main research gap exists in applying overpressure analysis to HEN synthesis. This requires developing two separate formulations. The first shall underestimate the safety of an individual exchanger, and the second shall optimize a network configuration to meet predetermined safety thresholds. Furthermore, these two formulations must also be able to account for changes in phases.

The final research gap exists in applying artificial neural networks for predicting the severity of overpressure scenarios. If successful, these models can be used as the foundation for real-time overpressure prediction monitoring.

1.5 Research objectives

Based on the aforementioned challenges that exist in mitigating heat exchanger tube ruptures, the overall objectives of the proposal are as follows:

- Objective 1: Developing a methodology for dynamically modeling and sizing single heat exchanger tube ruptures
- Objective 2: Developing an approach for designing minimum cost tube-rupture-resilient heat exchanger networks for single phase exchangers
- Objective 3: Developing an approach for designing minimum cost tube-rupture-resilient heat exchanger networks for multi-phase exchangers
- Objective 4: Developing an artificial neural network model to predict the severity of tube ruptures.

For objective 1, a first-principles model is proposed that captures the transient mass flux and respective fluid properties of each component entering, exiting, and remaining in the shell side. The existence of choked flow for the tube side fluid is included. The transient effects of the relief valve are incorporated in the model, and by extension, a potential tube rupture's severity. The effects of varying shell volume and tube diameter are likewise accounted for. This framework is capable of accurately modeling liquid-liquid, vapor-liquid, and flashing-liquid liquid tube ruptures. This model is successfully leveraged to understand the relative severity of the three main types of tube ruptures, liquid-liquid, vapor-liquid, and flashing-liquid liquid tube ruptures. Lastly, a dimensionless analysis is performed to identify which parameters result in the most significant tube ruptures.

For objective 2, the output of the first-principles model in objective 1, the peak transient pressure, is normalized. This normalization, referred to as the safety rating, is done by assigning a weight for a tube rupture's maximum pressure relative to the exchanger's shell design pressure. The safety rating can now be used to compare the severity of multiple exchanger configurations at

different process conditions, a requirement for designing an economical tube-rupture-resilient heat exchanger network. An exchanger's hydrotest pressure is used as the transient pressure ceiling that cannot be exceeded during a tube rupture. This ceiling is in line with API 521 which itself recommends that exchangers undergoing a tube rupture not exceed their hydrotest pressure. This threshold is equivalent to a safety rating of 67. At this value and above, an exchanger is protected during a tube rupture. An exchanger is not protected vice versa. The safety rating and the relief valve's economics are subsequently incorporated within the well-known SYNHEAT model. The end result is that we are able to design tube-rupture-resilient networks that operate at a minimal annual cost while satisfying the network's heating and cooling requirements.

For objective 3, a modified SYNHEAT model is used that accounts for streams undergoing a non-isothermal phase change. One of the main challenges of this objective is that the safety rating significantly varies with a stream's temperature across multiple phases. This is overcome by leveraging an existing optimization framework that underestimates the safety rating, ensuring our safety rating results are always conservative.

1.6 Original contributions

The original contributions of this proposal are as follows:

- A robust approach to predicting the severity of liquid-liquid, vapor-liquid, and flashing-liquid liquid tube ruptures.
- The introduction of a novel safety rating that serves as a benchmark for tube rupture safety.
- A framework for incorporating tube rupture safety in HEN synthesis, including the ability to handle single phase and multi-phase tube ruptures
- A framework for implementing ANN-based tube rupture monitoring

The novel contributions of this work include a step-by-step methodology on dynamically sizing a relief system for a tube rupture. The model will be useful in answering critical safety related questions such as what is the maximum pressure the shell-side reaches, how long after the tube

rupture is maximum pressure reached, and how long is the shell design pressure exceeded. Examples on how to apply this methodology to a liquid-liquid, vapor-liquid, and flashing liquid-liquid system are given. This work explains how to use process simulation software to generate the necessary thermophysical properties required for accurate pressure profile predictions. Finally, a dimensionless analysis of properties that affect tube ruptures is performed.

Chapter 2 is organized as follows. Chapter 2 provides a background on this overpressure event, in addition to examining the common causes of heat exchanger tubes failing. Chapter 2 also provides a brief overview of ASME VIII pressure vessel code and its relation to the tube rupture scenario. This helps to specify an acceptable pressure limit during a tube rupture event. Lastly, Chapter 2 also describes the differences in relief devices used to protect exchangers and their associated response times. Chapter 2 models the tube rupture. Chapter 2 first lists the assumptions in this model, followed by the modeling of each component that is fed into a tube rupture dynamic pressure profile algorithm. Chapter 2 also illustrates how the equations are used in a practical setting, with examples on liquid-liquid, vapor-liquid, and flashing liquid-liquid systems. A discussion on the differences between these systems is included. A dimensionless analysis is also performed for a liquid-liquid tube rupture. Also included are some strategies on mitigating a tube rupture.

The second novel contribution regards HEN synthesis. In general, one shortcoming for HEN synthesis is that most assume an isobaric system. This simplification neglects pressure-related process safety metrics, including the potential for overpressure. Note that some exceptions to this incorporate the pressure drop in HEN design [75, 76, 77, 78]. However, the pressure aspect is incorporated for the purpose of more accurately sizing the heat exchanger, which ultimately affects the economics of the network. To the best of our knowledge, no formulation has been developed with the explicit goal of preventing overpressure scenarios. By integrating process safety principles with optimization, a formulation for how to design a heat exchanger network to assess the risk of tube rupture failures is presented. Given a set of hot and cold streams, it is desired to design a HEN that maximizes energy recovery while protecting for a tube rupture. This work uses the SYNHEAT model in conjunction with the BARON algorithm as the basis for designing the HEN [79].

Chapter 3 is organized as follows: First, a motivating example of the applicability of tube ruptures in HEN is provided along with a discussion on the tradeoffs that exist between process safety and heat exchanger economics. Next, the development of a safety metric that captures the severity of a tube rupture event is given. Chapter 3 also outlines the optimization model for the design of a heat exchanger network that incorporates this safety metric. Here, the safety metric is first applied to the design of a single heat exchanger. This is followed by an application to a heat exchanger network problem.

Chapter 4 offers the framework for the neural network model. A comparison is made between traditional consequence modeling and a real-time detection system. An overview of ANN is also given, followed by the training of the model towards two tube rupture case studies.

Lastly, Chapter 5 offers concluding remarks.

2. FRAMEWORK FOR DYNAMIC MODELING OF LIQUID-LIQUID, VAPOR-LIQUID, AND FLASHING-LIQUID LIQUID HEAT EXCHANGER TUBE RUPTURES[1]

2.1 Model Assumptions

A tube in an exchanger can fail from fatigue, corrosion, increased temperature, and conflict with baffling [80]. A case study from SABIC Europe shows baffle hammering as having the potential to damage tubes [81]. Depending on the tolerance between the baffle and tubes, excessive movement by the tubes will result in continued striking against the baffle. Over time, this has the possibility to form a cavity. This creates a weak point in the tube, effectively reducing the design pressure of the tube. Similarly, Shahrani et al studied the failure mechanism of heat exchanger tubes in a plant [82]. It was concluded that fretting between the baffles and tubes, in combination with the corrosion due to the presence of sulfur, led to the tube failing. Vibration from equipment such as compressors can also cause tube failures via baffle hammering. One way to counter this is to reduce the velocity to minimize vibrations. For new exchangers, materials of construction and/or adding design features such as baffle spacing may also allow for increased vibration.

Metal erosion from high velocity particulates over time can also thin tubes and result in a rupture [80]. The erosion rate primarily depends on the velocity, diameter, pipe thickness, and mass of particulates. The impact angle also affects the severity of erosion. Because of the need for the fluid to change direction, in a piping system, pipe bends frequently exhibit higher rates of erosion [83]. Another case study by Khilnaney examines the failures of tube ruptures at a nuclear plant cooling water exchanger [84]. In this study, hydrogen sulfide was detected in the cooling tower, thus suspecting a tube leak had occurred. It was found that in 50% of these tubes, fluid elastic instability across the tube may have played a role in their failure. Lastly, corrosion from harsh chemicals such as sulfur and caustic chemicals can weaken tubes to the point of failure.

ASME VIII code governs the performance of pressure vessels. It specifically applies to pres-

[1]This chapter was reprinted in whole or in part with permission from "Dynamic modeling of heat exchanger tube rupture" by Harhara, A., & Hasan, M. M, 2020. *BMC Chemical Engineering*, 2(1), 1-20, Copyright 2022 by Harhara, A., & Hasan, M. M.

sure vessels operating at or exceeding 15 psig [85]. Most exchangers in a plant have operating pressures that fall under this criterion and are consequently governed by ASME VIII code. The code also defines a maximum allowable working pressure (MAWP) based on an equipment's material, thickness, and other mechanical properties. During overpressure scenarios, pressure vessels must vent excess pressure to a flare, recycled to the process, or to the environment (depending on the fluid being vented). For the most part, pressure relief valves are set at or below the MAWP. There are exceptions to this when dealing with multiple relief valves. Note that the MAWP and the design pressure often refer to the same pressure and are used interchangeably. This paper makes no distinction between the two terms.

For a single pressure relief valve protecting a system, a 10% accumulation in pressure beyond the MAWP is allowed [85]. For multiple relief valves providing protection, the accumulation is allowed to increase to 16% above the MAWP [85]. The last common overpressure scenario is for dealing with external fire, in which case, accumulation can increase up to 21% beyond the MAWP [85]. For pressure vessels, the hydrotest pressure is tested anywhere between 1.3 to 1.5 times the MAWP [86]. This work assumes a hydrotest pressure of 1.5 times the design pressure. This work can easily be reformulated to apply to a hydrotest pressure of 1.3 times the design pressure, however. Lastly, because of the low probability of tube ruptures occurring in comparison with other more common relief events, and because a tube rupture occurs over a short period of time, the shell-side hydrotest pressure is set as the upper bound. Some plants may not even consider an overpressure scenario up to the hydrotest pressure to be a layer of protection analysis (LOPA) scenario [87]. Figure 2.1 shows an overview of where the different pressures are located in relation to one another. The range of pressures for a tube rupture scenario can theoretically vary from the shell-side operating pressure to the tube-side hydrotest pressure. A normal operating window for the shell-side is between its operating pressure and design pressure. Somewhere between these pressures, a pressure relief device is set to open. Similarly, the tube-side also has an operating window between its operating pressure and design pressure, as well as a relief device set between these pressures. The next threshold after the shell-side design pressure is its hydrotest pressure.

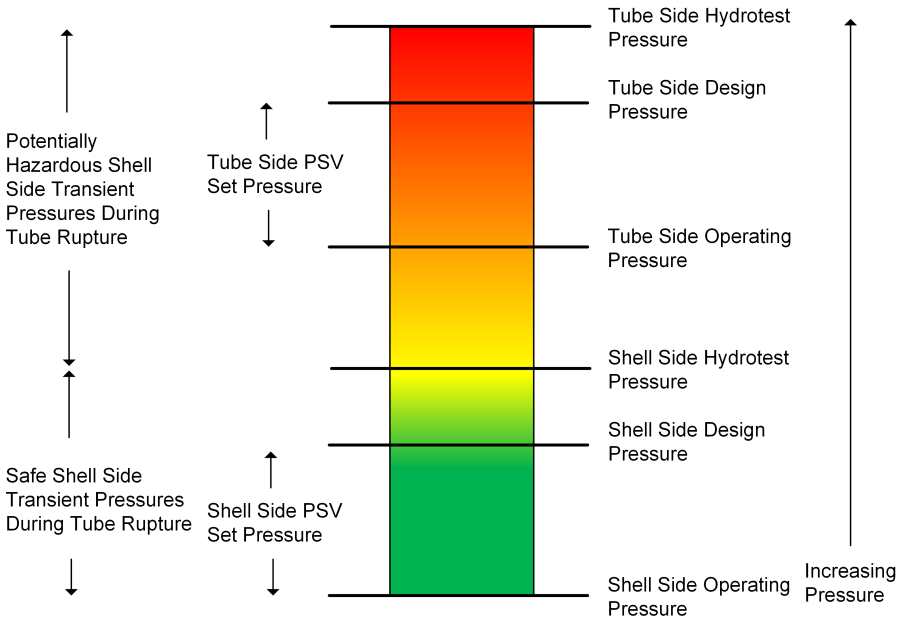

Figure 2.1: Range of pressures for tube rupture scenario

When modeling the dynamic pressure profile, any pressure between the operating pressure and hydrotest pressure will be considered acceptable. Beyond this pressure, the severity of a tube rupture and the likelihood of the shell-side failing increase with pressure (shown as the region in yellow-to-red region in Figure 2.1).

For most overpressure scenarios, relief valves are able to open in time for pressure increases. With heat exchanger tube ruptures however, there is some concern that tube ruptures (which can generate peak pressures in milliseconds) can overpressure the shell-side of an exchanger before a pressure relief valve can take effect. A 2002 study prepared by Pipeline Simulation and Integrity Ltd for the United Kingdom's Health and Safety Executive tested the response times of pressure relief valves and rupture disks [13]. The study found that fast-acting relief valves do exist. Note that if a vendor includes a datasheet that lists the response time, that should be used in the model. An if-statement can be included that doesn't allow any fluid to vent through the relief valve from the initial rupture until the response time has been met.

This paper examines the three most common tube rupture scenarios: the liquid-liquid system, the vapor-liquid system, and the flashing liquid-liquid system. For all shell and tube exchanger

configurations, tube ruptures can be divided into four distinct phases [88]:

- Phase I: Sudden rupture
- Phase II: Development of transient shell-side pressure wave
- Phase III: Shell-side liquid discharges through pressure relief system
- Phase IV: Shell-side vapor discharges through pressure relief system

The first phase generates a shock wave from the rupture of the tube. This is, however, considered to be nearly instantaneous and is not modeled. With an open path, the high pressure side fluid enters the low pressure side. Because the tube-side fluid acts against the shell-side fluid, the shell-side fluid is pushed into the relief system. Once this is complete, the tube-side fluid (either vapor or liquid) has a path to exit the exchanger. Phases II, III, and IV are modeled with the following assumptions:

- Only one tube is assumed to rupture.
- The rupture is assumed to be a full-bore rupture.
- A tube rupture exposes both ends of the severed tube, allowing fluid to enter the shell-side at twice the cross-sectional area of one tube.
- The tube-side fluid enters the shell-side as an isentropic nozzle flow.
- The effects of temperature are ignored (e.g., increased heating resulting in the buildup of pressure).
- An infinite reservoir of tube-side fluid exists. This is a conservative assumption. Without this assumption, one would need to determine what is the quantity of tube-side fluid available (from upstream and downstream units). One can also determine what is the rate of tube-side pressure loss (and decrease in velocity) as the fluid is being lost to the shell-side.

- Pressure relief systems have an instantaneous response time (i.e., zero milliseconds).
- No credit is taken for outflow via inlet or outlet piping. The phrase "taking credit for outflow" allows one to reduce the relieving requirements for overpressure scenarios by accounting for fluid leaving the system. This however comes with a set of requirements to ensure than an open path exists (and is adequately sized) for fluid to escape. For this model, all excess pressure must be vented through available relief systems.
- All areas of the exchanger's shell-side are in equilibrium. The effects of localized pressure are ignored.
- The exchanger shell-side can safely handle pressures up to the hydrotest pressure.

What follows describes how one can model and predict the liquid and vapor flow rates, flashing liquid flow rates, vapor densities, mass fluxes from the tube to shell-side and from the shell-side to outside through a pressure relief valve, and the dynamic pressure profiles as a consequence of tube rupture in a shell and tube heat exchanger.

2.2 Liquid Flow Rate

The volumetric energy balance for isentropic nozzle flow is given by Equation 2.1.[89]

$$G^2 = \frac{2 \times \int_{P_1}^{P_2} v \, dP}{v_t^2} \tag{2.1}$$

Where G is the tube-side mass flux entering the shell (kg/s-m^2), v is the specific volume of the tube-side fluid (m^3/kg), P_1 and P_2 are the pressure (Pa) the tube-side fluid experiences at the inlet and outlet, respectively, and t is the fluid condition at the throat of the nozzle where the cross-sectional area is minimized. Assuming a constant pressure step size, the integration portion in Equation 2.1 can be expressed via Equation 2.2.

$$\int_{P_1}^{P_2} v \, dP = \frac{h}{2} \left(v_1 + v_n + 2 \times \sum_{j=2}^{n-1} v_j \right) \tag{2.2}$$

Where v is the specific volume of the tube-side fluid (m^3/kg), h is the constant pressure step size chosen for summation purposes (Pa), n is the index for fluid conditions at the assumed throat pressure (i.e. the assumed endpoint pressure for the integral), and j is the increment counter used for summation purposes. Combining Equations 2.1 and 2.2, we are able to obtain the mass flux equation for liquid flow through a tube (Equation 2.3).

$$G^2 = \frac{h\left(v_1 + v_n + 2 \times \sum_{j=2}^{n-1} v_j\right)}{v_t^2} \tag{2.3}$$

Once G is determined for different pressure intervals, the mass flux should be fitted against pressure by using a quadratic fit in the following format (Equation 2.4), where $A1$, $A2$, and $A3$ are the coefficients that give the best fit (e.g., method of least squares). Smaller pressure intervals will increase the accuracy of G. The end result is a continuous function that yields a mass flux for all pressures between the shell and tube-side pressure.

$$G = A1 \times P(t)^2 + A2 \times P(t) + A3 \tag{2.4}$$

2.3 Vapor Flow Rate

The methodology for the calculation of vapor flow through the ruptured tube is very similar to that of the liquid flow rate. A series of isentropic flashes from high pressure to low pressure conditions are performed. Using the relationship between pressure and specific volume, Equations 2.1 - 2.3 are solved to yield a mass flux as a function of pressure. Up to this point, the solution method for the liquid flow rate and the vapor flow rate are identical. However, for most vapor-liquid tube ruptures, a choked flow condition will be present. The mass flux function, G, when calculated, will show whether or not a choked condition exists. If that is the case, the mass flux versus pressure must be adjusted to reflect the choked condition. This is fitted using a cubic fit in the following format (Equation 2.5), where $\alpha 1$, $\alpha 2$, $\alpha 3$, and $\alpha 4$ are the coefficients that give the best fit (e.g., method of least squares). An example of how this is performed is presented later.

$$G = \alpha 1 \times P(t)^3 + \alpha 2 \times P(t)^2 + \alpha 3 \times P(t) + \alpha 4 \tag{2.5}$$

2.4 Flashing Liquid Flow Rate

The flow rate of a flashing liquid entering the shell-side incorporates techniques used in calculating the liquid flow rate and vapor flow rate. First, a series of isentropic flashes from the tube-side pressure to the shell-side pressure are performed. Equations 2.1 - 2.3 are solved to yield a mass flux as a function of pressure. If a choked condition does result, then the mass flux should be fitted as a cubic equation (Equation 2.5). These steps are identical to the ones performed in Section 2.3. The main difference, however, is that the downstream phase in a flashing liquid may take the form of a vapor, two-phase, or liquid, depending on its pressure. Thus, the vapor phase fraction at each pressure interval needs to be calculated in addition to the total mass flux. The vapor phase fraction, y_t, is expressed as a piecewise function as follows:

$$y_t = \begin{cases} C1 \times P(t) + C2 & if\ P(t) \leq P_{tbp} \\ 0 & otherwise \end{cases} \tag{2.6}$$

Where $C1$ and $C2$ are the coefficients that give the best fit, and P_{tbp} is the tube-side fluid's bubble point pressure. The vapor phase fraction can then be multiplied with the total mass flux, G, to yield the tube-side vapor mass flux, G_v, and one minus the vapor phase fraction multiplied by G yields the tube-side liquid mass flux, G_l:

$$G_v = G \times y_t \tag{2.7}$$

$$G_l = G \times (1 - y_t) \tag{2.8}$$

2.5 Density of Tube-Side Vapor, ρ_{tv}

With liquid-liquid systems, the density is assumed to be constant. However, with vapor-liquid systems, density must be changed as a function of pressure. If the vapor density is treated as an ideal gas, it would be inaccurate at high pressures and low temperatures. If density versus pressure is fitted using experimental data, the results will be accurate. The problem with this, however, is that the number of gases available to deploy this method are limited. A general way is to use an equation of state to determine the density versus pressure relationship. This can be accomplished by using widely available process simulation software (e.g., Aspen HYSYS). Density and pressure are expressed via a linear relationship as follows:

$$\rho_{tv} = B1 \times P(t) + B2 \tag{2.9}$$

Where $B1$ and $B2$ are the coefficients that give the best fit.

2.6 Rate of Tube-Side Fluid Entering Shell-Side

With the tube-side mass flux, G, determined, the area of a single tube and the tube-side mass flow rate can be obtained by Equations 2.10, 2.11, and 2.12. Note that the mass flow rate is listed as two times the flux multiplied by the area. This is because the flow entering the shell-side will be entering from upstream of one ruptured tube and downstream of the other ruptured tube.

$$A_{tube} = \pi r_{tube}^2 \tag{2.10}$$

$$\dot{m}_{tl} = 2G_l A_{tube} \tag{2.11}$$

$$\dot{m}_{tv} = 2G_v A_{tube} \tag{2.12}$$

2.7 Rate of Shell-Side Fluid Exiting Relief Device

Assuming a pressure relief valve can be modeled as flow through an orifice, the following gives the mass flow rate exiting the relief device:

$$\dot{m_{psv}} = \left\{ \begin{array}{cc} A_{psv} C_0 \sqrt{2 \rho_{sl} g_c P(t)} & if\ P(t) \geq P_{set} \\ 0 & otherwise \end{array} \right\} \tag{2.13}$$

Note that the equations used for flow through a pressure relief valve can be modified to model spring loaded, balanced bellows, and pilot valves. An example of this performed is by Singh who developed a one-dimensional dynamic model for a spring loaded pressure safety valve (PSV) [90]. Moreover, any equations of flow through a PSV provided by a vendor can also be substituted here. The expression can also be modified to reflect the reseat pressure of a relief valve.

2.8 Bulk Modulus of Elasticity

Interpolation should be used to determine the bulk modulus for a fluid, B, shown in Equation 2.14. While using the same temperature as that of the system, the high and low side pressures (P_1 and P_0) and their respective volumes (V_1 and V_0) are chosen to calculate the bulk modulus. Although the bulk modulus does vary, it is reasonable to assume it is constant throughout the entire range of pressures during the overpressure event.

$$B = \frac{P_1 - P_0}{\frac{V_1 - V_0}{V_0}} \tag{2.14}$$

2.9 Tube-Side Vapor and Liquid Volumes Present in Shell, V_{tv} and V_{tl}

V_{tv} and V_{tl} represent the tube-side vapor and tube-side liquid volumes that are present in the exchanger shell. At the beginning of a tube rupture, no tube-side fluid is present in the shell. As fluid starts entering the shell-side, V_{tv} and V_{tl}, are calculated by the following Equations:

$$\frac{d\dot{V}_{tv}}{dt} = \frac{\dot{m}_{tv}}{\rho_{tv}} \tag{2.15}$$

$$\frac{d\dot{V}_{tl}}{dt} = \frac{\dot{m}_{tl}}{\rho_{tl}} \tag{2.16}$$

Where $\dot{m}_{tv}$ and ρ_{tv} are the tube-side vapor mass flow rate (kg/s) and density (kg/m^3), respectively. And $\dot{m}_{tl}$ and ρ_{tl} are the tube-side liquid mass flow rate (kg/s) and density (kg/m^3), respectively.

2.10 Shell Pressurization

A conservation of volume balance on the exchanger shell yields Equation 2.17 [23]. This allows one to determine the change in pressure over time during a tube rupture. For liquid-liquid systems, the vapor associated terms $\dot{m}_{tv}$, ρ_{tv}, V_{tv}, and c_{tv0} are removed from the equation. Similarly, for vapor-liquid systems, the terms $\dot{m}_{tl}$, ρ_{tl}, V_{tl}, and B_{tl} are removed from the equation. In the case of a flashing tube-side liquid with liquid on the shell-side, all terms in Equation 2.17 would be present.

$$\left(\frac{dP}{dt}\right) = \frac{\frac{\dot{m}_{tv}}{\rho_{tv}} + \frac{\dot{m}_{tl}}{\rho_{tl}} - \frac{\dot{m}_{psv}}{\rho_{sl}}}{\Omega + \frac{V_{sl}}{B_{sl}} + \frac{V_{shell}}{B_{shell}}} \tag{2.17}$$

$$\Omega = \left\{ \begin{array}{cc} \frac{V_{tv}}{c_{tv0}^2 \rho_{tv}} & vapor \\ \frac{V_{tl}}{B_{tl}} & liquid \\ \frac{V_{tv}}{c_{tv0}^2 \rho_{tv}} + \frac{V_{tl}}{B_{tl}} & flashing\, liquid \end{array} \right\} \tag{2.18}$$

Where $\dot{m}_{tv}$ and ρ_{tv} are the tube-side vapor mass flow rate (kg/s) and density (kg/m^3), respectively. $\dot{m}_{tl}$ and ρ_{tl} are the tube-side liquid mass flow rate (kg/s) and density (kg/m^3), respectively. $\dot{m}_{psv}$ and ρ_{sl} are the PSV mass flow rate (kg/s) and shell-side liquid density (kg/m^3), respectively. Ω represents the tube-side volume and bulk modulus terms. V_{sl} and B_{sl} are the volume of shell-side liquid (m^3) remaining in the shell-side and the shell-side liquid's bulk modulus (Pa), respectively. V_{shell} and B_{shell} are the shell volume (m^3) and the bulk modulus (Pa) of the shell material of construction (e.g., carbon steel), respectively. The three cases for Ω are given by Equation 2.18. V_{tv} and c_{tv0} are the volume of tube-side vapor (m^3) that has entered the shell-side and the tube-side va-

por's speed of sound (m/s), respectively. V_{tl} and B_{tl} are the volume of tube-side liquid (m^3) that has entered the shell-side and the tube-side liquid's bulk modulus (Pa), respectively. This differential equation is the main mathematical model that will be solved and is valid for liquid-liquid, vapor-liquid, and flashing liquid-liquid systems. The previous variables, described in earlier subsections all feed into this model.

Since the initial shell-side pressure in Equation 2.17 is known, this differential model can be viewed as an initial value problem. Furthermore, this equation is a first order differential equation. A simple explicit method can be used to solve the model. Euler's method is used for this paper. Using Matlab, a custom algorithm based on Euler's method is developed [91]. The accuracy of this method increases with a smaller step size. Because tube ruptures can exhibit peak pressures in milliseconds, a step size of no larger than 0.1 millisecond is appropriate.

Figure 2.2 lists the major steps in generating a tube rupture pressure profile. The first step in modeling a tube rupture is collecting the appropriate data about the system. These include, but are not limited to, equipment diagrams, process simulation parameters (pressure, temperature, density, etc.), and relief valve datasheets. The second step is to obtain the necessary thermodynamic properties. One way to achieve this is by creating a table of isentropic flashes from the tube-side conditions to the shell-side conditions. Table 2.1 lists the isentropic flashes for the liquid-liquid system solved in Section 4.1. The integral term in Table 2.1 refers to the solution of Equation 2.2. These properties are used to determine the tube-side mass flux which can be used to calculate the mass flow rate entering the shell-side. The bulk modulus is also calculated at this stage. Once the above information are obtained, the equations relating the mass flux and pressurization of the shell are used to calculate the shell-side pressure. An appropriate time-step is selected to solve Equation 2.17 numerically. If the time-step is too large, then the resolution will not be detailed enough. If this occurs, the dynamic pressure profile obtained may not display the true peak of the tube rupture phenomena. Too small a time-step, on the other hand, increases the number of iterations needed to achieve a solution.

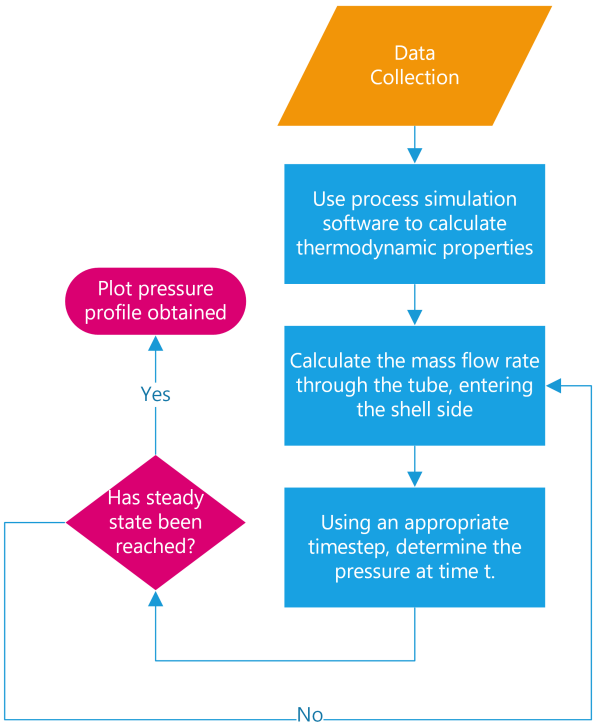

Figure 2.2: Steps needed to generate dynamic pressure profile during tube rupture.

2.11 Liquid-Liquid System Case Study

Consider the following example. A carbon steel shell and tube exchanger has ethylene glycol in the tube-side and cooling water in the shell-side. The exchanger contains 150 tubes each 2 meters long with an inner diameter of 15 mm. The shell's volume is 7.5 m^3. The high and low side operating pressures are 10 bar and 1 bar, respectively. The high and low side operating temperatures are 100 °C and 20 °C, respectively. The shell-side has a PSV set pressure of 1.2 bar (equal to its design pressure) and a hydrotest pressure of 1.8 bar. The following steps are used to determine the required PSV size in order to adequately protect this system.

Step 1: Obtain the physical properties of the liquid-liquid system.

Using the Peng-Robinson equation of state, at 1 bar and 20 °C, the density of water is 1011 kg/m^3. Similarly, at 10 bar and 100 °C, the density of ethylene glycol is 1055 kg/m^3. We then determine the bulk modulus for each fluid. It is determined that water has a bulk modulus of 3.44931×10^9 Pa, and ethylene glycol has a bulk modulus of 0.89769×10^9 Pa. The bulk modulus

of common metals can be found in engineering reference manuals [92]. Carbon steel has a bulk modulus (B_{shell}) of 159 $\times$ 10^9 Pa.

Step 2: Use process simulation software to calculate thermodynamic properties.

Using Aspen HYSYS [93], a property table is created for the tube-side fluid. Isentropic flash calculations (in increments of 1 bar) are performed for ethylene glycol from the tube-side pressure (10 bar) to the shell-side pressure (1 bar). The results are listed in Table 2.1.

Step 3: Calculate the mass flow rate through the tube, entering the shell-side.

Using the mass flux equation and property table, the mass flux can be calculated (shown in Table 2.1). Once the mass flux for each pressure is determined, the data is then fitted to a quadratic equation in order to obtain the mass flux as a function of pressure. For the ethylene-glycol water system described, Equation 2.4 is generated with coefficients $A1$, $A2$, $A3$ equal to -434.4, 526.4, and 41854.5, respectively. Note that the pressure in Equation 2.4 refers to the shell-side pressure. At a pressure of 1 bar and 10 bar, this equation yields the maximum and minimum tube-side flow rates. This is reasonable since the largest driving force exists when the shell-side pressure is 1 bar. Similarly, when the shell-side is at 10 bar, no driving force exists.

Step 4: Using an appropriate time-step, determine the pressure at time t.

At time is equal to zero, the shell-side pressure is set to 1 bar. Using Matlab [91], Equations 4, 9-13, and 15-16 are then simultaneously solved using a time-step of 1 millisecond. The required data are shown in Table 2.2. Note the calculations presented shall assume a zero second response time for relief valves.

Table 2.1: Properties of ethylene-glycol isentropic flashes and mass flux at different pressure intervals. Molar Entropy = -131 kJ/kgmole-°C.

Pressure bar	Mass Density kg/m^3	Specific Volume 1e4 $\times$ m^3/kg	Integral Term m^2/s^2	Mass Flux kg/s-m^2
10	1055	9.482		
9	1054	9.483	95	14522
8	1054	9.484	190	20536
7	1054	9.485	285	25149
6	1054	9.486	379	29037
5	1054	9.487	474	32462
4	1054	9.488	569	35558
3	1054	9.489	664	38404
2	1054	9.490	759	41052
1	1054	9.491	854	43539

Table 2.2: Parameters used in liquid-liquid, vapor-liquid, and flashing liquid-liquid systems.

Ethylene-glycol & Water		Methane & Water		Propane & Water	
Parameter	Value	Parameter	Value	Parameter	Value
r_{tube}	0.0075 m	r_{tube}	0.005 m	r_{tube}	0.005 m
ρ_{tl}	1055 kg/m^3	c_{tv0}	505.2 m/s	c_{tv0}	228 m/s
B_{tl}	8.9769 $\times$ 10^8 Pa	ρ_{sl}	1011 kg/m^3	ρ_{sl}	1011 kg/m^3
ρ_{tl}	1011 kg/m^3	B_{sl}	3.4493 x 10^9 Pa	B_{sl}	3.4493 x 10^9 Pa
B_{sl}	3.4493 $\times$ 10^9 Pa	V_{sl}	7.5 m^3	V_{sl}	7.5 m^3
V_{shell}	7.5 m^3	V_{shell}	7.5 m^3	V_{shell}	7.5 m^3
V_{sl}	7.5 m^3	B_{shell}	159 x 10^9 Pa	B_{shell}	159 x 10^9 Pa
B_{shell}	159 $\times$ 10^9 Pa	$\alpha 1$	-34.219	$\alpha 1$	-8.131
$A1$	-434.4	$\alpha 2$	219.62	$\alpha 2$	323.33
$A2$	526.4	$\alpha 3$	-439.53	$\alpha 3$	-3295.7
$A3$	41854.5	$\alpha 4$	997.29	$\alpha 4$	27649
		$B1$	0.4747	$B1$	2.32
		$B2$	0.58	$B2$	-1.5468
				$C1$	-0.025
				$C2$	0.5285

The pressure profiles for the liquid-liquid system are shown in Figure 2.3. The pressure (bar) is plotted against time (milliseconds) for various standard PSV orifice sizes. This figure uses a time axis of 500 milliseconds, enough to capture the pseudo steady state pressures for all orifice sizes. A dotted line representing the hydrotest pressure (1.8 bar) is shown. As stated earlier, we do not wish to exceed the hydrotest pressure for this scenario. At time is equal to 0 milliseconds, the tube rupture begins. This period in time has the largest difference in pressure between the two exchanger sides.For orifice sizes D, E, F, and G, the hydrotest pressure is exceeded at 25 milliseconds. An 10 additional miliseconds shows orifice size H exceeding the hydrotest pressure. These orifice sizes reach a pseudo steady state condition at approximately 300 miliseconds, with shell-side pressures

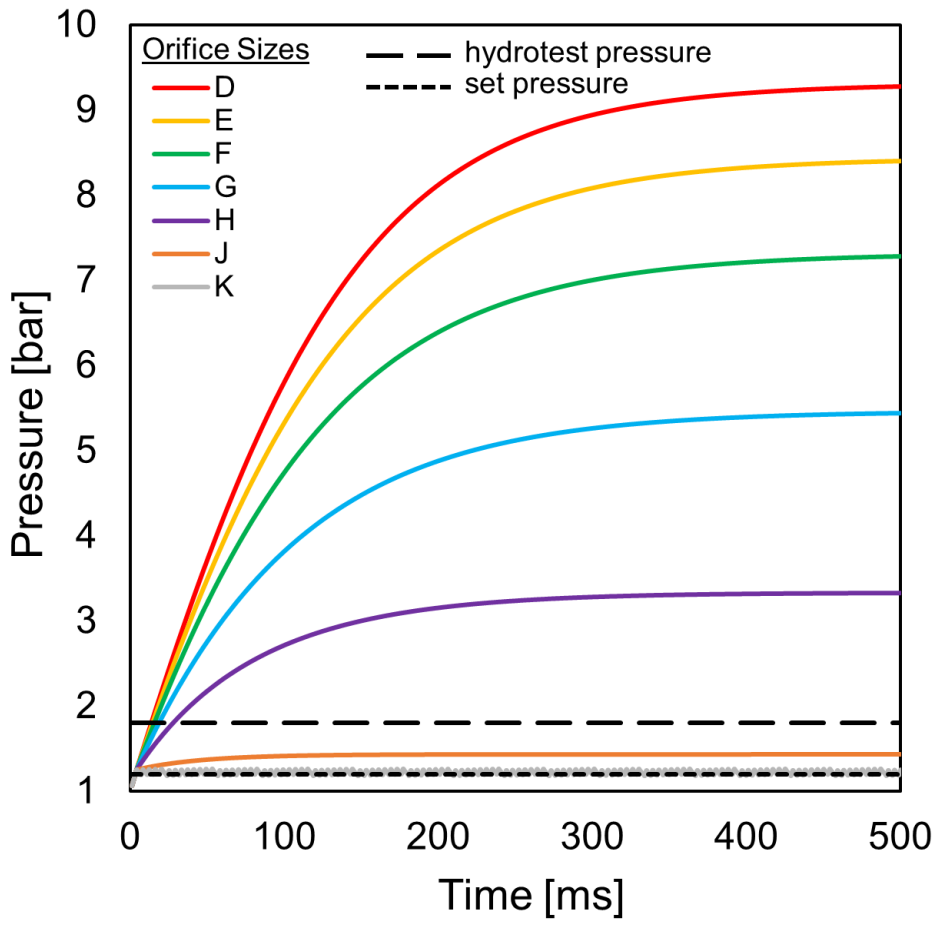

Figure 2.3: Shell-side pressure profiles for ethylene-glycol water systems for different PSV sizes.

ranging from 3 bar to above 9 bar. Thus, for orifice sizes D, E, F, G, and H, the shell-side failing is almost certain due to the hydrotest pressure being significantly exceeded. Orifice sizes J and K are the only PSV sizes that adequately protect against this overpressure event. While orifice size J does exceed the design pressure, it is comfortably below the hydrotest pressure. Orifice size K is even more conservative with shell-side pressures not exceeding the design pressure during this tube rupture. Due to the lower cost of the J orifice PSV (resulting from its smaller size), this PSV would most likely be preferred in a plant.

2.12 Vapor-Liquid System Case Study

Consider the following example. A carbon steel shell and tube exchanger has methane in the tube-side and cooling water in the shell-side. The exchanger contains 100 tubes each 3 meters long with an inner diameter of 10 mm. The shell's volume is 7.5 m^3. The high and low side operating pressures are 5 bar and 1 bar, respectively. The high and low side operating temperatures are 100 °C and 20 °C, respectively. The shell-side has a PSV set pressure of 1.2 bar (equal to its design pressure) and a hydrotest pressure of 1.8 bar. We would like to determine the required PSV size in order to adequately protect this system following the steps:

Step 1: Obtain the physical properties of the vapor-liquid system.

Using the Peng-Robinson equation of state, at 1 bar and 20 °C, the density of water is 1011 kg/m^3. Between 5 bar and 1 bar, the density of methane in kg/m^3 is given by Equation 2.9 with coefficients $B1$ and $B2$ equal to 0.4747 and 0.58, respectively. As previously stated, water has a bulk modulus of 3.44931 $\times$ 10^9 Pa. Similarly, carbon steel has a bulk modulus (B_{shell}) of 159 $\times$ 10^9 Pa.

Step 2: Use process simulation software to calculate thermodynamic properties.

Using Aspen HYSYS [93], a property table is created for the tube-side fluid. Isentropic flash calculations (in increments of 0.4 bar) are performed for methane from the tube-side pressure (5 bar) to the shell-side pressure (1 bar). The results are listed in Table 2.3.

Step 3: Calculate the mass flow rate through the tube, entering the shell-side.

Using the mass flux equation and property table, the mass flux can be calculated and is given in Table 2.3. Note that the methane will exhibit choked flow, and the mass flux must reflect this (see Figure 2.4). Thus, the mass flux versus pressure data is fitted by a cubic polynomial (Equation 2.5) with the coefficients $\alpha1$, $\alpha2$, $\alpha3$, and $\alpha4$ equal to -34.219, 219.62, -439.53, and 997.29, respectively. Between 1 bar and 5 bar, this equation yields the maximum and minimum tube-side flow rates.

Step 4: Using an appropriate time-step, determine the pressure at time t.

At time is equal to zero, the shell-side pressure is set to 1 bar. Using Matlab [91], Equations 5,

9-14, and 16 are then simultaneously solved using a time-step of 1 millisecond. The required data are shown in Table 2.2. Note the calculations presented shall assume a zero second response time for relief valves.

Table 2.3: Properties of methane isentropic flashes and mass flux at different pressure intervals. Molar Entropy = 178.5 kJ/kgmole-°C.

Pressure bar	Mass Density kg/m^3	Specific Volume m^3/kg	Integral Term m^2/s^2	Mass Flux kg/s-m^2	Corrected Mass Flux kg/s-m^2
5.0	2.598	0.3849			
4.6	2.433	0.4110	7698	302	302
4.2	2.265	0.4414	25287	509	509
3.8	2.095	0.4774	43663	619	619
3.4	1.921	0.5207	63625	685	685
3.0	1.742	0.5740	85518	721	721
2.6	1.559	0.6414	109826	731	731
2.2	1.370	0.7299	137252	718	731
1.8	1.174	0.8518	168886	682	731
1.4	0.968	1.0328	206578	622	731
1.0	0.749	1.3348	253931	534	731

Figure 2.4 shows the mass flux profile for methane at various downstream pressures. Two mass flux profiles for methane are included, one which takes into account choked flow (listed as red circles) and one that excludes the effects of choked flow (listed as blue triangles). The choked flow region is roughly between downstream pressures of 1 bar and 2.6 bar. In other words, from an initial pressure and temperature of 5 bar and 100 °C, the mass flow rate of methane transported through an isentropic nozzle (as is the case in a tube rupture) increases with decreasing downstream pressure until 2.6 bar. Between downstream pressures of 1 bar and 2.6 bar, the mass flow rate of methane is constant and at its maximum (731 kg/s-m^2). Neglecting the effects of choked flow can

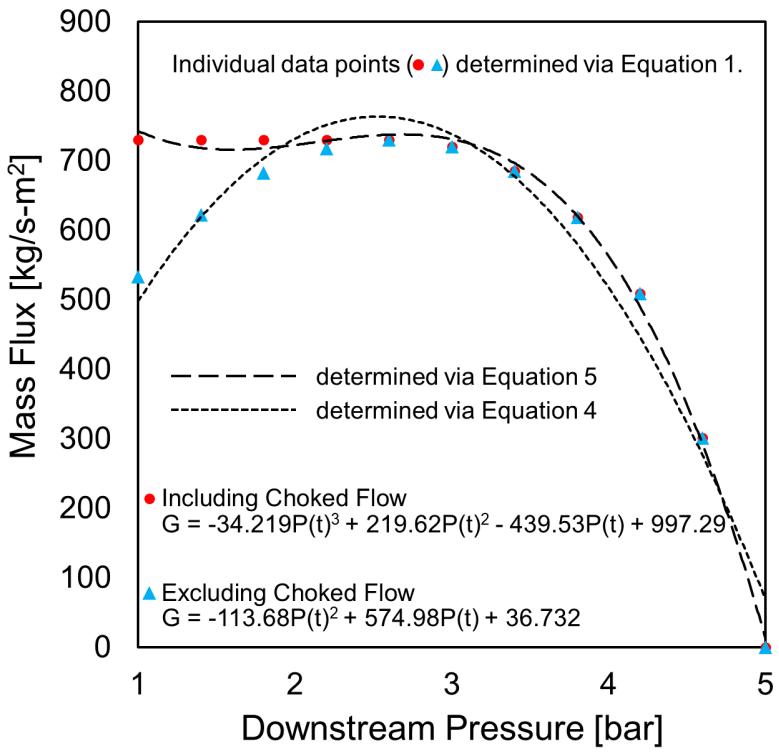

Figure 2.4: Tube-side mass flux vs. downstream pressure for methane with an initial pressure of 5 bar and initial temperature of 100 °C.

result in a misleading mass flux, as can be seen by the negative parabolic shaped trendline in Figure 2.4. Accepting this erroneous mass flux may lead to an undersized relief system.

The pressure profiles for the methane water system are shown in Figure 2.5. By plotting the pressure (bar) versus time (milliseconds), the effects of selecting different PSV orifice sizes (D, J, N, P, Q, R, and T) to protect this system are shown. A dotted line representing the hydrotest pressure (1.8 bar) is included. For this tube rupture, orifice size Q appears to provide adequate overpressure protection, without being conservative. One notable difference between this system and the liquid-liquid system is the speed at which pseudo steady state pressure is reached. Figure 2.5 took approximately 30 milliseconds as opposed to 300 milliseconds in Figure 2.3. This highlights the severity of a tube rupture in vapor-liquid systems.

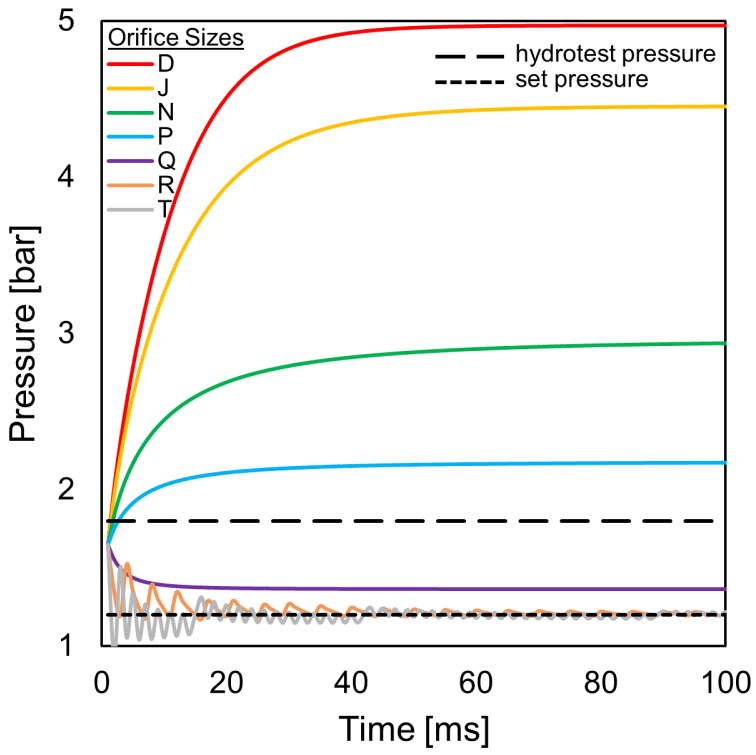

Figure 2.5: Shell-side pressure profiles for methane water systems for different PSV sizes.

2.13 Comparison of Liquid-Liquid and Vapor-Liquid Systems

Assuming the same tube and shell-side pressures, for an equivalent mass entering the shell-side, a vapor-liquid system reaches peak pressure significantly faster (and as a result is more severe) than that of a liquid-liquid system. This is true even though the fluid flow (on a mass basis) that enters the shell-side for vapors is significantly less than that of liquids. The vapor-liquid simulations indicate that the peak pressures are reached in less than 50 ms as opposed to the liquid-liquid cases which took between 100 and 300 ms, depending on the size of the PSV orifice. Shell-side transient peak pressures are able to significantly exceed their hydrotest pressures. For systems left with inadequate overpressure protection, these simulations demonstrate the consequences of tube ruptures.

The T and R orifices, as shown in Figure 2.5, resulted in the pressure oscillating above and below the set pressure. These pressure oscillations can be broken into a series of steps. First,

the system pressure builds up due to an overpressure event, causing the PSV to open. Because the PSV is sufficiently large to handle the influx of fluid entering, the PSV vents all of the excess fluid along with additional fluid. At this point, the system pressure decreases, eventually dropping below the set pressure. Since the system pressure is below the set pressure, the PSV reseats to its original position. This cycle repeats for the duration of the overpressure event. More sophisticated modeling can include the effects of the PSV reseating. The rapid opening and closing of the relief valve is known as chattering and has been documented as affecting the reliability of a PSV [94]. Chattering can occur due to oversizing a relief valve, which appears to be the case for orifices T and R. For more common overpressure scenarios such as blocked outlet, control valve failures, and fires, plants may desire to select a relief valve that avoids chattering. However, because of the low frequency of tube ruptures in plants, chattering is not considered to be a primary concern.

Another distinction between vapor-liquid and liquid-liquid systems is the presence of choked flow. For vapor-liquid systems, ignoring choked flow can result in a relief system being undersized. Figure 6 shows the tube-side mass flux when including and excluding choked flow. For downstream pressures that are close to the upstream pressures, it is possible the fluid may not enter the choked region. This would yield the same mass flow rate whether choked flow is included or excluded. This is seen in the pressure interval between 5 bar and 2.6 bar in both Table 2.3 and Figure 2.4. This should not be left to chance however. Testing for choked flow should always be performed.

2.14 Flashing Liquid-Liquid System

Consider the following example. A carbon steel shell and tube exchanger has propane in the tube-side and cooling water in the shell-side. The exchanger contains 100 tubes each 4 meters long with an inner diameter of 10 mm. The shell's volume is 7.5 m^3. The high and low side operating pressures are 30 bar and 6 bar, respectively. The high and low side operating temperatures are 60 °C and 6 °C, respectively. The shell-side has a PSV set pressure of 7.2 bar (equal to its design pressure) and a hydrotest pressure of 10.8 bar. We would like to determine the required PSV size in order to adequately protect this system following the steps:

Step 1: Obtain the physical properties of the flashing liquid-liquid system.

Using the Peng-Robinson equation of state, the density of 60 °C liquid propane between 30 bar and 6 bar is on average 446 kg/m^3. The density of vapor propane between 21 bar and 6 bar is given by Equation 2.9 with coefficients $B1$ and $B2$ equal to 2.32 and -1.5468, respectively. As previously stated, water has a density of 1011 kg/m^3 and a bulk modulus of 3.44931 $\times$ 10^9 Pa. Liquid propane has a bulk modulus of 0.1536 $\times$ 10^9 Pa. Carbon steel has a bulk modulus (B_{shell}) of 159 $\times$ 10^9 Pa.

Step 2: Use process simulation software to calculate thermodynamic properties.

Using Aspen HYSYS [93], a property table is created for the tube-side fluid. Isentropic flash calculations (in increments of 1.5 bar) are performed for propane from the tube-side pressure (30 bar) to the shell-side pressure (6 bar). Because vapor is generated, the vapor fraction is included in the property table. The results are listed in Table 2.4.

Step 3: Calculate the mass flow rate through the tube, entering the shell-side.

Using the mass flux equation and property table, the mass flux can be calculated and is given in Table 2.4. Methane exhibits choked flow with a maximum mass flux of 27170 kg/s-m^2. The corrected mass flux versus pressure is fitted against a cubic polynomial (Equation 2.5) with the coefficients $\alpha1$, $\alpha2$, $\alpha3$, and $\alpha4$ equal to -8.131, 323.33, -3295.7, and 27649, respectively. The vapor fraction is expressed as Equation 2.6 with coefficients $C1$ and $C2$ equal to -0.025 and 0.5285, respectively. The vapor fraction equation is only valid between pressures 6 bar and 21 bar (the tube-side bubble point pressure).

Step 4: Using an appropriate time-step, determine the pressure at time t.

At time is equal to zero, the shell-side pressure is set to 6 bar. Using Matlab [91], Equations 6-16, and 16 are then simultaneously solved using a time-step of 1 millisecond. The required data are shown in Table 2.2. Note the calculations presented shall assume a zero second response time for relief valves.

Table 2.4: Properties of propane isentropic flashes and mass flux at different pressure intervals. Molar Entropy = 104.5 kJ/kgmole-°C.

Pressure bar	Mass Density kg/m^3	Integral Term m^2/s^2	Mass Flux kg/s-m^2	Corrected Mass Flux kg/s-m^2	Vapor Fraction
30.0	434.9				
28.5	434.5	172	8069	8069	0
27.0	434.1	589	14900	14900	0
25.5	433.6	935	18751	18751	0
24.0	433.2	1281	21928	21928	0
22.5	432.8	1627	24692	24692	0
21.0	432.4	1974	27170	27170	0
19.5	330.7	2374	22786	27170	0.0367
18.0	248.5	2903	18936	27170	0.0791
16.5	192.2	3595	16294	27170	0.1194
15.0	151.0	4482	14294	27170	0.1581
13.5	119.6	5606	12662	27170	0.1954
12.0	94.8	7024	11242	27170	0.2318
10.5	74.9	8816	9943	27170	0.2675
9.0	58.4	11102	8707	27170	0.3029
7.5	44.7	14064	7493	27170	0.3384
6.0	33.0	18014	6267	27170	0.3747

Figure 2.6 describes the vapor and liquid mass fluxes for propane with changes in pressure. The x-axis is the downstream pressure in bar. This downstream pressure is equivalent to the shell-side pressure. Thus, Figure 2.6 can be interpreted as beginning from the left of the graph (at a downstream pressure of 6 bar), and shifting to the right as the tube rupture develops. If no PSV is present, this would continue until the downstream pressure is in equilibrium with the upstream pressure (30 bar). In addition to the x-axis, two y-axis are shown, one being the mass flux (kg/s-m^2) and the other being the vapor fraction. Between downstream pressures of 21 bar and 30 bar,

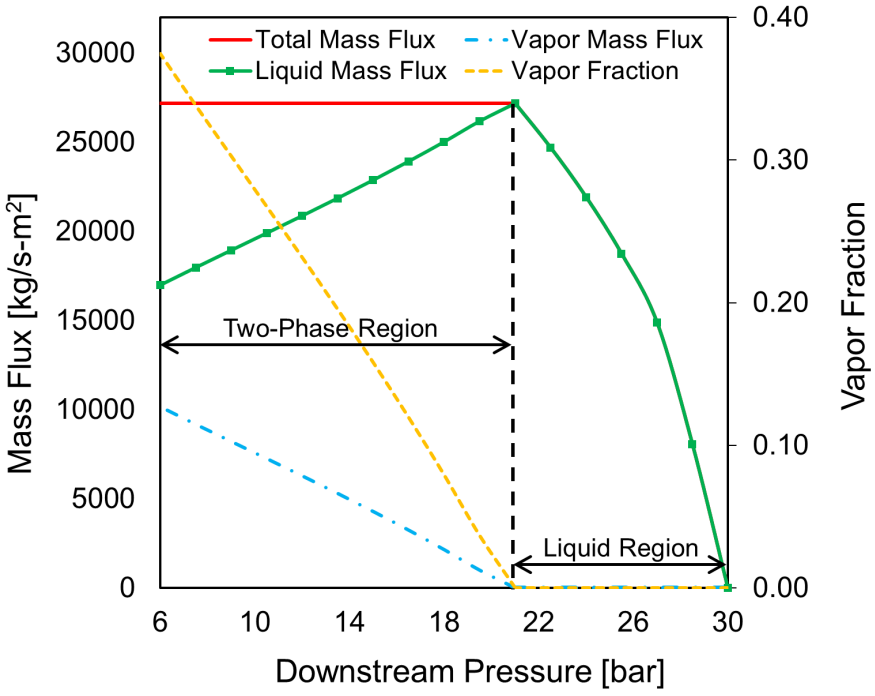

Figure 2.6: Tube-side mass flux vs. downstream pressure for propane with an initial pressure of 30 bar and initial temperature of 60 °C.

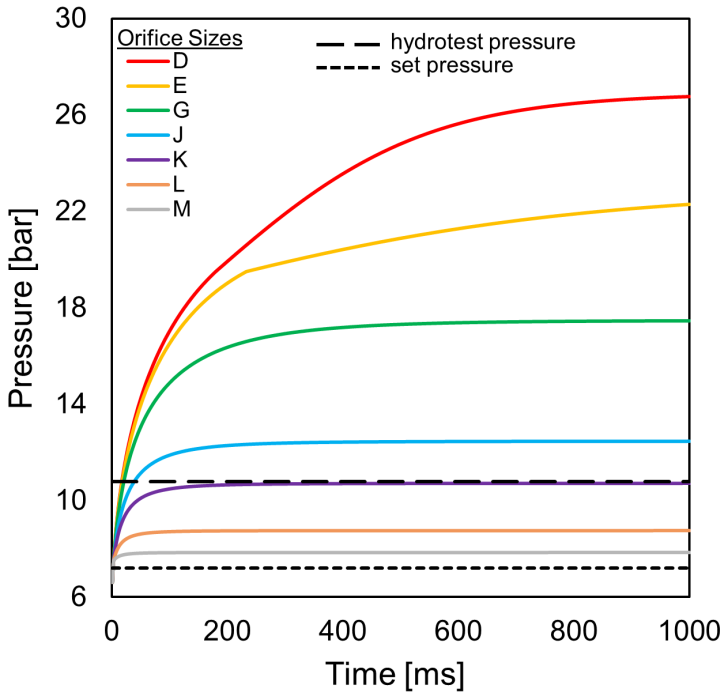

Figure 2.7: Shell-side pressure profiles for propane water systems for different PSV sizes.

the vapor fraction is zero. Between pressures 6 bar and 21 bar, the vapor fraction increases with decreasing downstream pressure. The vapor mass flux is generated by multiplying the total mass flux with the vapor fraction. Therefore, no vapor mass flux is present between the downstream pressures 21 bar and 30 bar.

The pressure profiles for the propane water system are shown in Figure 2.7. Compared to the previous two cases, this system requires roughly between 100 to 200 milliseconds before reaching pseudo steady state. A dotted line line at 10.8 bar represents the hydrotest pressure. The smallest PSV orifice size that does not exceed this pressure is K. One interesting feature of this system is that it functions as both a liquid-liquid and vapor-liquid tube rupture. In other words, as the tube rupture begins, the high pressure liquid flashes when exposed to the shell-side. This phase of the tube rupture is closely associated with a vapor-liquid rupture. Over time, pressure builds up and the amount of flashing decreases. Eventually, the liquid exiting the tube-side will fully remain a liquid in the shell-side, exhibiting characteristics similar to that of a liquid-liquid rupture. Orifice sizes D and E are both piece-wise functions since around 20 bar, the shell-side is entirely a liquid due to the high pressure.

2.15 Dimensionless Analysis of Tube Rupture

The severity of a tube rupture can be affected by a myriad of properties. These include the fluid's density, phase, pressure, and temperature. Exchanger properties such as the shell volume and tube diameter affect the flux and the rate of pressure increase. Lastly, pressure relief properties (e.g. valve size and opening times) affect the rate of fluid exiting the shell. To better understand the different parameters that can affect a tube rupture, properties were grouped together to form dimensionless numbers. The following numbers are proposed:

$$\tau = \frac{D_{tube}/D_c}{V_{shell}/V_c} \tag{2.19}$$

$$P_{ratio} = \frac{P_{tube}}{P_{shell}} \tag{2.20}$$

$$P_{max} = \frac{P(t)_{shell\ max}}{P_{shell\ design}} \tag{2.21}$$

$$\rho_{ratio} = \frac{\rho_{tube}}{\rho_{shell}} \tag{2.22}$$

τ in Equation 2.19 evaluates the size of the tube in relation to the exchanger shell. A larger tube diameter increases the severity of a tube rupture, while a larger shell volume slows the accumulation of pressure. For Equation 2.19, characteristic lengths of 1e-4 m and 1 m^3 for D_c and V_c were selected. The pressure ratio (Equation 2.20) is investigated because it is most likely the primary driver in the severity of a tube rupture. In fact, API 521 recommends a dynamic simulation when pressure differences exceed 1000 psi. The dimensionless number P_{max} in Equation 2.21 is the maximum pressure the shell-side experiences during a tube rupture divided by the shell design pressure. Lastly, the effects of the density ratio's (Equation 2.22) impact on tube rupture will be studied. A series of liquid-liquid tube rupture simulations were performed. In addition to the dimensionless numbers proposed, these simulations also measure the time it takes to reach the maximum pressure. The simulations contained ethylene-glycol and water on the tube and shell-side, respectively. In Figure 2.8, for a constant pressure ratio of 10, the maximum pressure was plotted against the density ratio (which was adjusted from 0.1 to 10). The dimensionless number, τ, was set at 13.3, 20, and 40. These values for τ are obtained from a 7.5 m^3 shell with 1 cm, 1.5 cm, and 3 cm diameter tubes, respectively.

From Figure 2.8, it is seen that the density ratio can significantly affect the ability of an exchanger to pressurize. A high density ratio reduces the ability of a tube rupture to result in overpressure. There exists for each system a density ratio threshold, in which no increase in pressure is present for this overpressure scenario. This relationship can be explained by thinking of an infinitely large density ratio. This would mean that the tube-side fluid is infinitely small and cannot pressurize the system. In mathematical terms, an infinite tube-side density forces the $\frac{dP}{dt}$ term in Equation 2.17 to zero. Alternatively, low density ratios were able to reach 10 bar regardless of the tube diameter and shell volume. When looking at the effects of τ, for the maximum pressure

a system experiences, a low value for τ results in a lower peak pressure. This is due to the fact that a low τ value results in a small tube diameter in relation to the shell volume. Thus, the cross sectional area of flow will be less, allowing a pressure relief device to mitigate the tube rupture's impact.

A second set of simulations were performed with the aim of studying the time it takes to reach the system peak pressure, P_{max}. This parameter is important to accurately capturing the severity of a tube rupture. A scenario that reaches peak pressure quickly may result in the shell-side failing due to the PSV not opening in time. This is in contrast to a longer time to reach P_{max}, which allows the PSV to open, limiting our concern to the maximum pressure the system reaches. The same pressure ratio (held constant at 10), density ratios, and values for τ as Figure 2.8 were used. The results are shown in Figure 2.9. All else being equal, it is preferred to have a tube rupture with a longer time to reach maximum pressure. For an equivalent density ratio, a faster time to reach P_{max} is observed for higher τ values. For a fixed τ, a higher density ratio increases the time it takes for a system to reach its maximum pressure. In addition, for all values of τ, the maximum pressure is achieved in less than 350 milliseconds.

The third set of dimensionless analysis simulations (Figure 2.10) study the impact the pressure ratio has on the severity of a tube rupture. The pressure ratio was varied, in increments of 2, from 2 bar to 10 bar. Two values of τ were used, 20 and 40. Similarly, three values for the density ratio were used, 0.49, 1.09, and 5.04. From Figure 2.10, a higher pressure ratio leads to a higher maximum pressure. This is not surprising. What is interesting to note, however, is how strong the density ratio can affect this peak pressure. As an example, a pressure ratio of 10 with a τ of 20, can yield a maximum pressure of 1.2 bar, 3 bar, or 7 bar. This wide variation in maximum pressure is due to the systems having density ratios of 5.04, 1.09, and 0.49, respectively. An increase in τ also shows an increase in a tube rupture's maximum pressure, although not as severe as the density ratio. A pressure ratio of 8, with a density ratio of 0.49 yields a maximum pressure of 5 bar (τ equal to 20) and 8 bar (τ equal to 40).

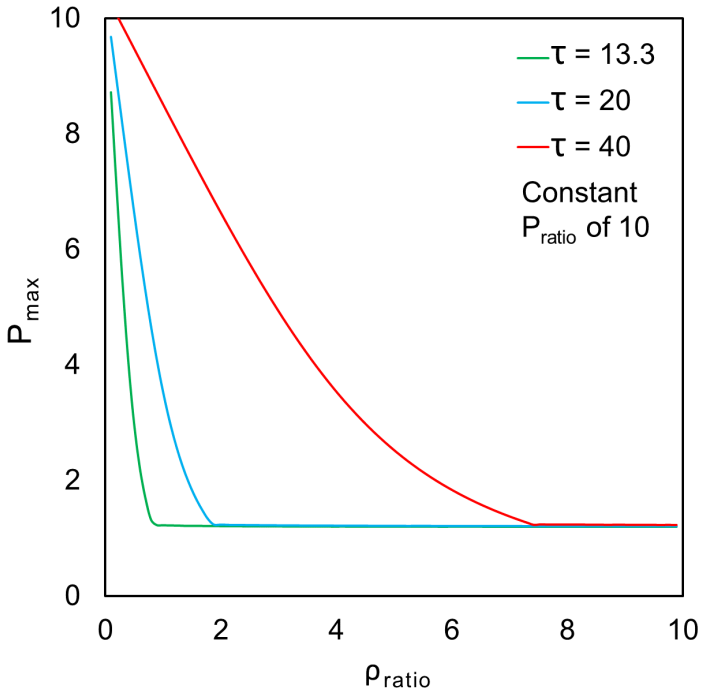

Figure 2.8: Shell-side peak pressure vs. density ratio for varying τ with a pressure ratio of 10.

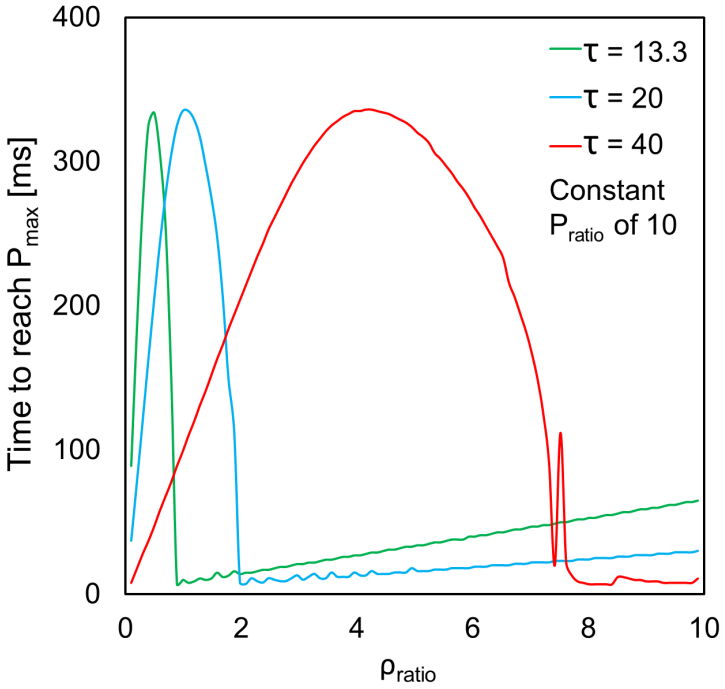

Figure 2.9: Time from initial rupture to peak pressure vs. density ratio for varying τ with a pressure ratio of 10.

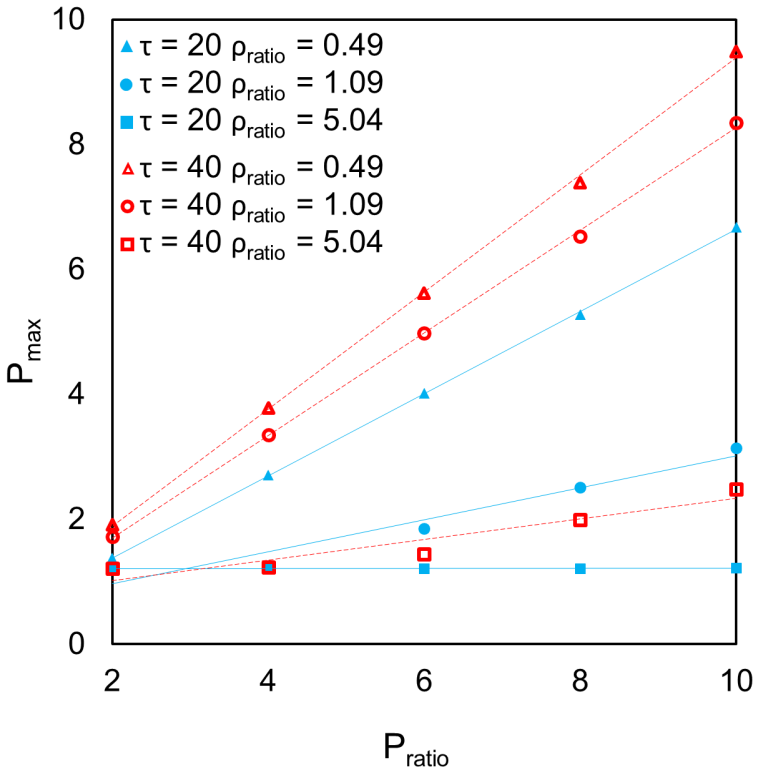

Figure 2.10: Shell-side peak pressure vs. pressure ratio relationship for varying τ and density ratios.

2.16 Mitigating Tube Rupture Scenarios

Depending on how far along in the lifecycle of an exchanger a plant is, mitigating the severity of tube rupture incidents can be done through one of several ways. First, one should flag exchangers that will have large differences in pressure. These exchangers are most susceptible to failure in the event of a tube rupture. For exchangers that are still in the design phase, increasing the strength of the exchanger is one way of mitigating the effects of a tube rupture. This design change does increase the investment cost of the exchanger, however. If the exchanger is upgraded to comply with the two-thirds rule, then a pressure relief valve would not be required for that system. Another strategy to mitigate tube ruptures is preventing exchanger tubes from failing in the first place. Nowadays, nondestructive technology such as eddy current testing can help estimate the remaining life of exchanger tubes [95]. This technology can be used to more frequently monitor exchangers

that are more susceptible to erosion and corrosion. Proactive prevention can also focus on detecting future operational hazards, such as by incorporating alarms within a process model [96].

One can also select an appropriately sized relief valve to handle a tube rupture scenario. For the ethylene-glycol water example in Section 4.1, without a pressure relief valve, the shell-side would be pressurized from 1 bar to 9 bar in 300 ms. However, by installing either relief valve sizes J or K, the shell-side would exhibit peak pressures of 1.43 and 1.27 bar, respectively. Moreover, while relief size K exhibits chattering during this tube rupture, relief size J does not. Furthermore, the results from this paper indicate vapor-liquid and flashing liquid-liquid ruptures to be more severe than liquid-liquid tube ruptures. Thus, more resources (e.g., increased design pressure and larger PSV orifice sizes) can be dedicated to these higher risk exchangers. Lastly, it was found that the density ratio and pressure ratio can significantly affect the ability of a shell to pressurize. As a result, systems with a high density ratio and low pressure ratio are preferred for this overpressure scenario.

3. HEAT EXCHANGER NETWORK SYNTHESIS WITH PROCESS SAFETY[1]

In process industries, pressure relief valves are commonly referred to as the last line of defense. Code requires that when a process fails, regardless of its built-in redundancies, there exists an independent protection system (e.g., pressure relief valve) powered by the medium it protects. [15] Therefore, correct pressure relief valve sizing is critical to ensure the protection of equipment, property, and life. Fortunately, for most overpressure scenarios, pressure relief standards set by API 521 help guide engineers on how to tackle various overpressure scenarios. For heat exchanger tube ruptures, an overpressure event that has been documented in industry, API 521 recommends a dynamic analysis be performed when there exist large differences in pressure. [40] However, a framework for dynamically modeling tube rupture scenarios is not given. A sketch of the tube rupture scenario is given in Figure 1.1. This scenario involves a heat exchanger with high pressure on the tube-side and low pressure on the shell-side. Exchanger tubes over time can weaken (shown as a zigzag stress pattern in Figure 1.1). If unnoticed or not replaced in time, this weak point may fail. High pressure tube-side fluid enters the shell-side, increasing the system pressure. At the set point, a pressure relief valve opens, venting shell-side fluid to the flare. With heat exchangers in the offshore industry having tube-side pressures into the hundreds of bar, dynamic modeling is critical to selecting an appropriate relief device. An additional benefit of accurately sizing overpressure scenarios via dynamic analysis is the potential to reduce the weight of equipment, lowering capital costs. [97] This is especially important in the offshore industry, where topside weight reduction is an important design criterion.

3.1 Introduction of a Safety Rating

In the event of a tube rupture, it is desired to determine how adequately an exchanger is protected from a tube rupture. The tube rupture scenario is a non-steady state process whereby the low

[1]This chapter was reprinted in whole or in part with permission from "Dynamic modeling of heat exchanger tube rupture" by Harhara, A., & Hasan, M. M, 2020. *BMC Chemical Engineering*, 2(1), 1-20, Copyright 2022 by Springer Nature.

pressure side is pressurized by the high pressure side. This pressurization can occur in a timespan as short as milliseconds. There exist simplified steady state calculations (also referred to as the the two-thirds rule) but transient calculations are considered more robust. Calculating the pressure at different time intervals yields a pressure profile. These are critical in allowing one to determine how long a pressure threshold has been exceeded and other important design questions. Ultimately, when compared to steady state calculations, the dynamic calculations more easily allow one to determine when the integrity of an exchanger will be compromised. Some common assumptions that simplify the calculations involved include modeling the tube rupture as a guillotine cut, ignoring the effects of adjacent equipment and piping, approximating relief valve response times as instantaneous, and that the shell side of the exchanger is homogeneous throughout the duration of this scenario [23].

To summarize the process of determining the severity of a single heat exchanger tube rupture, consider an exchanger with the properties of Table 3.2. For a detailed step-by-step procedure on how this is performed, the reader is referred to our previous work [98]. Appendix A lists the equations used in the dynamic tube rupture model. First, we take note of the system's phases. In this case, both sides are liquid, simplifying the complexity of this calculation. Constant entropy flashes from the tube side to the shell side are then performed, yielding the tube side mass flux for octane. Aspen Plus is used to determine the necessary thermodynamic properties, including the density and bulk modulus of each component. This information is then inputted into a shell pressurization equation. This equation, in effect a mass balance on an exchanger, also accounts for the effects of outflow via the PSV. The pressure profile is then determined from the start of the tube rupture, up until a pseudo steady state pressure is reached (at roughly 300 ms). From the pressure profile, the maximum pressure the system experiences is selected.

To quantify the severity of a tube rupture in an exchanger, we introduce a metric that accounts for overpressure safety. We refer to this metric as an exchanger's Safety Rating (SR). For a single heat exchanger, the safety rating can be described by Equation (3.1),

$$SR_{HE} = \frac{P_{design}}{P(t)_{max}} \times 100, \tag{3.1}$$

where SR_{HE} represents the safety rating of a single heat exchanger, P_{design} is the design pressure of the shell side, and $P(t)_{max}$ is the maximum transient shell side pressure that is experienced during a tube rupture. The benefit of the SR_{HE} metric is that it relates the severity of a tube rupture (in terms of the maximum pressure reached) with the design pressure of the shell. This allows a plant to specify a tolerance/threshold that is acceptable for their facility. An SR_{HE} score of 67 or above is considered to be adequate for a tube rupture. An SR_{HE} score of less than 67 may mean that a heat exchanger is inadequately designed for the possibility of overpressure from a tube rupture. Table 3.1 is a more comprehensive reference on how to interpret an SR_{HE} score. It should be noted that the SR_{HE} metric resembles that of the common industry rule-of-thumb known as the "two-thirds rule". Moreover, Table 3.1 lists an SR_{HE} score of 67 as the cutoff point for whether or not an exchanger is able to withstand a tube rupture. The difference between the SR_{HE} metric and the two-thirds rule is that the SR_{HE} metric is intended to use the maximum transient shell side pressure while the two-thirds rule only compares the design pressure and hydrotest pressure of the tube and shell sides, respectively. In addition, due to the fact that the SR metric requires the maximum transient shell side pressure, it may incorporate the use of a pressure relief device to increase its score (making the process safer). Thus, for determining the safety rating of an exchanger, it is entirely possible that an exchanger with a tube side pressure of 100 bar and a shell side pressure of 10 bar have an SR_{HE} score of 100. The way that an exchanger may obtain an SR_{HE} of 100 can be if it has a pressure relief valve adequately sized to handle the influx of incoming tube side fluid. The exchanger may also have a larger volume, smaller tube size, and many other design variations in order to obtain an SR_{HE} of 100.

The addition of using the SR_{HE} as a safety metric begs the question: why not instead calculate the risk of a tube rupture? Quantifying the risk for this scenario is a difficult task, primarily because little publicly available data exists on the probability of heat exchanger tube ruptures. This makes

Table 3.1: Interpretation guide for safety rating values. The higher the rating, the safer the tube rupture event. A safety rating of 67 signifies that the tube rupture does not exceed the hydrotest pressure (the boundary between the safe and unsafe region).

Safety Rating	Interpretation
100	Maximum transient shell side pressure experienced during tube rupture does not exceed the design pressure of the shell side.
>67	Maximum transient shell side pressure experienced during tube rupture exceeds the design pressure of the shell side, but does not exceed 1.5 times the design pressure of the shell side.
67	Maximum transient shell side pressure experienced during tube rupture equals 1.5 times the design pressure of the shell side.
<67	Maximum transient shell side pressure experienced during tube rupture exceeds 1.5 times the design pressure of the shell side.

risk calculations highly unreliable. The SR_{HE} metric does however indirectly measure the risk of a tube rupture. This is because the SR_{HE} metric incorporates the transient pressure in the shell side and compares it to its design pressure (the pressure that the equipment is rated for). For a tube rupture scenario that barely exceeds the shell's design pressure (interpreted as a high SR_{HE}), minimal impact to the exchanger is expected. However, for a tube rupture that greatly exceeds the shell's hydrotest pressure (interpreted as a low SR_{HE}), a catastrophic failure may occur.

This is then used to calculate the safety rating. For the liquid-liquid system in Table 3.2 with a K PSV orifice size, we determine the maximum transient shell side pressure to be 2.45 bar. Dividing the design pressure by this pressure, and multiplying by 100, yields a safety rating of 97. This safety rating is above the minimum 67 required for adequate protection in the event of a tube rupture. Thus, this system does not need any additional overpressure protection for this scenario.

Without considering the effects of a PSV, the maximum shell side pressure can reach 8 bar, the tube side operating pressure. Dividing the design pressure (2.4 bar) by the tube side operating pressure, and multiplying by 100, yields a safety rating of 30. This safety rating is significantly less than the minimum 67 required. Therefore, this shorthand simplified safety rating suggests

that a dynamic safety rating is more appropriate. Incorporating the PSV will reduce the maximum pressure the shell side experiences, increasing the system's safety rating.

This distinction between determining the safety rating using the simplified method, versus using a dynamic model, can result in an overly conservative exchanger design. The advantage of using a safety rating in the design of a heat exchanger is that we can compare the relative safety of different exchangers. This is critical as it allows the safety rating to be extended to heat exchanger networks.

Shell Side	
Fluid	Water
Operating Temperature	20 °C
Operating Pressure	2 bar
Shell Volume	10 m^3
PSV Set Pressure	2.4 bar
PSV Orifice	K
Design Pressure	2.4 bar
Hydrotest Pressure	3.6 bar
Tube Side	
Fluid	Octane
Operating Temperature	80 °C
Operating Pressure	8 bar
Tube Diameter	2 cm
No. Tubes	200

Table 3.2: Water Octane System Properties

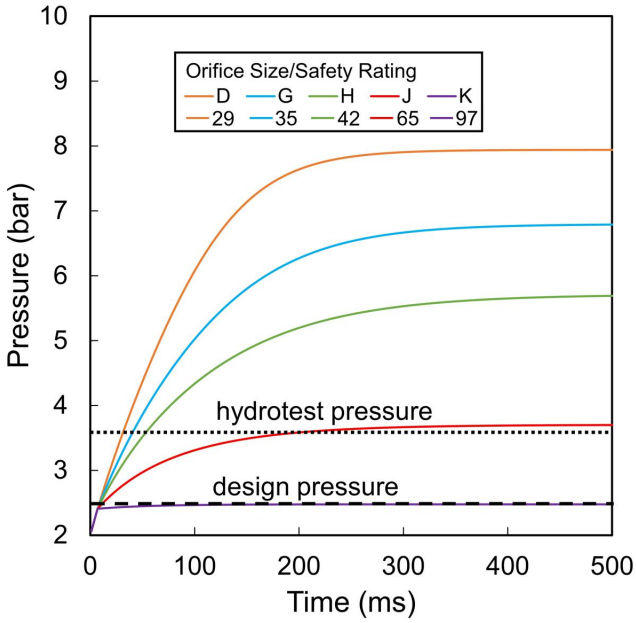

Figure 3.1: Impact of Different PSV Orifice Sizes on Water Octane System

A tube rupture event may occur to any shell and tube exchanger present in a plant. Factors such as the age of tubes, erosion, corrosion, and vibration all affect the life of a tube [80, 81, 82, 83, 84]. For the purpose of designing a safe process, as long as the potential for a high pressure tube entering the shell side exists, a tube rupture should be assumed to occur. This is in line with API 521's recommendation that a heat exchanger tube rupture should be considered a remote but possible

event [40]. Consequently, this also means tube ruptures must be considered in heat exchanger networks. To demonstrate this, consider the stream information shown in Table 3.3. There exist two hot streams and two cold streams, each with their own inlet and outlet temperature. A hot utility and cold utility and their respective costs are also included. A pressure associated with the hot and cold streams is also included. This pressure value will become necessary when evaluating the possibility of a tube rupture to negatively affect the safety of a HEN. We wish to design a HEN with the minimal annual operating cost. However, we also wish to protect the system from exposure to tube rupture events. Following the work of Yee and Grossmann (1990), the SYNHEAT GAMS model is used to generate the optimal HEN [35]. The optimal HEN was obtained via the BARON solver. A HEN diagram of the optimal solution is presented in Figure 3.2a. The optimal solution selects three exchangers to recover energy between streams H1-C1, H2-C1, and H1-C2. A heater with a duty of 491 kW raises the temperature of C1 from 617 K to 650 K. A cooler with a duty of 168 kW is used to cool stream H1 from 387 K to 370 K. A second cooler with a duty of 1973 kW cools stream H2 from 469 K to 370 K. The annual cost for this network is $154,997, the lowest possible cost for this stream information.

Table 3.3: Example HEN stream information. The pressure for each stream is included in order to be able to analyze the potential for a tube rupture. The safety rating is calculated for each exchanger in Figure 3.2b.

Component	Stream	Tin	Tout	P	FCp	Cost
	K	K	bar	kW K^{-1}	\$ $kW^{-1}yr^{-1}$	
Dodecane	H1	650	370	22	10	-
Benzene	H2	590	370	100	20	-
Ethylene Glycol	C1	410	650	85	15	-
Cyclohexane	C2	350	440	15	13	-
Steam	HU	680	680	-	-	80
Cooling Water	CU	300	320	-	-	15

This optimal solution however does not consider safety criteria when deciding on a match between hot streams and cold streams. More specifically, this particular HEN configuration puts the potential severity of a tube rupture very high, assuming there are no further overpressure protection measures. For example, exchanger E-101 in Figure 3.2 matches streams H1 and C1. These streams have a stream pressure of 22 bar and 85 bar, respectively. In heat exchanger design, the tube side is traditionally the higher pressure fluid [99, 100]. Thus, this exchanger will have C1 on the tube side, and H1 on the shell side. If a tube rupture occurred, and no pressure safety valve (PSV) is attached to the shell side, the shell side would pressurize until it is in equilibrium with the tube side (85 bar). Because shell and tube side of an exchanger frequently operate under different conditions (e.g., different pressures, different fluid in service, etc), they typically have different pressure ratings. When given an operating pressure, a plant may choose an equipment to have a pressure rating 10-20% above this pressure. Therefore, for a 22 bar operating pressure, the shell side of an exchanger may be rated to 25 bar. Thus, if such a shell were to be pressurized to 85 bar in the event of a tube rupture, this would almost certainly result in the failure of the shell side. This exchanger failure has the potential to result in a plant shutdown, downtime, environmental damage, and may harm operators nearby.

For Figure 3.2, the safety for exchanger E-101 has been evaluated. However, this HEN also resulted in two further exchangers being built, E-102 and E-103. For E-102, energy is recovered between streams H2 and C1. The pressure for these streams is 100 bar and 85 bar, respectively. For exchanger E-102, H2 would be located on the tube side and C1 would be located on the shell side. Similar to the previous exchanger, this design choice would be due to H2 having a higher pressure than C1. If a heat exchanger tube were to fail for E-102, the shell side would eventually pressurize to 100 bar. Once again, this assumes that no PSV, rupture disc, or other overpressure mitigation system is in place. Unlike exchanger E-101 however, E-102 can be considered a safe exchanger when evaluating the consequences tube rupture event. The primary reason is that the difference in pressure between the two sides is not as large as was the case for E-101. For E-102's shell side having an operating pressure of 85 bar, its pressure rating will likely be around 100 bar. This

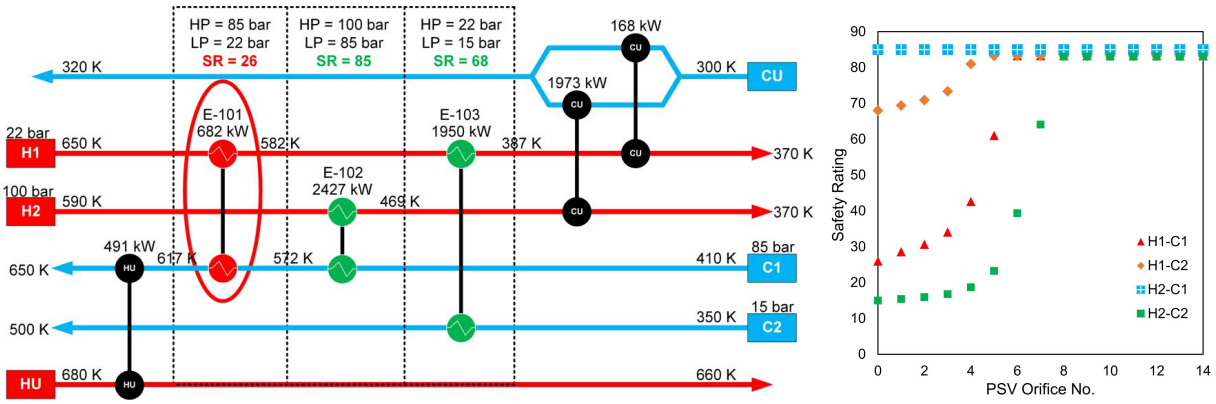

(a) Optimal network via SYNHEAT model

(b) Safety rating for all possible exchanger matches in 3a

Figure 3.2: Optimal network via SYNHEAT. For the hot and cold streams present, the SYNHEAT model yielded this network. The proposed configuration was then analyzed for exposure to a tube rupture event. The analysis performed was the simplified safety rating calculation. This calculation only considers the pressure of the streams and assumes no additional protection devices exist. In the figure, the high pressure (HP) and low pressure (LP) stream for each exchanger is identified and displayed alongside the safety rating. The HP and LP streams will occupy the tube and shell side of the exchanger, respectively. The safety ratings for exchangers E-101, E-102, and E-103 are 26, 85, and 68, respectively. The safe limit is greater than or equal to 67. The two exchangers, E-102 and E-103 (highlighted in green), are safe during a tube rupture. The exchanger E-101 (highlighted in red) with a safety rating of 26, however, would fail unless other mitigation measures were in place.

would be able to withstand the tube side pressure. Furthermore, even if the the shell side pressure rating were to be less than 100 bar (e.g., 90 bar), the shell side would still be able to tolerate the maximum tube side pressure of 100 bar. This is because in pressure vessel design, the pressure rating is not the maximum pressure a vessel can withstand. Instead, the pressure rating serves as the maximum pressure a vessel can handle under normal operation. To account for process upsets, a safety margin exists between the pressure rating and the pressure that an equipment will fail [101]. The limits of how much a pressure vessel can exceed its pressure rating is governed by pressure vessel codes. For the United States, these limits are specified under ASME Boiler and Pressure Vessel Code, Section VIII [85]. Because a tube rupture is not considered normal operation, the pressure rating can be exceeded for a short duration of time. The amount that this can be exceeded is up to the hydrotest pressure. This pressure is the maximum pressure a vessel is tested at before

it is put in service. This pressure is usually set 50% above the design pressure.

Similar to E-102, E-103 is also protected in the event of a tube rupture. The low and high pressure side for E-103 are 15 bar and 22 bar, respectively. Conventional heat exchanger design suggests the hydrotest pressure for the shell side of E-103 would be 50% above 15 bar, or 22.5 bar. Thus, if a tube rupture occurred and the low pressure side was pressurized up to the maximum pressure possible (22 bar), this exchanger would be protected from this overpressure event. This HEN demonstrates that the consequence of a tube rupture should be evaluated at every exchanger. Furthermore, it can be seen that while a stream in one exchanger may not be exposed to a tube rupture, that same stream in a different exchanger may result in a tube rupture (e.g., H1 in E-101 versus H1 in E-103).

For any process design decision, there will always exist trade-offs. Examples of these in the field of process safety may include: evaluating the cost of installing scrubbers versus paying a fine for exceeding allowable emissions; reducing the size of inventory to reduce the worst case scenario and lower storage costs, but this will come at the expense of reducing operational flexibility. Similarly, the equipment pressure can be reduced, but at the expense of less throughput. Plants also have the option to adjust their maintenance schedules. Since these exchanger properties can be quantified in terms of cost, these tradeoffs can be represented through the use of a Pareto curve. A heat exchanger's capital costs are directly related to the shell and tube design pressures, which indicate what pressures the heat exchanger is able to withstand. Thus, a heat exchanger with a low cost on the Pareto curve represents a lower safety rating, and vice versa. Similarly, one can expect there to be a second Pareto curve, which includes the effects of adding a pressure safety valve (PSV). When deciding on how to increase the safety of an exchanger, there are two main ways to accomplish this. The first is by physically changing the exchanger's properties (e.g., design pressure). The second is by increasing the relief capacity of the system. When comparing the economics between these decisions, the latter is a significantly more cost effective approach to increasing an exchanger's safety. In the following sections, the tube-rupture safe HENS optimization formulation is presented.

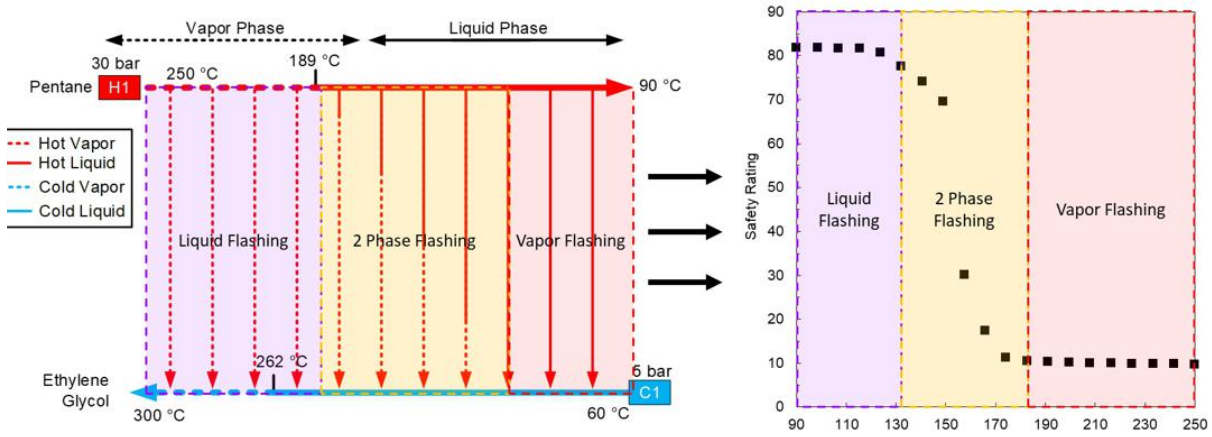

Figure 3.3: On the left, pentane is shown flashing from 30 bar to 5 bar. The pentane stream enters as a vapor and condenses at 189 °C. Note that depending on where pentane begins to flash, it will end up as either a liquid, two-phase, or vapor. Using this knowledge, on the right, a safety rating temperature profile is generated. This demonstrates the importance of properly determining which temperature the tube rupture will occur at.

3.2 Tight Piecewise Linear Underestimation of Safety Rating

One challenge in incorporating the safety rating into a HEN synthesis model lies in the fact that the exchanger temperature is not known apriori. Rather, exchanger temperatures are determined once the optimization model converges. For fluids that enter and exit as a liquid, this does not raise safety concerns. However, for fluids undergoing a phase change, the safety rating can vary significantly with changes in the fluid's phase. An example of this is shown in Figure 3.3. From the figure, one can see that while pentane is a liquid, its safety rating easily exceeds the safe SR threshold of 67. However, between temperatures 130 °C and 189 °C, the SR changes from a maximum of 78 to a minimum 12. Thus, a safe HEN synthesis model must be able to underestimate the safety rating. To achieve this, we propose a piecewise linear underestimation of the safety rating based on the work of Rebennack and Kallrath (2015) [39].

This underestimation formulation must adhere to a few principles: 1) That the temperature values of our breakpoints are bounded to the interval $[T_+, T_-]$. 2) That a minimum of two breakpoints exist for each system. 3) That there exist breakpoints at our endpoints, T_+ and T_-. 4) That the temperature value of each breakpoint must be successive. In other words, the temperature value

of one breakpoint cannot increase and subsequently decrease for a future breakpoint. 5) That a continuous piecewise linear function across all breakpoints, our safety rating, must lie within an pre-specified error. From this, the model is given below along with a brief summary at the end.

Indices:

$b =$ index for breakpoints 1, ..., B

$i =$ index for grid points 1, ..., I

Sets:

$\mathbb{B} = \{b \,|\, b \text{ denotes the existence of a breakpoint}\}$

$\mathbb{I} = \{i \,|\, i \text{ denotes the location of the grid point}\}$

Parameters:

$t_i =$ temperature at grid point i

$T_- =$ lower bound temperature for interval

$T_+ =$ upper bound temperature for interval

$1/M =$ machine precision error (e.g., 10^{-3})

$\delta =$ allowable error between approximation and input data

$I =$ total number of grid points

$B =$ maximum number of breakpoints

Variables:

$T_b =$ temperature at breakpoint b

$$\chi_b = \begin{cases} 1 & \text{if breakpoint } b \text{ exists,} \\ 0 & \text{otherwise} \end{cases}$$

$$\chi_{bi} = \begin{cases} 1 & \text{if breakpoint } b \text{ exists at grid point } i, \\ 0 & \text{otherwise} \end{cases}$$

$l_{bi} =$ line at grid point i, between temperatures T_b and T_{b-1}

$l_i =$ piecewise linear function combining l_{bi} for all χ_{bi}

$w_b =$ distance between T_b and T_{b-1}

Equations

$$t_i = \frac{i}{I}(T_+ - T_-) + T_- \tag{3.2}$$

$$z^* = \min \sum_{b \in \mathbb{B}} \chi_b \tag{3.3}$$

$$T_{b-1} \leq T_b, \ \forall b \in \mathbb{B} \tag{3.4}$$

$$T_b \geq T_- + (T_+ - T_-)(1 - \chi_b), \ \forall b \in \mathbb{B} \tag{3.5}$$

$$T_b - T_{b-1} \geq \frac{1}{M}\chi_b, \ \forall b \in \mathbb{B} \tag{3.6}$$

$$T_b - T_{b-1} \leq (T_+ - T_-)\chi_b, \ \forall b \in \mathbb{B} \tag{3.7}$$

$$w_b = T_b - T_{b-1} + (T_+ - T_-)(1 - \chi_b), \ \forall b \in \mathbb{B} \tag{3.8}$$

$$\sum_{b \in \mathbb{B}} \chi_{bi} = 1, \ \forall i \in \mathbb{I} \tag{3.9}$$

$$T_{b-1} - (T_+ - T_-)(1 - \chi_{bi}) \leq t_i \leq T_b + (T_+ - T_-)(1 - \chi_{bi}), \ \forall b \in B, \ \forall i \in \mathbb{I} \tag{3.10}$$

$$l_{bi} = \phi(T_{b-1}) + \frac{\phi(T_b) - \phi(T_{b-1})}{w_b}(t_i - T_{b-1}), \ \forall b \in B, \ \forall i \in \mathbb{I} \tag{3.11}$$

$$l_i = \sum_{b \epsilon B} l_{bi}\chi_{bi}, \ \forall i \in \mathbb{I} \tag{3.12}$$

$$|l_i - SR(t_i)| \leq \delta, \ \forall i \in \mathbb{I} \tag{3.13}$$

$$T_b \in [T_-, T_+], \ \chi_b \in \{0, 1\}, \ \chi_{bi} \in \{0, 1\}, \ w_b \geqslant \frac{1}{M}, \tag{3.14}$$

$$s_b \in [-\delta, +\delta],\ l_b \text{ free},\ l_{bi} \text{ free},\ \forall b \in \mathbb{B},\ \forall i \in \mathbb{I} \tag{3.15}$$

As shown in Equation (3.2), t_i represents the temperature at grid point i. t_i spans across the maximum and minimum temperatures, T_+ and T_- respectively. I represents the total number of grid points. The objective of this formulation is to determine the minimum number of breakpoints whose piecewise linear function guarantees an overestimation, underestimation, or approximation within a specified tolerance. We assign the binary variable χ_b to represent the existence of a breakpoint at b, contained within the set $\mathbb{B}$. This gives us the objective function, Equation (3.3). The logical constraint, Equation (3.4), ensures that the temperature at each breakpoint, T_b, is successive. The next logical constraint, Equation (3.5), applies the lower bound T_- to T_b when χ_b is one (i.e., when a breakpoint at b exists). If instead χ_b is zero, T_b is given the lower bound, T_+. With Equation (3.6), two successive breakpoints must be at least a minimum distance apart, represented as $\frac{1}{M}$. In Equation (3.7), the difference between two successive breakpoints cannot exceed the range of the temperature interval, $[T_+, T_-]$. In Equation (3.8), the temperature difference between two breakpoints is represented by w_b. For each grid point, i, Equations (3.9) and (3.10) require that t_i shall be in between two breakpoints, T_{b-1} and T_b. This is needed as the piecewise linear approximation will be compared to the original grid point. Between each two breakpoints, the line segment between l_{bi} can be expressed by Equation (3.11). All line segments are then grouped into a single piecewise linear function by Equation (3.12). Finally, the difference between the piecewise linear function and the original function must be within a specified tolerance, delta, for all grid points, i, represented by Equation (3.13). This ultimately yields the minimum number of breakpoints, given a tolerance. An example of this formulation is shown in Figure 3.4 where the sample function, x^2, is overestimated, underestimated, and approximated between an x_b of 0 and 20.

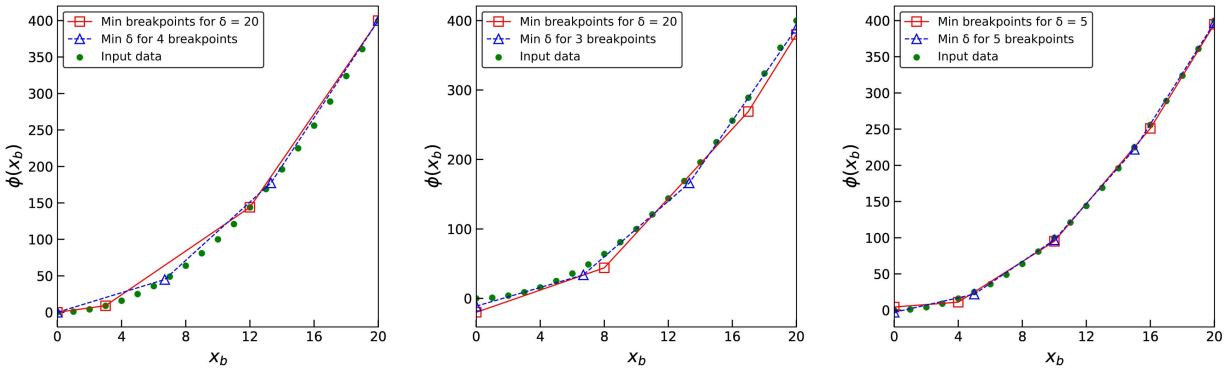

(a) Overestimation, x^2 (b) Underestimation, x^2 (c) Approximation, x^2

Figure 3.4: Over, under, and delta approximations of x^2. The input data (i.e., the function x^2) is shown in green. The minimum breakpoints needed to achieve δ (specified on each subplot) are shown. (3.4a) Four breakpoints are needed to overestimate x^2, given a δ of 20. (3.4b) Four breakpoints are needed to underestimate x^2, given a δ of 20. (3.4c) Five breakpoints are needed to approximate x^2, given a δ of 5.

3.3 MINLP for HENS Incorporating Process Safety

From the formulation in Section 3, one is able to conservatively underestimate the safety rating across a range of temperatures. Since HENs take advantage of different stream temperatures to capture energy savings, the safety rating can now be determined for any location in the HEN superstructure. This section presents the formulation for developing a safe HEN. The design of a heat exchanger network that incorporates the safety rating can be described through the following optimization problem: given a set of performance requirements for a heat exchanger network (flow rate, temperature, etc.), design a network with the least total annual cost while ensuring the safety rating exceeds a specified threshold. Specifically, we now present an extended SYNHEAT model with consideration of minimum safety rating for selected heat exchangers:

Indices:

$i =$ index for hot process streams

$j =$ index for cold process streams

$k =$ index for temperature locations

$l =$ index for standard PSV size 1,...,15

$r =$ index for temperature regions

Sets:

$HP =$ hot process streams

$CP =$ cold process streams

$HU =$ hot utility

$CU =$ cold utility

$ST =$ stages

$\mathbb{L} = \{l \mid l \text{ is a standard PSV size}\}$

$\mathbb{R} = \{r \mid r \text{ is a temperature region}\}$

Parameters:

$CCU =$ cold utility per unit cost

$CHU =$ hot utility per unit cost

$TIN =$ inlet temperature

$TOUT =$ outlet temperature

$F =$ heat capacity flow rate

$NOK =$ total number of stages

$U =$ overall heat transfer coefficient

$C =$ area cost coefficient

$CF =$ fixed exchanger cost

$B =$ area cost exponent

$\Omega =$ heat exchange uppper bound

$\Gamma =$ temperature difference upper bound

$SR_{min} =$ minimum exchanger safety rating

$SRm_{ijlr} =$ slope of temperature-safety rating underestimation for exchanger (i, j) with PSV size l at temperature region r

$SRb_{ijlr} =$ intercept of temperature-safety rating underestimation for exchanger (i, j) with PSV size l at temperature region r

$A_{PSV,ijl} =$ orifice area for exchanger (i, j) with PSV l

$C_{PSV} =$ fixed coefficient used in PSV power-sizing model

$B_{PSV} =$ fixed exponent used in PSV power-sizing model

$t_{i,r}^{lower} =$ lower bound temperature for hot stream i at temperature region r

$t_{i,r}^{upper} =$ upper bound temperature for hot stream i at temperature region r

Variables:

$$z_{ijk} = \begin{cases} 1 & \text{where exchanger } (i, j, k) \text{ exists,} \\ 0 & \text{otherwise} \end{cases}$$

$$zcu_i = \begin{cases} 1 & \text{where cooler } (i) \text{ exists,} \\ 0 & \text{otherwise} \end{cases}$$

$$zhu_j = \begin{cases} 1 & \text{where heater } (j) \text{ exists,} \\ 0 & \text{otherwise} \end{cases}$$

$q_{ijk} =$ exchanger duty

$qcu_i =$ cooler duty

$qhu_j =$ heater duty

$dt_{ijk} =$ approach temperature

$dtcu_i =$ approach temperature between cold utility and stream i

$dthu_j =$ approach temperature between hot utility and stream j

$t_{ik} =$ hot stream temperature i at end of stage k

$t_{jk} =$ cold stream temperature j at end of stage k

$SR_{ijk} =$ safety rating for exchanger (i, j) in stage k

$sr_{ijk} =$ safety rating region for exchanger (i, j) in stage k

$A^0_{PSV,ijk} =$ PSV area for exchanger (i, j) in stage k

$$y_{ijl} = \begin{cases} 1 & \text{if PSV } l \text{ exists for stream match } (i, j), \\ 0 & \text{otherwise} \end{cases}$$

$th_{ik} =$ temperature of hot stream i in stage k

$tr_{ikr} =$ temperature of hot stream i in stage k in temperature region r

$$zr_{ikr} = \begin{cases} 1 & \text{if hot stream } i \text{ in stage } k \text{ is assigned temperature region } r, \\ 0 & \text{otherwise} \end{cases}$$

Objective function:

$$\begin{aligned}
&\min \sum_{i \in HP} CCUqcu_i + \sum_{j \in CP} CHUqhu_j + \sum_{i \in HP} \sum_{j \in CP} \sum_{k \in ST} CF_{ij} z_{ijk} \\
&+ \sum_{i \in HP} CF_{CU,i} zcu_i + \sum_{j \in CP} CF_{HU,j} zhu_j \\
&+ \sum_{i \in HP} \sum_{j \in CP} \sum_{k \in ST} C_{ij}[q_{ijk}/(U_{ij}[(dt_{ijk})(dt_{ijk+1})(dt_{ijk} + dt_{ijk+1})/2]^{1/3})]^{B_{ij}} \\
&+ \sum_{i \in HP} C_{CU,i}[qcu_i/U_{CU,i}[dtcu_i(TOUT_i - TIN_{cu}) \times \frac{dtcu_i + (TOUT_i - TIN_{cu})}{2}]^{1/3}]^{B_{CU,i}} \\
&+ \sum_{j \in CP} C_{HU,j}[qhu_j/U_{HU,j}[dthu_j(TIN_{HU} - TOUT_j) \times \frac{dthu_i + (TIN_{HU} - TOUT_j)}{2}]^{1/3}]^{B_{HU,j}} \\
&+ \sum_{i \in HP} \sum_{j \in CP} \sum_{k \in ST} C_{PSV} {A^0_{PSV,ijk}}^{B_{PSV}} z_{ijk} \qquad (3.16)
\end{aligned}$$

Constraints:

$$(TIN_i - TOUT_i)F_i = \sum_{k \in ST} \sum_{j \in CP} q_{ijk} + qcu_i \quad i \in HP \qquad (3.17)$$

$$(TOUT_j - TIN_j)F_j = \sum_{k \in ST} \sum_{i \in HP} q_{ijk} + qhu_j \quad j \in CP \qquad (3.18)$$

$$(t_{i,k} - t_{i,k+1})F_i = \sum_{j \in CP} q_{ijk} \qquad k \in ST, \quad i \in HP \qquad (3.19)$$

$$(t_{j,k} - t_{j,k+1})F_j = \sum_{i \in HP} q_{ijk} \qquad k \in ST, \quad j \in CP \qquad (3.20)$$

$$TIN_i = t_{i,1} \qquad i \in HP \qquad (3.21)$$

$$TIN_j = t_{j,NOK+1} \qquad j \in CP \qquad (3.22)$$

$$t_{i,k} \geq t_{i,k+1}, \qquad k \in ST, \quad i \in HP \qquad (3.23)$$

$$t_{j,k} \geq t_{j,k+1}, \qquad k \in ST, \quad j \in CP \tag{3.24}$$

$$TOUT_i \leq t_{i,NOK+1}, \qquad i \in HP \tag{3.25}$$

$$TOUT_j \geq t_{j,1}, \qquad j \in CP \tag{3.26}$$

$$(t_{i,NOK+1} - TOUT_i)F_i = qcu_i, \qquad i \in HP \tag{3.27}$$

$$(TOUT_j - t_{j,1})F_j = qhu_j, \qquad j \in CP \tag{3.28}$$

$$q_{ijk} - \Omega z_{ijk} \leq 0, \qquad i \in HP, \quad j \in CP, \quad k \in ST \tag{3.29}$$

$$qcu_i - \Omega zcu_i \leq 0, \qquad i \in HP \tag{3.30}$$

$$qhu_j - \Omega zhu_j \leq 0, \qquad j \in CP \tag{3.31}$$

$$z_{ijk}, zcu_i, zhu_j = 0, 1 \tag{3.32}$$

$$dt_{ijk} \leq t_{i,k} - t_{j,k} + \Gamma(1 - z_{ijk}) \qquad i \in HP, \quad j \in CP, \quad k \in ST \tag{3.33}$$

$$dt_{ijk+1} \leq t_{i,k+1} - t_{j,k+1} + \Gamma(1 - z_{ijk}) \qquad i \in HP, \quad j \in CP, \quad k \in ST \tag{3.34}$$

$$dtcu_i \leq t_{i,NOK+1} - TOUT_{CU} + \Gamma(1 - zcu_i) \qquad i \in HP \tag{3.35}$$

$$dthu_j \leq TOUT_{HU} - t_{j,1} + \Gamma(1 - zcu_i) \qquad j \in CP \tag{3.36}$$

$$dt_{ijk} \geq \epsilon \qquad j \in CP \tag{3.37}$$

$$A^0_{PSV,ijk} = \sum_{l \in L} A_{PSV,ijl}\, y_{ijl} \qquad i \in HP, \quad j \in CP, \quad k \in ST \tag{3.38}$$

$$\sum_{l \in L} y_{ijl} = 1 \qquad i \in HP, \quad j \in CP \tag{3.39}$$

$$SR_{ijk} \geq SR_{min}\, z_{ijk} \qquad i \in HP, \quad j \in CP, \quad k \in ST \tag{3.40}$$

$$th_{ik} = \sum_{r \in R} tr_{ikr} zr_{ikr} \qquad i \in HP, \quad k \in ST \tag{3.41}$$

$$tr_{ikr} \leq \sum_{l \in L} \sum_{j \in CP} t_{ir}^{upper} zr_{ikr} \qquad i \in HP, \quad k \in ST, \quad r \in \mathbb{R} \tag{3.42}$$

$$tr_{ikr} \geq \sum_{l \in L} \sum_{j \in CP} t_{ir}^{lower} zr_{ikr} \qquad i \in HP, \quad k \in ST, \quad r \in \mathbb{R} \tag{3.43}$$

$$\sum_{r \in R} zr_{ikr} = 1 \qquad i \in HP, \quad k \in ST \tag{3.44}$$

$$sr_{ijk} = \sum_{l \in L} \sum_{r \in R} (SRm_{ijlr} y_{ijl}) tr_{ikr} zr_{ikr} + \sum_{l \in L} \sum_{r \in R} (SRb_{ijlr} y_{ijl}) zr_{ikr} \; i \in HP, \; j \in CP, \; k \in ST \tag{3.45}$$

$$SR_{ijk} = \sum_{r \in R} sr_{ijk} zr_{ikr} \qquad i \in HP, \quad j \in CP, \quad k \in ST \tag{3.46}$$

The SYNHEAT model is integrated with our safety rating model using the equations above. More specifically, dynamic tube rupture simulations which yield the severity of each overpressure event are performed for all exchanger matches. For each simulation, the continuous piecewise linear formulation shown in the previous section gives us the safety rating as a function of temperature. To account for safety within the HEN model, Equations (38) to (46) are added. Ultimately, this model will yield the minimum cost HEN that meets our safety criteria. One important feature is the model's ability to handle safety liquid-liquid, vapor-liquid, and flashing liquid-liquid systems for pure component streams. For each exchanger, the model will also determine the appropriately sized PSV in order to meet our safety rating of 67.

A brief summary of the modifications applied to the SYNHEAT model each step is given here. First, the index, l, is added to represent the 15 standard PSV sizes. As a point of clarification, an l of one represents no PSV in our system (e.g., an exchanger without any external relief device attached). The values for l anywhere from two to 15 correspond to PSV sizes D to T. The index, r, is used to represent the different temperature regions for a given exchanger match. In practice, this r is the temperature breakpoint location obtained from the underestimation of safety ratings across an exchanger's temperature region. A parameter representing the minimum exchanger safety rating, SR_{min}, is included. As previously discussed, a value for SR_{min} greater than or equal to 67 is considered adequate protection in the event of a tube rupture. Using AspenTech HYSYS and Matlab, tube rupture simulations are performed for every possible hot and cold stream combina-

tion. For more details on how this is performed, we refer the reader to our previous work [98]. The maximum pressure of every stream combination is used to calculate the safety rating as a function of temperature and ultimately inputted as parameters SRm_{ijlr} and SRb_{ijlr}. These two parameters help to represent the safety rating as a piecewise linear function. More importantly, they also serve as a underestimation of the safety rating, vital to ensuring a conservative exchanger design. If the slopes and intercepts of the piecewise linear function were not inputted as parameters, this would require reformulating the optimization model from an MINLP problem to an MINLDP problem since the tube rupture problem itself requires a robust dynamic simulation. Two other parameters inputted that are related to this piecewise formulation are $t_{i,r}^{lower}$ and $t_{i,r}^{upper}$. These are the temperatures themselves that serve as the breakpoints for the piecewise linear underestimator.

A brief description of Equations (38) to (46) is as follows. Equation (38) assigns the orifice area of PSV l to the variable $Area_{ijk}$. Equation (39) limits the selection of PSVs so that no more than one PSV can exist on any given hot or cold stream exchanger. Because Equation (39) includes an l of 1, this equation is able to select no PSV when appropriate. Note that the only time this would be the case is when an exchanger is already protected from a tube rupture without the need for a PSV. Equation (40) requires that the safety rating of each exchanger be equal to or greater than the minimum safety rating (typically 67). Equation (41) takes the hot stream temperature of stream i at stage$k$ from the existing HEN model th_{ik} and assigns it equal to sum over $\mathbb{R}$ of the product of $tr_{ikr}zr_{ikr}$. Effectively, this assigns only one hot temperature region to th_{ik}. This is because zr_{ikr} is limited to one over $\mathbb{R}$ by Equation (44). For Equations (42) and (43), the temperature of each hot region tr_{ikr} is bounded between the upper and lower region temperatures obtained by the underestimator. The previous equations are all posed to solve Equation (46). This equation calculates the safety rating for each exchanger. Lastly, the modified objective function is given by Equation (3.16). This objective function includes the cost of the PSV as well as its area. A PSV may or may not exist for each exchanger in streams (i, j). With the formulation presented above, two case studies demonstrating these principles are presented in the next section.

3.4 Results and Discussion

3.4.1 Case Study 1

In Section 3.1, we applied process safety principles to a single heat exchanger. Using the models from Section 3 and 4, we can apply the same logic to heat exchanger networks. Heat exchangers are one of the most popular, if not the most popular, equipment in plants. Within heat exchangers, shell and tube heat exchangers are the most popular types of exchangers. Thus, by the sheer number of exchangers in a plant, designing for tube rupture scenarios should not be overlooked. To show more advanced case studies leveraging the safety rating, Cases 1 and 2 use the HENS model proposed by Ponce Ortega et. al (2008) [38]. For other scenarios, a different HENS model may also be used, provided that one can still accurately capture the safety rating for different conditions across the HEN. The stream summary for Case 1 is shown in Table 3.4. In total, four streams must be analyzed, two hot and two cold. The problem contains different types of hot and cold streams. HPS1, HPS2, and HPS3 represent streams that require sensible heat, latent heat, and a combination of both, respectively. For cold streams, CPS1, CPS2, and CPS3 follow a similar logic. The inlet and outlet temperatures are represented in Kelvin. The heat capacity and heat of vaporization multiplied by the flow rate are given as FCp and Fλ, respectively. Both the heat capacity and heat of vaporization were obtained from HYSYS. The bubble/dew point temperatures are also included. Only two streams will undergo a phase change. Benzene at 45 bar will undergo a phase change at 550 K, and cyclohexane at 30 bar will undergo a phase change at 529 K. Next, note the pressures included in this table (represented in bar). The highest and lowest system pressures belong to streams H1 (55 bar) and C2 (30 bar), respectively. This is needed in order to be able to analyze the potential for tube rupture scenarios. In addition, included with each stream is its real component name. Without this information, one is limited to calculating a more conservative safety rating based on stream pressure information alone. While this calculation will still ensure safety, it does not allow one to take credit for PSVs. By including the component names (e.g., ammonia), one is able to leverage robust dynamic tube rupture simulations and use PSVs to

improve a network's system safety. Ultimately, with the addition of an appropriately sized relief system, this may result in some of the initially infeasible matches to be feasible. For this HEN case study, the logic shown in Figure 3.5 is used as a guide in determining the appropriate way to approach a system. Alongside Figure 3.5, Figure 3.6 details the different levels of complexity in modeling tube rupture scenarios for HENs.

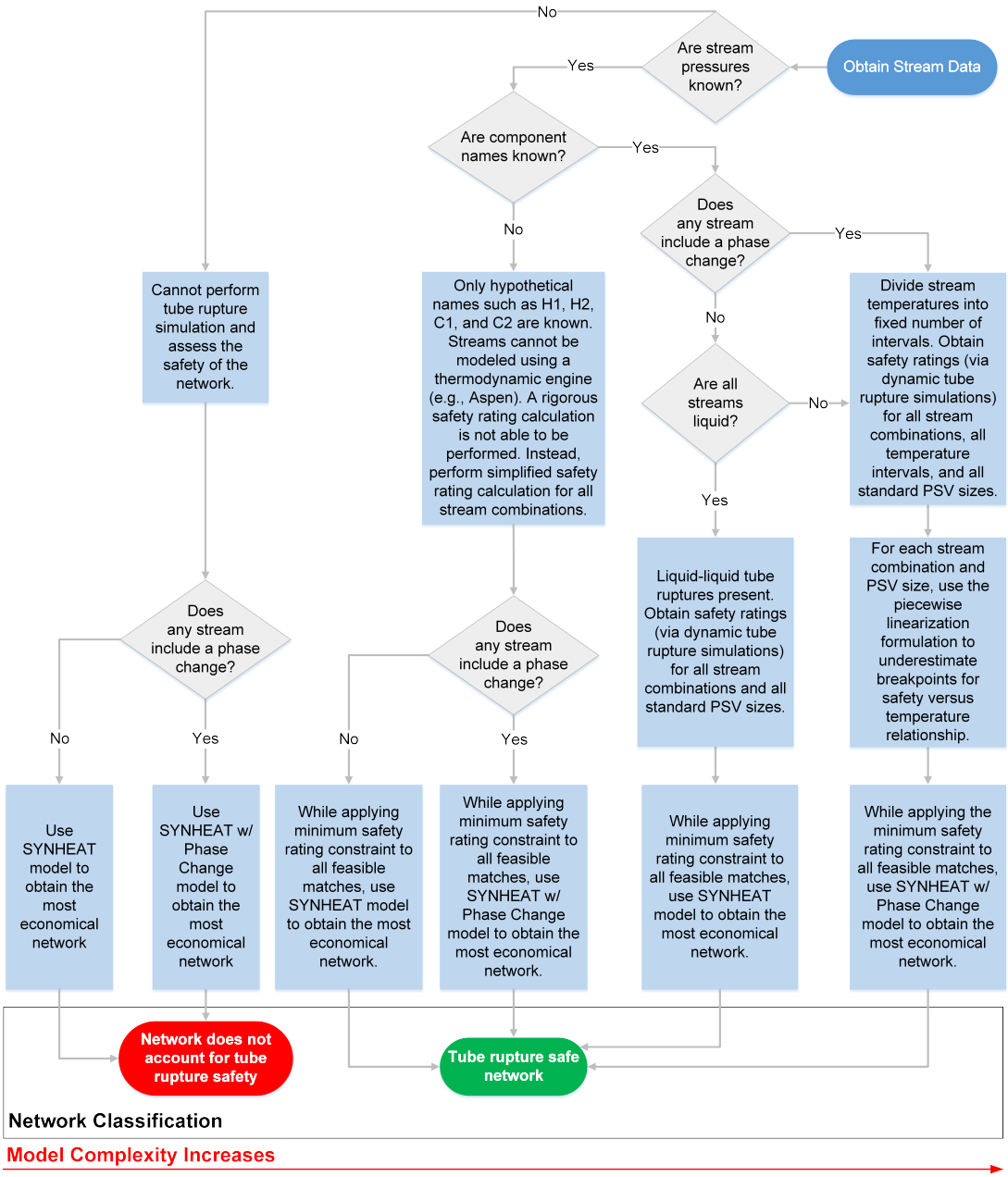

Figure 3.5: Logic flow diagram on modeling tube rupture safety in HEN. First, stream data is obtained via a commercial thermodynamic package. In order to analyze safety in the context of a tube rupture, stream pressures must be known. If stream pressure is excluded, only HEN economic analyses can be performed. If stream pressure is known, however, the safety rating metric that can be applied will depend on whether or not the network's component names are known. For real components (e.g., methane), the more rigorous safety rating calculation can be implemented. If this is not known, however, the network should default to using the simplified safety rating calculation (i.e., the two-thirds rule). Note that the simplified safety rating calculation will require a more conservative network, thus increasing the network's annual cost.

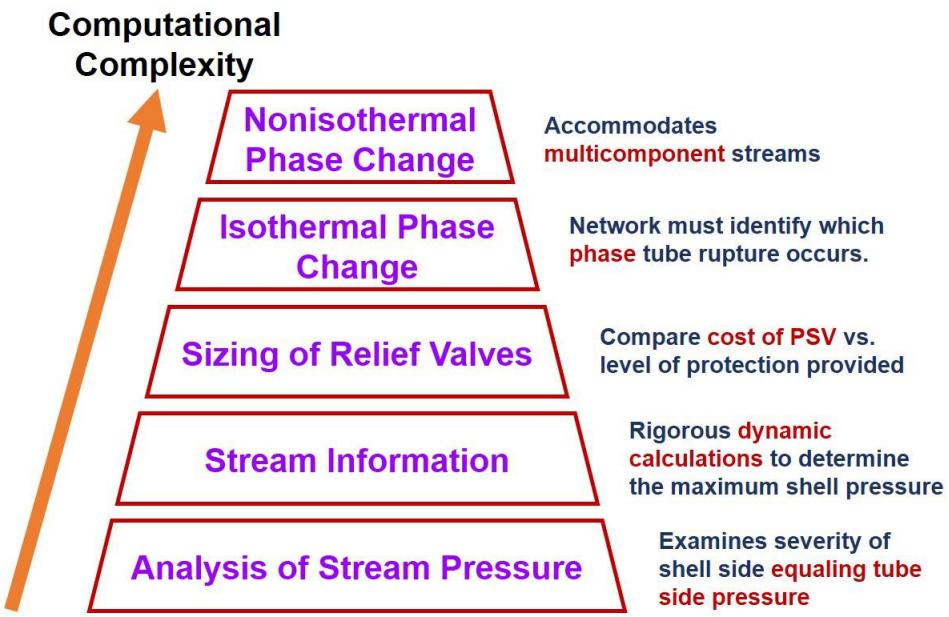

Figure 3.6: Complexity of incorporating tube rupture safety in heat exchanger networks. The first layer "Analysis of Stream Pressure" analyzes a tube rupture using the the two-thirds rule and excludes the possibility of a pressure safety valve providing protection. The second and third layers incorporate the exchangers's thermophysical properties and relief valve sizing in order to perform a dynamic tube rupture simulation. The fourth layer "Isothermal Phase Change" accounts for tube ruptures in streams that undergo a phase change, and is the main subject of this manuscript. The fifth layer build on the previous layers and is able to accommodate multi-component streams.

Table 3.4: Case study 1 stream summary

Component	Stream	Tin	Tout	P	FCp	Fλ	Type	T_{change}^{phase}	Cost
		K	K	bar	kW K^{-1}	kW		K	\$ kW^{-1}yr^{-1}
Ammonia	H1	620	440	55	34.7	-	HPS1	-	-
Benzene	H2	590	450	45	45.9	826	HPS3	550	-
Carbon Dioxide	C1	350	420	20	30.6	-	CPS1	-	-
Cyclohexane	C2	529	529	30	58.5	1924	CPS2	529	-
Steam	HU	627	627	-	-	-	-	-	80
Cooling Water	CU	303	315	-	-	-	-	-	15

First, the optimal network configuration excluding safety as a criteria is shown in Figure 3.7a. In other words, this figure represents the HEN configuration for a network-wide minimum acceptable safety rating (SR_{min}) of zero. As shown from the figure, the network includes four heat exchangers and two coolers. One heat exchanger (E-101) transfers energy between H1 and C2. Three heat exchangers (E-102, E-103, and E-104) transfer energy between H2 and C1. To meet the outlet temperature targets, a cooler is placed on each hot stream. No heat exchanger is assumed to have any additional overpressure protection equipment. It is worth re-emphasizing that this does not necessarily result in an exchanger being unsafe. However, if one side of an exchanger has a design pressure 50% greater than another, it may result in an exchanger failure. For this network, exchangers E-102, E-103, and E-104 have a high side pressure of 45 bar and a low side pressure of 20 bar. As a result, each of these exchangers has a safety rating of 44 (excluding any additional PSVs). Exchanger E-101 has a high side pressure of 55 bar and a low side pressure of 30 bar. As a result, E-101 has a safety rating of 55 (excluding any additional PSVs). Therefore, all exchangers in this network are at risk in the event of a tube rupture. For each exchanger combination, the safety rating with different PSV sizes is shown in Figure 3.7b.

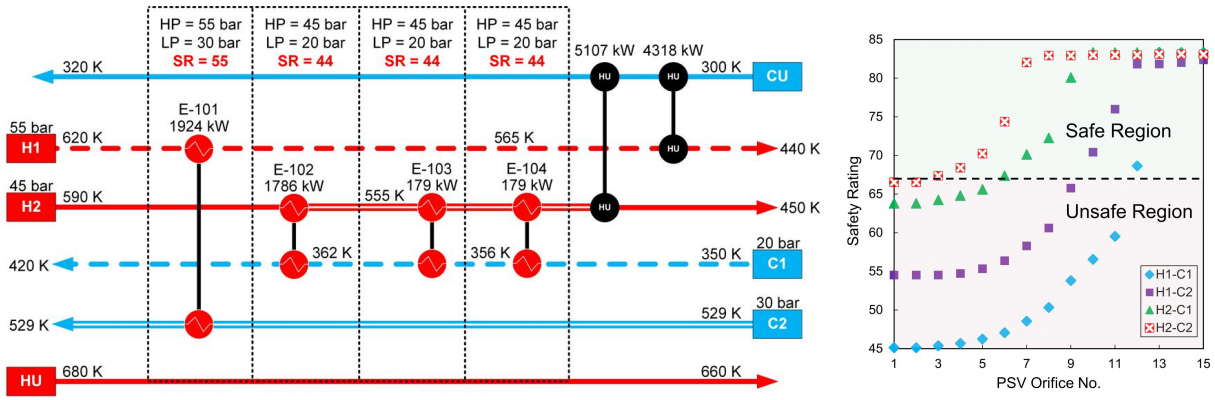

(a) Optimal network configuration excluding tube rupture safety considerations.

(b) Safety rating for all possible exchanger matches in Case 1

Figure 3.7: 3.7a) Optimal network configuration via the SYNHEAT method. 3.7b) For the hot and cold streams present, the SYNHEAT model yielded this network. The proposed configuration was then analyzed for exposure to a tube rupture event. This calculation only considers the pressure of the streams and assumes no additional protection devices exist. In the figure, the HP and LP stream for each exchanger is identified and displayed alongside the safety rating. The HP and LP streams will occupy the tube and shell side of the exchanger, respectively. The safety ratings for exchangers E-101, E-102, E-103, and E-104 are 55, 44, 44, and 44, respectively. All exchangers are less than the safe threshold of 67. Thus, all exchangers would fail in the event of a tube rupture unless other mitigation measures were in place.

To determine an alternative network configuration for Case 1 that results in the minimum annual cost while meeting our safety rating threshold, the steps in Figure 3.5 are used as a guide. In the flow diagram, the first step listed is obtaining the stream data. For this case study, Table 3.4 lists the necessary stream information. The second step in Figure 3.5 requires that stream pressures must be known. Without this information, it is not possible to analyze the network for overpressure safety scenarios. From Table 3.4, the pressures for streams H1, H2, C1, and C2 are 55, 45, 20, and 30 bar, respectively. The third step in Figure 3.5 is whether or not component names are known. The component names are required to perform a dynamic tube rupture. In this case, streams H1, H2, C1, and C2 are identified as ammonia, benzene, carbon dioxide, and cyclohexane, respectively. Step four in Figure 3.5 is whether or not any stream includes a phase change. Streams H2 and C2 both experience a phase change. Up to this point, enough information is known to perform a tube rupture calculation.

The next step determines how exactly the tube rupture calculation shall be performed. Here, there exists two options of tube rupture calculations. The first (and simpler) option is to only perform liquid-liquid tube ruptures. The logic behind this is that the tube side density at a fixed pressure remains relatively constant at a range of temperatures. This obviously wouldn't apply to a vapor stream since its density is a stronger function of temperature than that of a liquid. The second option is to perform tube rupture calculations at temperature steps. This second approach is required for streams that are vapor, two-phases, or undergoing a phase change. By performing tube rupture calculations at multiple temperatures, the safety rating changes from being a single value into a profile. This can then be converted into a underestimated continuous piecewise linear function. This is needed in order to accurately represent the safety rating.

For this case study, this second approach is used. Tube rupture calculations have to be performed for all possible exchanger matches. The possible exchanger matches are H1-C1, H1-C2, H2-C1, and H2-C2. Table 3.5 shows a summary of each potential exchanger match. For each match, the stream selected to be on the tube and shell side is given along with their pressures. In Table 3.5, H1 is divided into 20 temperature steps between 620 K and 440 K. H2 is likewise divided into 20 temperature steps between 590 K to 450 K. Table 3.5 also includes the shell side temperatures. One may ask why a range of temperatures are used for the tube side while a single temperature is used for the shell side. This is because a single temperature used for the shell side, as opposed to a range, yields a conservative tube rupture. Take H1-C1 for example. C1 varies from 350K to 420K. However, only C1 at 350 K will be used in the tube rupture calculations. This is because C1 at 350 K will result in a more conservative safety rating than 420 K. More specifically, because C1 at 350 K is more dense than C1 at 420 K, it will result in a lower safety rating. The less dense the shell side is, the higher the safety rating. Therefore, for a conservative safety rating, it is appropriate to select the lower shell side temperature.

Table 3.5: Case 1 potential exchanger matches

	C_{tube}	C_{shell}	P_{tube} bar	P_{shell} bar	T_{range} K	T_{shell} K	T_{change}^{phase} K
H1-C1	H1	C1	55	20	620 to 440	350	-
H1-C2	H1	C2	55	30	620 to 440	529	-
H2-C1	H2	C1	45	20	590 to 450	350	550
H2-C2	H2	C2	45	30	590 to 450	529	550

All potential exchanger matches are assessed for tube rupture failure. This includes two hot streams, two cold streams, 15 standard pressure relief sizes, and 20 temperature steps. In total, for this case study, 1,200 tube rupture simulations are performed ($2 \times 2 \times 15 \times 20$). It's important to note that each tube rupture simulation yields a single safety rating value. According to Figure 3.5, a continuous piecewise linear function underestimating the safety rating for all temperatures must be performed. This allows the safety rating to vary depending on the location of an exchanger within a HEN. Figure 3.8 displays the safety rating versus temperature for all exchanger combinations. From the figure, it is clear there exists a large difference in the safety rating at different temperatures. Note that this figure only includes three out of the 15 standard PSV sizes. Still, it is evident that caution must be exercised in selecting an appropriately sized PSV.

For exchanger H1-C1, the safety rating for PSV orifices D, H,and M lies below 67 for all tube side temperatures. Thus, the final HEN configuration should not include matches between H1 and C1 unless PSV sizes higher than M yield a safety rating greater than or equal to 67. For exchanger H2-C2, the opposite appears to be true. The safety rating for orifices D, H, and M all lie above 67. Thus, H2-C2 is a feasible match for all tube side temperatures. For H1-C2, orifice size M has a safety rating greater than 67 for all tube side temperatures while orifice sizes D and H are considered unsafe for all tube side temperatures. Lastly, for H2-C2, orifice D is considered safe for tube side temperatures between 550 K to 590 K and unsafe for tube side temperatures between 450 K and 550 K.

From Figure 3.5, one is able to solve the MINLP model presented earlier. To do so, the previous underestimations are taken and inputted as parameters to the HEN MINLP model in Section 4. A minimum safety rating of 67 is applied and the network is solved. The case study results are shown in Figures 3.9 and 3.10. The base case of this design (Figure 3.7a) had a minimum safety rating of zero, or in other words, without imposing any safety constraints. A minimum safety rating of 67 adequately protects the network from a potential tube rupture. For this particular case study, it is quite inexpensive to achieve this (a less than 4% increase in the total annual cost). From Figure 3.10, note that the heaters and coolers do not have any safety rating calculations performed. This is by design. While the calculation procedure for a tube rupture for a heater or cooler would be exactly the same as that of a heat exchanger, the reasoning behind omitting a safety requirement for utility exchangers is that if a heater or cooler is unable to be safe, the network itself would be infeasible.

In further examining the results in Figure 3.10, four exchangers are proposed, two between H2 and C2, and two between H2 and C1. The PSV sizes selected are either E or G. From the HEN, it is clear all exchangers are at or exceed the 67 threshold specified in the problem statement. Note also that H1 does not have any matches with any cold streams. This is because of the high safety burden imposed by H1's pressure (55 bar). Upon examining Figure 3.8, H1-C1 yielded no feasible matches for orifices sizes D, H, and M. Similarly, H1-C2 only yielded a feasible match for orifice size M. This is in contrast to H2 which provided safe exchanger matches for much smaller PSV sizes and was also able to accommodate larger temperature ranges (critical in constructing economical HENs).

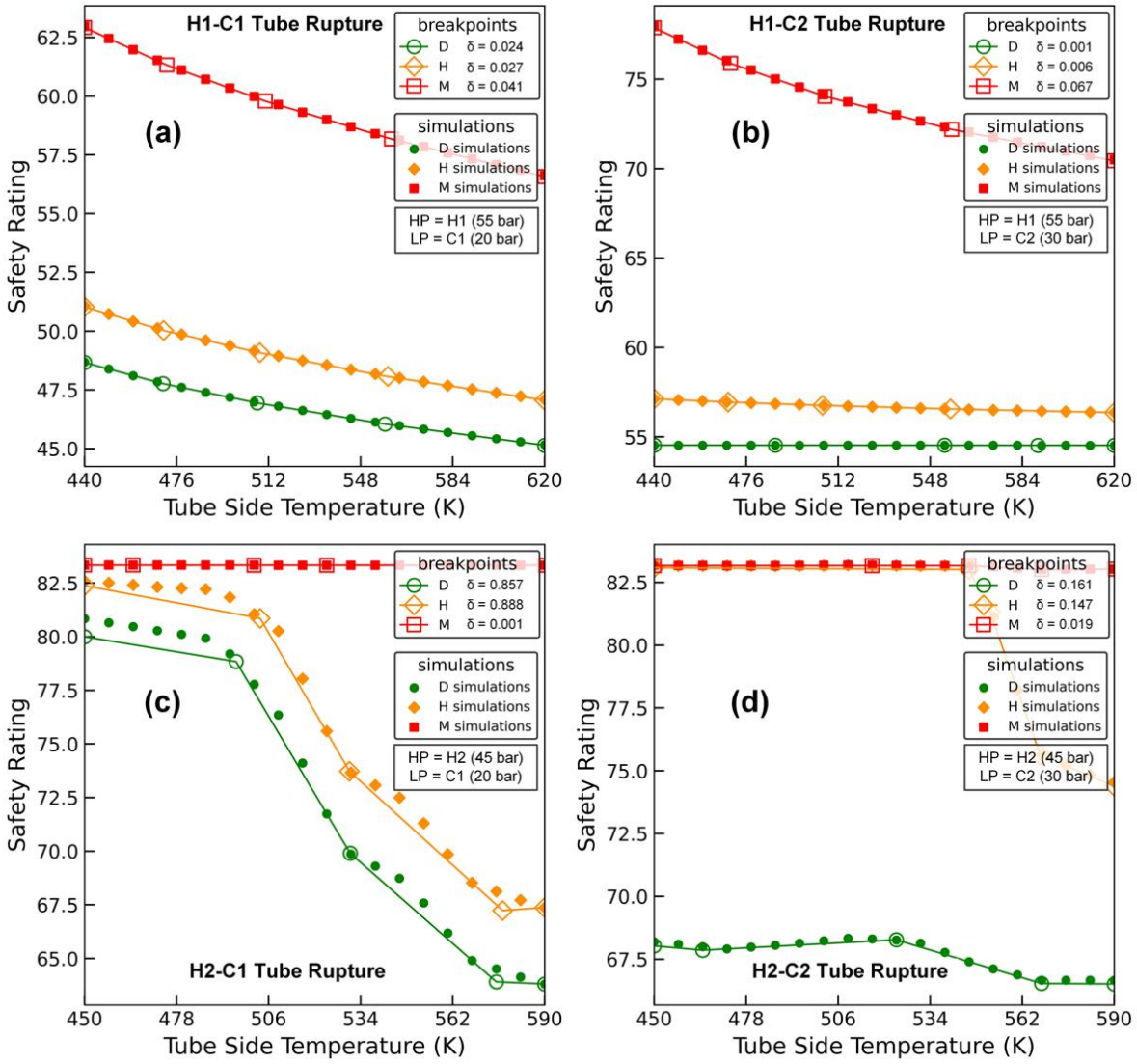

Figure 3.8: Underestimated safety rating for stream matches H1-C1, H1-C2, H2-C1, and H2-C2. Tube side temperatures vary according to Table 3.5. Note that while only three PSV sizes (D, H, and M) are shown in this figure, this underestimation is performed for all 15 PSV sizes. The error of the safety rating at the breakpoint locations for each PSV size is given as δ. A safety rating of 67 or higher is considered safe in the event of a tube rupture. For H1-C1, none of the PSV sizes shown in the figure satisfy this criteria. For H1-C1, a larger PSV size may however exceed an SR of 67. For H1-C2, PSV size M is considered safe for all tube side temperatures. For H2-C1, size D is only safe between temperatures 450K and 540K, while sizes H and M are considered safe for all tube side temperatures. For H2-C2, all PSV sizes shown are considered safe for all tube side temperatures.

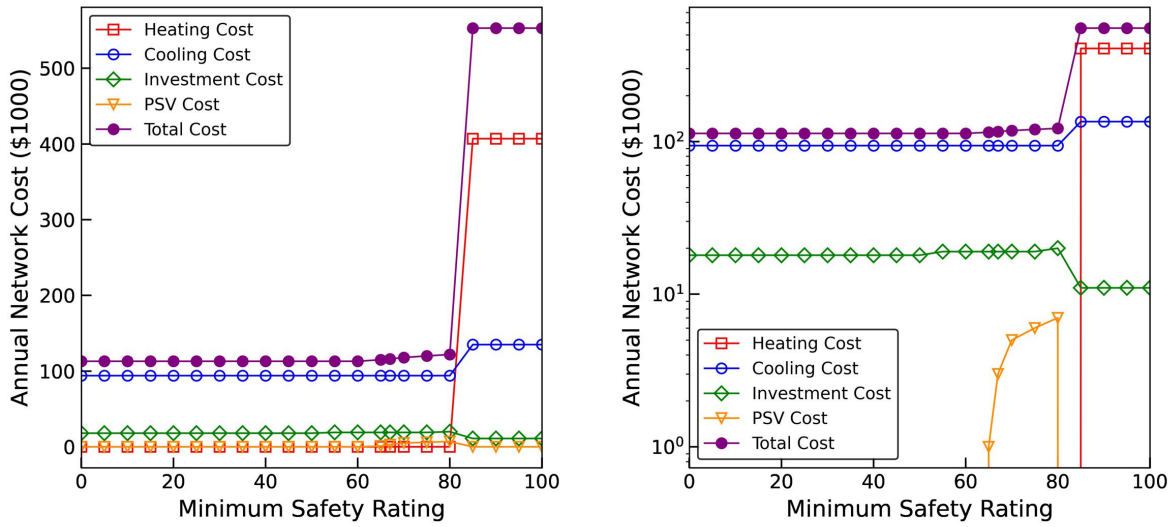

(a) Pareto curve

(b) Pareto curve log based

Figure 3.9: Pareto curves for Case 1. The total annual cost (TAC) of the network is the sum of the heating cost, cooling cost, investment cost, and PSV cost. From the figure, the heating cost closely follows the total annual cost. This is because as the minimum safety rating increases, less exchanger matches are feasible. As a result, the savings that would have been realized from the exchangers must go to either the heaters or coolers. At an SR_{min} of zero, the total annual network cost is \$112508 whereas an SR_{min} of 67 costs \$116131.

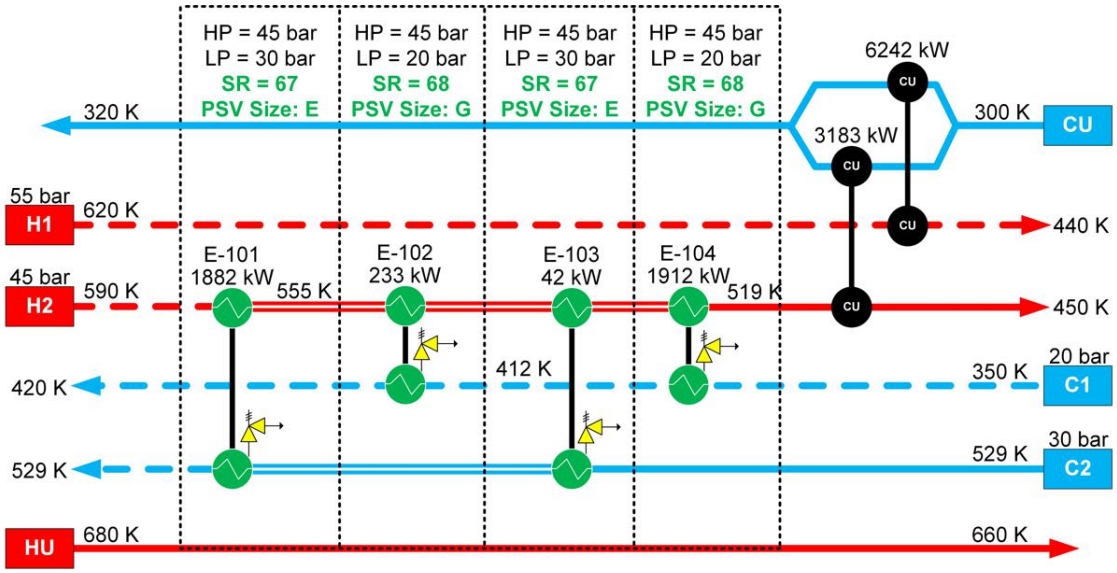

Figure 3.10: Case 1 optimal network configuration that provides protection in the event of a tube rupture.

3.4.2 Case Study 2

The HEN stream summary for Case 2 is shown in Table 3.6. Similar to Case 1, real components and not hypothetical components are used. There are a total of six streams, three hot (H1, H2, H3) and three cold (C1, C2, and C3). The pressures vary from 55 bar (H2) to 20 bar (C2). The temperatures vary from 700 K to 320 K. The stream types include HPS1, HPS3, CPS1, and CPS2. H1, H2, and C2 are vapors for both the inlet and outlet. H3 starts off as a vapor at 590 K, changes phase at 555 K, and exits as a liquid at 450 K. C1 only undergoes a phase change from a liquid to a vapor at 523 K. C3 enters and exits as a liquid. FCp and $F\lambda$ are included and were obtained from HYSYS.

Table 3.6: Case study 2 stream summary

Component	Stream	Tin	Tout	P	FCp	Fλ	Type	T_{change}^{phase}	Cost
		K	K	bar	kW K^{-1}	kW		K	\$ kW^{-1}yr^{-1}
Ammonia	H1	700	400	45	38	-	HPS1	-	-
Ammonia	H2	600	400	55	38	-	HPS1	-	-
Benzene	H3	590	450	45	45.9	826	HPS3	555	-
Benzene	C1	523	523	30	30	826	CPS2	523	-
Carbon Dioxide	C2	350	420	20	30.6	-	CPS1	-	-
Cyclohexane	C3	320	400	30	29	-	CPS1	-	-
Steam	HU	627	627	-	-	-	-	-	80
Cooling Water	CU	303	315	-	-	-	-	-	15

The network configuration excluding safety as a criteria is shown in Figure 3.7a. In other words, the minimum acceptable safety rating is zero. As shown from the figure, the network includes three heat exchangers and three coolers. The heat exchangers transfer energy between H1 and C1, H1 and C2, and H3 and C3. Coolers are placed on streams H1, H2, and H3. In first analyzing the network, heat exchangers are assumed not to have additional overpressure protection equipment. For this network, exchangers E-101, E-102, and E-103 have safety ratings of 66, 49, and 66 respectively (excluding any additional PSVs). Therefore, all exchangers in this network are at risk in the event of a tube rupture.

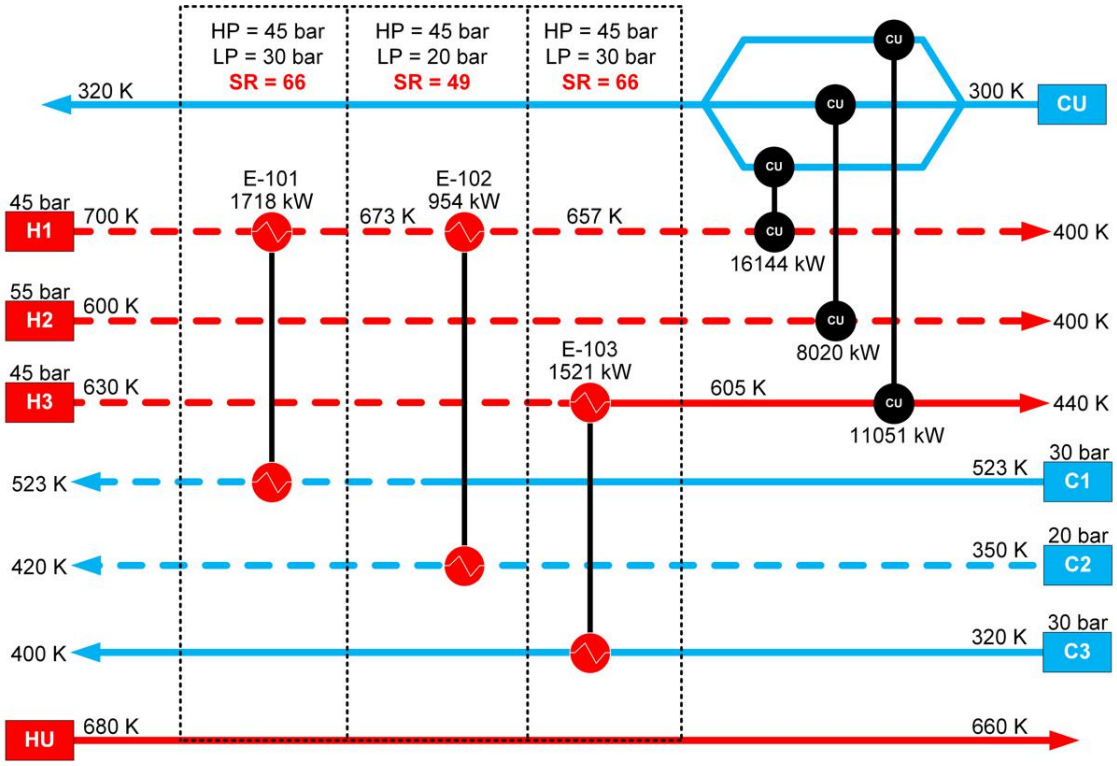

Figure 3.11: Case 2 optimal network configuration excluding tube rupture safety considerations.

To determine an alternative network configuration that yields the minimum cost and meets our safety rating threshold, the steps in Figure 3.5 are used. First, the stream data is obtained. Second, the stream pressures must be known. The pressures for streams H1, H2, H3, C1, C2, and C3 are 45, 55, 45, 30, 20, and 30 bar, respectively. Thus, it is possible to evaluate the network for tube rupture overpressure. Third, the component names are required. From Table 3.6, H1, H2, H3, C1, C2, and C3 are identified as ammonia, ammonia, benzene, benzene, carbon dioxide, and cyclohexane, respectively. The next step is proceeding to the tube rupture calculation. These are performed for all possible exchanger matches. The properties of each exchanger match (nine in total) are listed are listed in Table 3.7. From the table, two possible tube side pressures exist, 45 bar and 55 bar. Three different temperature ranges are present, 700 K to 400 K, 600 K to 400 K, and 590 K to 450 K. Three different shell side temperatures exist, 523 K, 350 K, and 320 K. Finally, only H3 at 555 K experiences a phase change.

Table 3.7: Case 2 potential exchanger matches

	C_{tube}	C_{shell}	P_{tube} bar	P_{shell} bar	T_{range} K	T_{shell} K	T_{change}^{phase} K
H1-C1	H1	C1	45	30	700 to 400	523	-
H1-C2	H1	C2	45	20	700 to 400	350	-
H1-C3	H1	C3	45	30	700 to 400	320	-
H2-C1	H2	C1	55	30	600 to 400	523	-
H2-C2	H2	C2	55	20	600 to 400	350	-
H2-C3	H2	C3	55	30	600 to 400	320	-
H3-C1	H3	C1	45	30	590 to 450	523	555
H3-C2	H3	C2	45	20	590 to 450	350	555
H3-C3	H3	C3	45	30	590 to 450	320	555

All potential exchanger matches are assessed for tube rupture failure. This includes three hot streams, three cold streams, 15 standard pressure relief sizes, and 20 temperature steps. In total, for this case study, 2,700 tube rupture simulations are performed ($3 \times 3 \times 15 \times 20$). The safety rating versus temperature for all exchanger combinations is shown in Figure 3.12. These underestimations are inputted as parameters to the HEN MINLP model in Section 4. A minimum safety rating of 67 is applied and the network is solved. The pareto curves for this case study are shown in Figure 3.13. The optimal HEN configuration is shown in Figure 3.14.

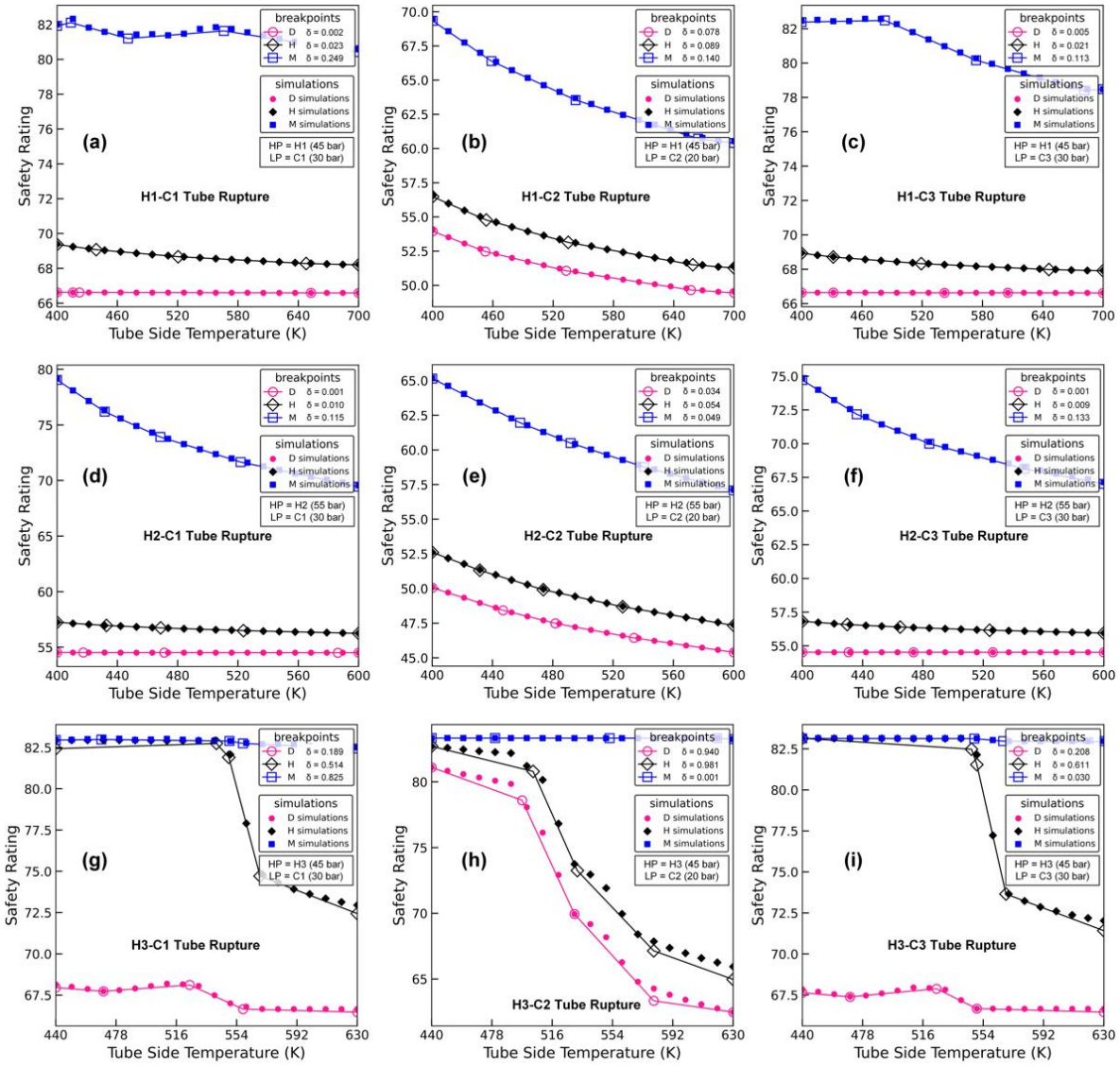

Figure 3.12: Optimal breakpoint locations for each potential exchanger match. Underestimated safety rating for all nine potential stream matches. Tube side temperatures vary according to Table 3.7. Note that while only three PSV sizes (D, H, and M) are shown in this figure, this underestimation is performed for all 15 PSV sizes. The error of the safety rating at the breakpoint locations for each PSV size is given as δ.

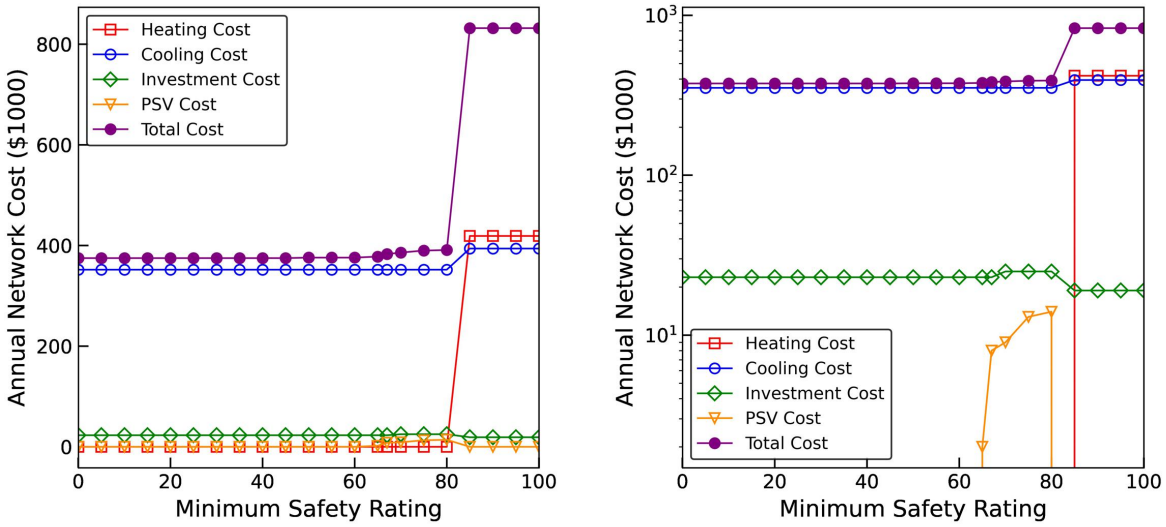

(a) Pareto curve

(b) Pareto curve log based

Figure 3.13: Pareto curves for Case 2. The total annual cost of the network is the sum of the heating cost, cooling cost, investment cost, and PSV cost. Annual network cost of $375,000 for an SR_{min} of 0. Annual network cost of $383,000 for an SR_{min} of 67, or roughly 2% above the base case.

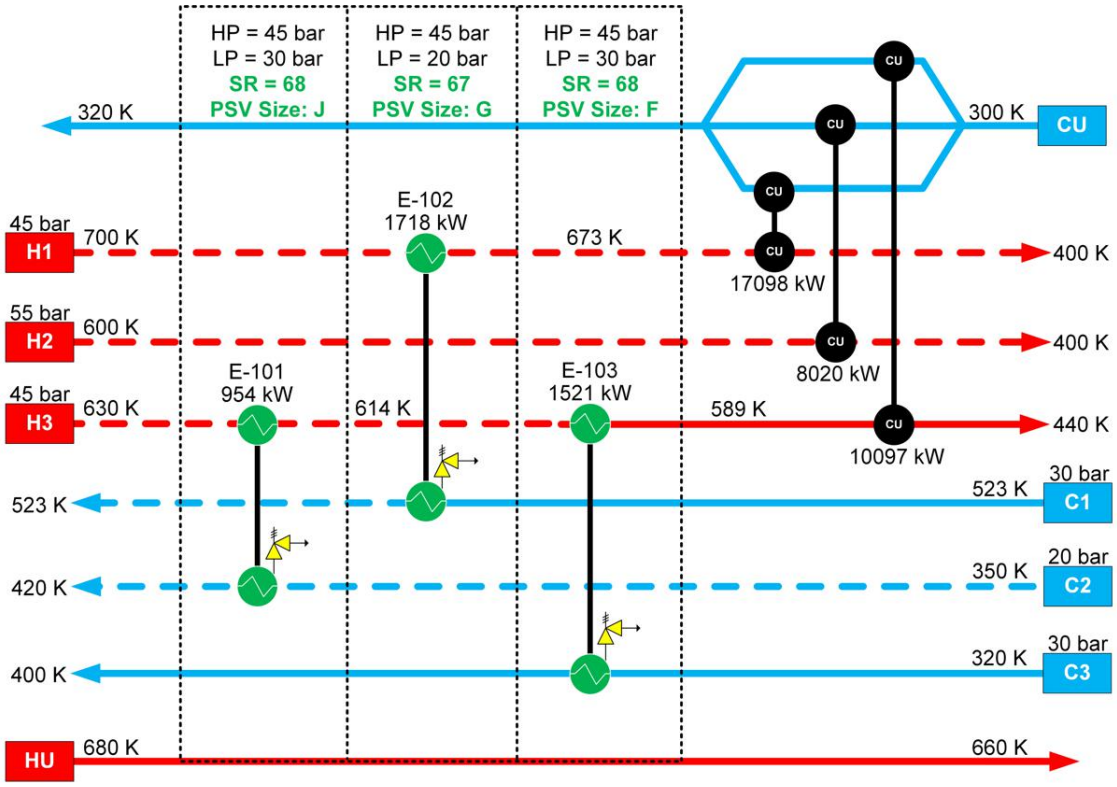

Figure 3.14: Case 2 optimal network configuration that provides protection in the event of a tube rupture.

3.5 Appendix A

In Equation (3.1), calculating the safety rating for each exchanger requires P_{design} and $P(t)_{max}$. The former is assumed given since it represents a basic equipment design property. The latter however represents the maximum pressure experienced during a tube rupture event and must be calculated. To calculate $P(t)_{max}$, the dynamic tube rupture model presented here is used. For a detailed discussion on this model, the reader is referred to our earlier work [42]. Here, a brief description of each equation is given. Equation (3.47) is used to calculate the change in shell side pressure over time during a tube rupture event. The numerator on the right amounts to a mass balance accounting for fluid entering via $\dot{m}_{tv}$ and $\dot{m}_{tl}$ and exiting via $\dot{m}_{psv}$. The denominator represents shell side conditions. Because these can vary depending on the type of tube rupture present, Ω is placed instead and defined in Equation (3.48). The individual terms in these two

equations are defined by Equations (3.49) to (3.58).

In Equation (3.49), G represents the mass flux between the tube side and shell side pressures. v_t, v_n, and v_1, v_n, and v_j represent different volumes obtained via flash calculations. G is then fitted against pressure in Equation (3.50). Equation (3.51) fits density as a function of pressure. Equations (3.53) and (3.54) determine the liquid and vapor mass flow rate of a tube, respectively. The flow rate of a PSV is modeled by (3.55). The bulk modulus, B, is calculated using Equation (3.56). Equations (3.57) and (3.58) represent the change in shell side volume from the tube side vapor and liquid, respectively. Equations (3.47) to (3.58) are then simultaneously solved to achieve pressure as a function time, from which $P(t)_{max}$ is obtained.

$$\left(\frac{dP}{dt}\right) = \frac{\frac{\dot{m}_{tv}}{\rho_{tv}} + \frac{\dot{m}_{tl}}{\rho_{tl}} - \frac{\dot{m}_{psv}}{\rho_{sl}}}{\Omega + \frac{V_{sl}}{B_{sl}} + \frac{V_{shell}}{B_{shell}}} \tag{3.47}$$

$$\Omega = \left\{ \begin{array}{cc} \frac{V_{tv}}{c_{tv0}^2 \rho_{tv}} & vapor \\ \frac{V_{tl}}{B_{tl}} & liquid \\ \frac{V_{tv}}{c_{tv0}^2 \rho_{tv}} + \frac{V_{tl}}{B_{tl}} & flashing\, liquid \end{array} \right\} \tag{3.48}$$

$$G^2 = \frac{h\left(v_1 + v_n + 2 \times \sum_{j=2}^{n-1} v_j\right)}{v_t^2} \tag{3.49}$$

$$G = \alpha 1 \times P(t)^3 + \alpha 2 \times P(t)^2 + \alpha 3 \times P(t) + \alpha 4 \tag{3.50}$$

$$\rho_{tv} = B1 \times P(t) + B2 \tag{3.51}$$

$$A_{tube} = \pi r_{tube}^2 \tag{3.52}$$

$$\dot{m_{tl}} = 2 G_l A_{tube} \tag{3.53}$$

$$\dot{m_{tv}} = 2 G_v A_{tube} \tag{3.54}$$

$$\dot{m_{psv}} = \left\{ \begin{array}{cc} A_{psv} C_0 \sqrt{2 \rho_{sl} g_c P(t)} & if\ P(t) \geq P_{set} \\ 0 & otherwise \end{array} \right\} \tag{3.55}$$

$$B = \frac{P_1 - P_0}{\frac{V_1 - V_0}{V_0}} \tag{3.56}$$

$$\frac{d\dot{V}_{tv}}{dt} = \frac{\dot{m}_{tv}}{\rho_{tv}} \tag{3.57}$$

$$\frac{d\dot{V}_{tl}}{dt} = \frac{\dot{m}_{tl}}{\rho_{tl}} \tag{3.58}$$

4. APPROXIMATING PROCESS SAFETY METRICS USING ARTIFICIAL NEURAL NETWORKS

4.1 Real-time consequence modeling

The motivation of this work is rethinking process safety modeling. To demonstrate, consider the following. Process safety scenarios are often highly specific, time intensive, and require many inputs. An example of the steps required in process safety consequence modeling can be shown in Figure 4.1. First, a process safety objective has to be determined. This can be things such as determining the size of a PSV required for a system, performing a dispersion model analysis, or some other related process safety calculation. After this is determined, this objective then has to be assigned to qualified personnel (i.e., someone with a background in process safety and consequence modeling). After that, the selected personnel responsible for consequence modeling must consult the appropriate standards or guidelines. This is in order to determine a model that is appropriate and also make sure that any model or solution they propose is in accordance with the latest process safety guidelines and is adopted throughout industry.

After this, the steps of actually solving the process safety calculation can begin. This requires collecting data from a plant. This data can include operating data and equipment data. Once that has been gathered, that can then be inputted into the process safety model. An example of this for dispersion modeling would be collecting data such as the local weather conditions and also including the chemicals within a plant in order to determine a safe evacuation zone. Once this is done, one must relay this information to another party to perform a secondary review of the model. This is particularly important in process safety because of the potential for severe consequences if any errors were made. From there, the design is either approved, or it is rejected. If it's the latter, one must return to the first step and repeat the process until a design is approved. What is clear from this diagram is that each of these steps takes time, is highly specific, requires personnel expertise, requires subject matter expertise, and is not scalable. In addition, these tasks require

niche infrastructure necessary to perform those calculations. This infrastructure could be in the form of required software, or it could be in terms of the training of the engineers to be able to do that calculation. Lastly, this process takes up valuable resources for a company.

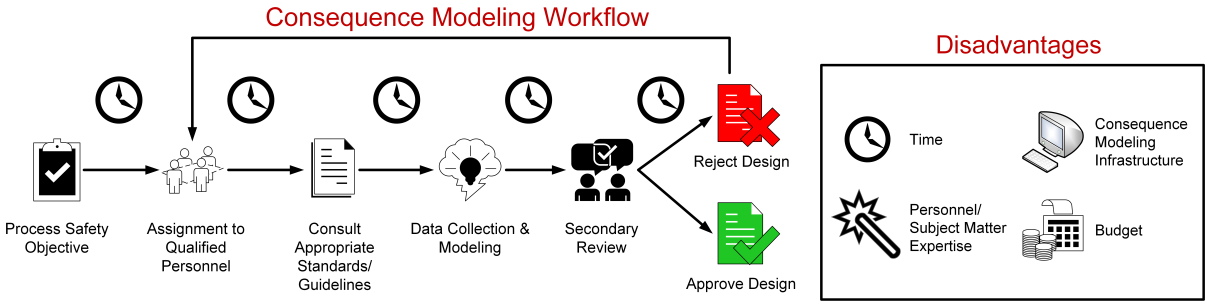

(a) Steps required in process safety consequence modeling. (b) Disadvantages

Figure 4.1: Consequence modeling for process safety scenarios are often highly specific, time-intensive, and require many inputs.

Because of the disadvantages presented earlier, we wish to reimagine the way that a calculation like this can be performed and in particular, we think fault detection techniques that are combined with ANN can be very promising in tackling these types of issues. Plant operating data that is often used for quality control, management decision making, and operator response is already present in most process plants. Therefore, all of this data can be integrated with an ANN model that has the ability to translate the real-time data to real-time process safety metrics providing significant value to plant operators. An ANN model also has the ability to increase access to process safety metrics. This is particularly important because it allows process safety to be communicated to more people which may lead to an increase in the safety of a plant. With the previous method shown, these process safety calculations are typically only known to those in the process safety community. An ANN model thus has the ability to increase access to those metrics which would get more input from shareholders in the plant (e.g., community, workers, contractors, etc.). An example of how this might work would be in Figure 4.9 where we see a distributed control system (DCS) that already exists. Two units are present, Unit-101 and Unit-102. For each unit, a vessel,

control valve, and a heat exchanger are present. For the vessel, the level of that vessel is being monitored, and is being transmitted through the DCS. For the control valve, its pressure is being monitored, and for the heat exchanger, its temperature is being monitored. Thus, for this plant configuration, all of the operating data is being fed through the DCS, which goes into a server, and then is used in the control room to monitor the performance of a plant. From the figure, this plant has the potential to take the aggregated data that already exists in the server and apply an ANN model to predict process safety metrics. In our particular case, this would be for a tube rupture. However, other applications of this and the way it can be extended is by having an ANN model for other process safety metrics such as dispersion modeling or fire modeling, all of which require operating data which already exists from the DCS and also equipment data, which is data that only has to be retrieved one time, making the cost of acquiring that data very low.

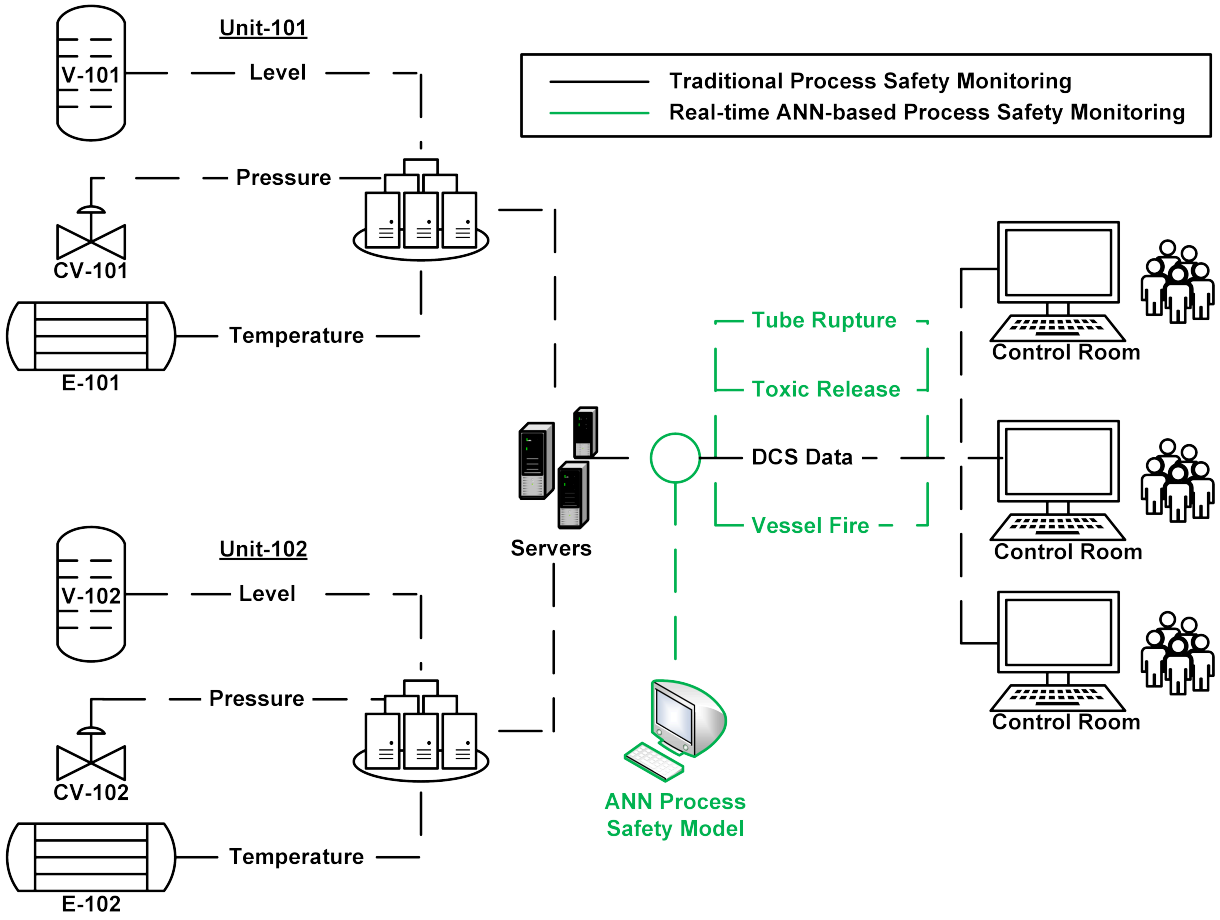

Figure 4.2: Diagram of a process' distributed control system data. Black displays traditional process safety modeling. ANN can be used to provide real-time assessments of potential overpressure events.

4.2 Artificial neural networks overview

The process of an artificial neuron is as follows: If we propose a model of the neuron with the summation and an activation function and we have several inputs. The process would be to multiply the input x_1 by a value known as weight w1, arriving here to be added with the input x_2 multiplied by w_n, and so on until we reach the input x_n multiplied by w_n plus a special input known as the bias. Once this value is obtained, it arrives at an activation function, which will cause this neuron to provide an output. Depending on this activation function, we end up with different responses for each neuron. The output is defined as a function evaluated over n, where n is the

result of the entire weighted sum plus the bias.

Note that there exist different types of activation functions. In Figure 4.3, the functions in equation and graph form of some of the most common activation functions are presented. The first function shown, Figure 4.3(a), is the linear function, which yields the value that is obtained directly from the sum of the inputs in the neuron. It delivers the input directly to the output without any modification. The rectified linear unit (ReLU) function shown in Figure 4.3(b) returns zero when the sum of the inputs is less than zero and returns a linear function if the result of the inputs of the neuron is greater than zero. The sigmoid function shown in Figure 4.3(c) returns a value approaching zero when the sum of the inputs is less than zero. It also approximately returns a linear function between inputs of negative two and positive two. Beyond positive two, sigmoid function approaches one. The tanh function shown in Figure 4.3(d) is simular to the sigmoid function, except that its output varies from negative one to one. The step function, Figure 4.3(e), which equals zero at the output of the neuron, provided that the sum of the inputs of the neuron is less than zero. The step function output equals one when the sum of the inputs is greater than or equal to zero. Next is the signum function, Figure 4.3(f), which is very similar to the step function, except that its output is from negative one to one instead of zero to one.

4.3 Modeling heat exchanger tube ruptures

Before we can begin developing the ANN Model, a brief discussion on heat exchangers and tube ruptures is presented. The shell side of a heat exchanger typically has three pressures, an operating pressure, a design pressure, and a hydrotest pressure. The operating pressure is where the heat exchanger will spend most of its life. The design pressure is the pressure that the shell side is designed for. It serves as an upper limit during normal plant operation. The hydrotest pressure is the maximum pressure the shell side has ever been tested at. This hydro test pressure is typically a multiple of the design pressure, the most common being 150% of the design pressure. For the tubes within a heat exchanger, they will be at higher pressures than the shell side. Similar to the shell side, they will also have three pressures, an operating pressure, a design pressure, and a hydrotest pressure. For both the shell and tube side, a PSV is placed and its set pressure is set

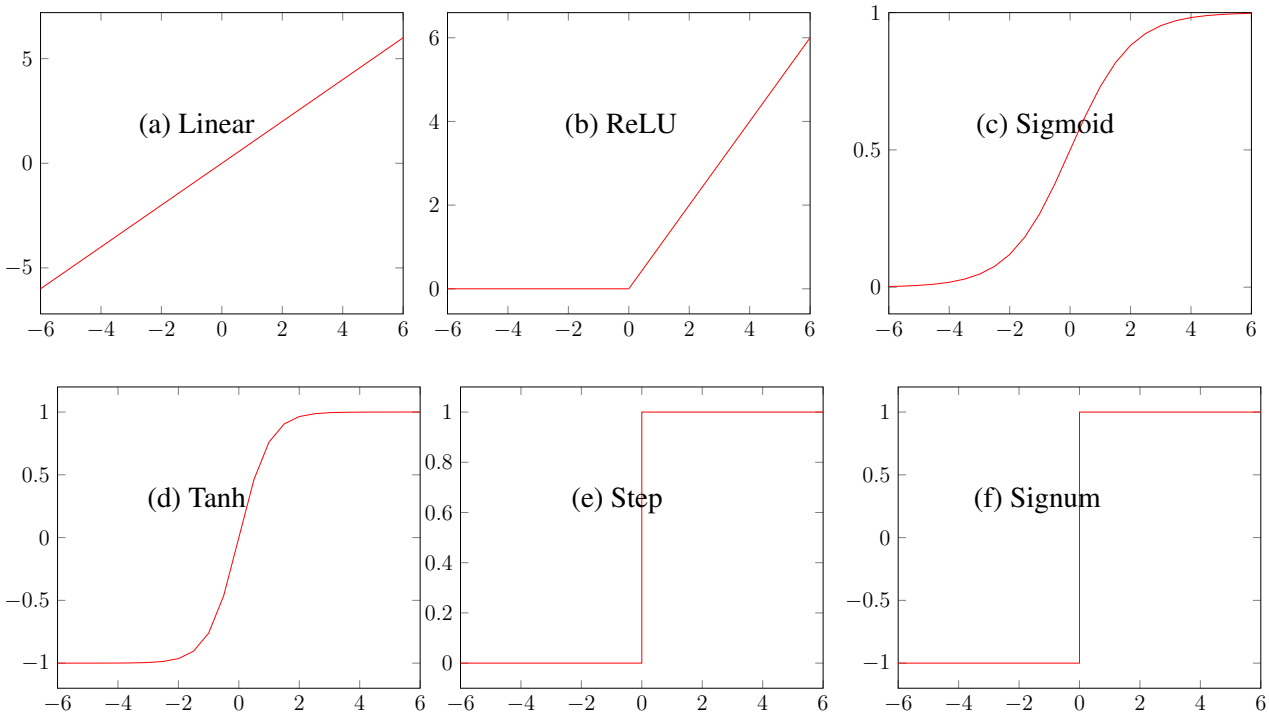

Figure 4.3: Common activation functions for training neural networks.

anywhere between the operating pressure and design pressure. The higher the set pressure of the PSV, the less that PSV would open and valuable products would escape to the flare. Within this heat exchanger design, API 521 allows a tube rupture to reach the shell side hydrotest pressure. Therefore, in the event of a tube rupture, there exists a safe and an unsafe region. The border of that safe and unsafe region is the shell side hydro test pressure. Therefore, for a safe heat exchanger design, a tube rupture that occurs cannot have the shell side exceed the hydrotest pressure.

The way a tube rupture is represented is through a pressurization equation in which the flow from the tube side fluid is modeled assuming isentropic nozzle flow. The properties that affect this rate of pressurization can be lumped into two categories. The first category are fluid properties. These include the fluid density, fluid phase, pressure temperature and whether or not any flashing exists. Examples of exchanger properties include attached piping, shell volume, tube diameter, relief valve size, and relief valve opening times. The shell pressurization equation can be summarized as a mass balance where the top portion of the equation represents tube side fluid (vapor or

liquid) entering the low pressure shell side minus any fluid exiting via a PSV. On the bottom of the equation, the volumes of the vapor, liquid, and shell are divided by their bulk modulus, which represents the compressibility of a fluid. For the shell, the bulk modulus represents the compressibility of carbon steel.

For a vapor-liquid tube rupture, the terms contributing to dP/dT are highlighted in blue. For a liquid-liquid tube rupture, the terms contributing to dP/dT are highlighted in orange. The terms common to any tube rupture scenario are highlighted in yellow.

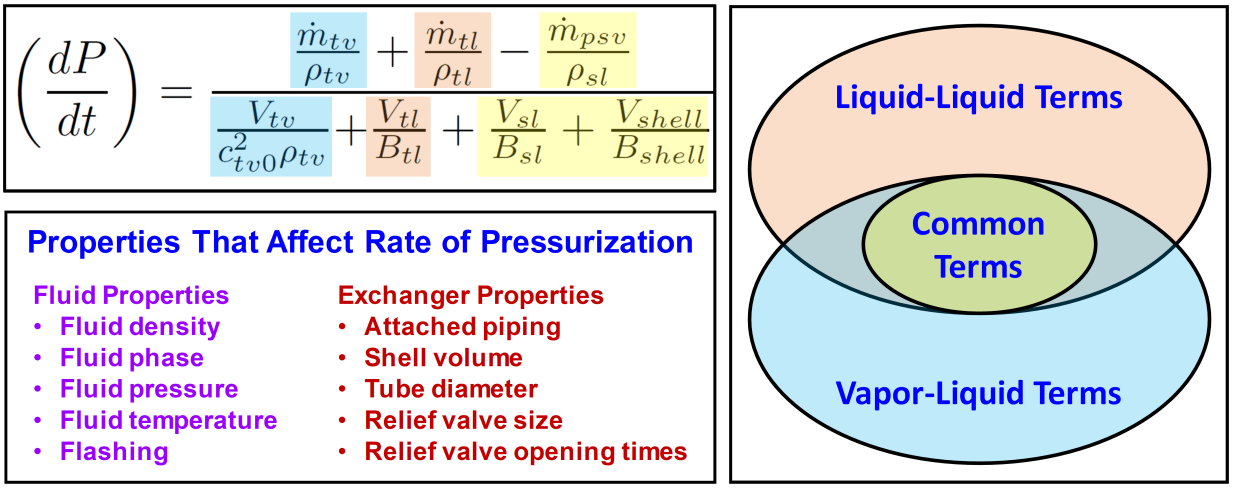

Figure 4.4: Dynamic shell pressurization equation.

To represent the severity of a heat exchanger tube rupture, the safety rating is used. The safety rating is defined as the design pressure divided by the maximum transient pressure during a tube rupture. The safety rating can be interpreted as a "normalized tube rupture severity rating". The details of the safety rating is presented in another work by Harhara and Hasan (2022). To briefly summarize, a safety rating score of 67 or greater represents a safe region for a tube rupture. The value 67 is used because it equals 1.5 times the design pressure of the shell side. More specifically, the maximum transient pressure during a tube rupture would equal 1.5 times the design pressure of the shell side. A safety rating of less than 67 means that the maximum transient pressure has

been exceeded past the shell side hydrotest pressure. Therefore, in constructing an ANN Model, the safety rating will be the output since it is what determines the severity of a tube rupture. The inputs to the ANN model will be all of the properties that are used to calculate the safety rating.

Here, an overview of ANN architecture is presented. The term artificial neural networks gets its name from modeling the behavior of neurons within the human brain. Because ANN models can be non-linear, this makes them useful in being able to predict data and recognize patterns within large sets of data. For heat exchangers, ANN applications have significantly increased in the literature. In the year 2000, only two papers reported heat exchanger-related studies on ANN. In 2009, almost 20 papers reported applications in heat exchangers (Mohanraj et al., 2015) [102]. With the increasing power and affordability of computing, being able to leverage ANN is much more available to the engineering community. In our particular case, the effects of parameters that cannot be easily accounted for, such as the temperature, pressure, and composition can be mapped and incorporated via ANN in developing a tube rupture prediction model. For our particular case, the inputs to the ANN model will be the exchanger design properties such as the tube diameter, shell volume, and PSV size, and also the exchanger operating conditions such as the temperature, pressure, and composition of each stream. These inputs will be fed into an artificial neural network and ultimately predict the safety rating.

The basic structure of a single processing unit within ANN is presented as follows. The inputs are represented by the variable x. The weights are represented by the variable w. For each input, a weight is given. These weighted inputs are then summed up and a bias is applied. The term is then fed into an activation function which then can be used to predict an output. In this particular case, a rectified linear unit activation (ReLU) function is used. The advantage of a rectified linear unit activation function is that it provides great flexibility while also being computationally less expensive.

Returning to the ANN network, it should be noted that within ANN, there exist hidden layers, each of which have a different numbers of nodes. Therefore, a neural network will have an input layer, an output layer and then multiple hidden layers with a certain node size. The way to deter-

mine the different number of layers needed is typically done by adjusting the number of layers to increase the accuracy of the output. To calculate the weights within a neural network, the network is trained against a large set of data. In our particular case, this will be the operating data and the output will be safety ratings calculated via our tube rupture model (Harhara and Hasan, 2020, and Harhara and Hasan, 2022) [98], . This then allows the neural network to estimate the weights and develop a neural network structure. This process is called training the network or learning. After that is done, the neural network is tested against a separate set of data to cross validate the accuracy of the network.

Using ANN, we present two case studies. The objective of both case studies is to test the feasibility of ANN. For the prediction of tube rupture safety ratings, the inputs to the case studies is information that is readily available to a plant. This is important because we do not include intermediate calculations as inputs to the ANN model. An example of this specific to tube ruptures would be including the tube rupture mass flux, which is something that a plant might not necessarily have readily available. However, a plant almost certainly has access to the compositions and stream flowrate data. Other parameters that will be used include the pressure and temperature of both tube and shell side as well as properties of the exchanges such as the diameter of its tubes, the volume of the shell, and the area of any PSVs on the exchanger. From this very basic and easily accessible data, these two case studies attempt to predict the safety rating.

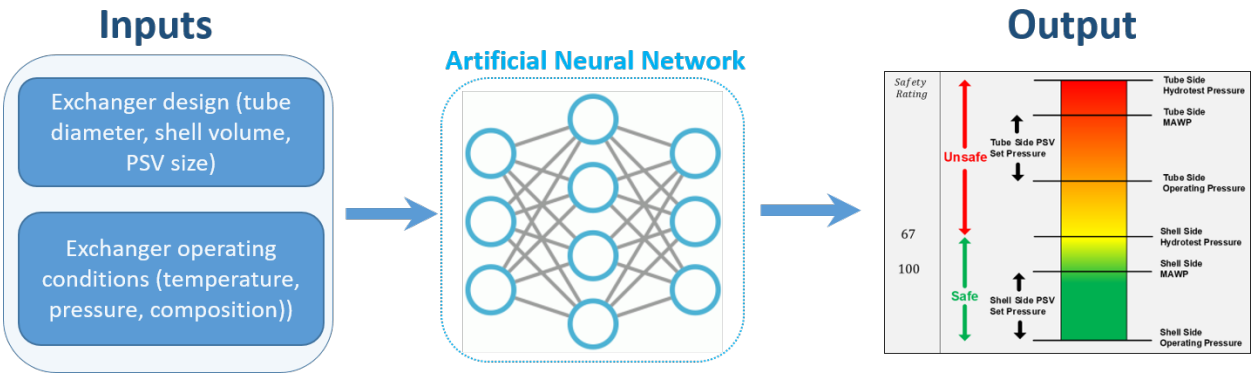

Figure 4.5: Exchanger design inputs and operating conditions can be fed to an ANN model to predict the safety rating.

4.4 Training the ANN model

The architecture and method for training Cases 1 and 2 is similar. They are summarized as follows. First, the following packages within Python are needed. These include numpy, pandas, keras and matplotlib. Within keras, the dense function, sequential function, and the callback function are imported. Next, the exchanger input data is normalized. This is done by creating a re-scale function within Pyton. The purpose of the re-scale function is to take the input values which are the composition, temperature, and pressure for the tube side and shell side and to normalize them in order to be able to fit them into the keras model. The lower and upper bound of the exchanger input data were obtained. In this case, these were pre-specfied. These are assumed to be ranges that a plant would know ahead of time.

For the Y values, they represent the temperatures within the tube side, and vary from 0 to 110. The x lower bound and the x upper bound, our first obtained similarly the why lower bound and the y upper bound are obtained after that we import the sample safety ratings that were calculated and that we will use to train our model. This sample consists of 1500 tube rupture simulations that were calculated and whose input data was varied using latin hyper cube sampling from this data. We obtained the X and the Y from the spreadsheet at this point, the X and the Y arrays can be re scaled using the lower and upper bounds.

At this point we define a few parameters that will be inputted into our ANN model. The first is the number of samples which is simply 1500. The second is the number of inputs, which would be 12 inputs and the number of outputs, which is the safety rating from there. We define a nodes array. And we specify the number of epochs to be 3000. The activation function that is used here is the rectified linear unit activation function. At this point we have enough information to be able to train the data. The data is trained via constructing a for loop for the number of nodes for for each node elements within the node array. The nodes are specified as in array of the array element in the outputs. The number of layers are taken as the shape of the number of nodes and then the ANN model architecture is defined. The ANN model architecture begins by calling the sequential function at this point. A dense layer consisting of a number of node is specified and an activation

function of relu is specified. The input shape is specified as the number of inputs. After this first layer, a for loop is then constructed, to iterate over the other nodes to create more layers within the network, and finally at the end, these are compiled. Finally, at the end of a final layer is added in this layer represents the output. This model is then compiled using the adam optimizer and the loss is measured as the mean squared error. A CSV file is used to log the training data. The model is then fit to X, Y. The number of epochs is set to 3000. The validation split is set equal to zero and the callbacks are set equal to the logger that were created after that. The model Is run and saved into an H5 file. For the 3000 epochs that were run, we try to obtain the model that resulted in the lowest loss.

After Case 1 has been trained, this is then used to predict the safety rating against 200 tube rupture samples. Once the re-scale function is called, a comparison function is created from the model that achieved the lowest loss function. The model that that had the highest R^2, representing the accuracy of the model, is selected. The H5 model is then imported and then the prediction is applied against the the cross validation data. From this, the figure below is presented. From the figure we can see the 200 samples. The safety rating varies from a low of 38 to a high of 72. These safety ratings were purposefully selected since they are near the safety rating of 67, the boundary which would yield a safe and unsafe safety rating. The R^2 value obtained 99.56, yielding a very high accuracy prediction for the safety rating.

4.5 Case study 1

Table 4.1: Case 1 input bounds for training feed forward artificial neural network.

Design Parameter	Parameter Definition	Unit	Lower Bound	Upper Bound
x_{tube_comp1}	Tube side mole fraction - component 1		0.076	0.114
x_{tube_comp2}	Tube side mole fraction - component 2		0.079	0.119
x_{tube_comp3}	Tube side mole fraction - component 3		0.185	0.277
x_{tube_comp4}	Tube side mole fraction - component 4		0.336	0.480
x_{shell_comp1}	Shell side mole fraction - component 1		0.212	0.318
x_{shell_comp2}	Shell side mole fraction - component 2		0.271	0.407
x_{shell_comp3}	Shell side mole fraction - component 3		0.147	0.221
x_{shell_comp4}	Shell side mole fraction - component 4		0.012	0.019
P_{tube}	Tube side pressure	bar	10	14
T_{tube}	Tube side temperature	°C	117	217
P_{shell}	Shell side pressure	bar	5	7
T_{shell}	Shell side temperature	°C	-3	93
d_{tube}	Tube diameter	cm	4	4
V_{shell}	Shell volume	m^3	7	7
A_{PSV}	Shell side pressure relief valve area	cm^2	23.23 (M Size)	23.23 (M Size)

For the first case study, the ANN model is limited to a single exchanger. More specifically, the compositions on both the tube and shell side are narrow. This is intended to represent operational variations of a stream's composition. Similarly, for the pressure and temperature, there is some variation that may exist within the normal operation of that process. The goal of the first case study is to test the feasibility of ANN in predicting the safety rating for individual heat exchangers in operation. The idea behind case one is for an exchanger that is already present and one wishes to monitor its safety rating performance. The second case study varies in that it is for creating a

generic ANN safety prediction model that can be used throughout a plant. The second case study does not have narrow compositions like case one. Instead, the composition can range from 0 to 1. Similarly, the pressure and temperature can vary widely for the second case study. Lastly, while the exchanger properties were fixed in case one, they are variables in case two. The advantage of the second case study is to present a generic safety rating model that can be used throughout a plant without needing modification. If successful, this would confirm the feasibility of a real time process safety monitoring program (presented earlier).

For case one, the parameters that are fixed are the exchanger properties including the tube diameter, shell volume, and shell side pressure relief valve area. The tube diameter is set to 4 cm. The shell volume is set to 7 cubic meters. The shell side pressure relief valve has an M sized orifice (23.23 cm²). The training data is comprised of 1500 sample points whereby the variables are inputted using Latin hypercube sampling. Similarly, 200 unique data points are then cross validated for case one.

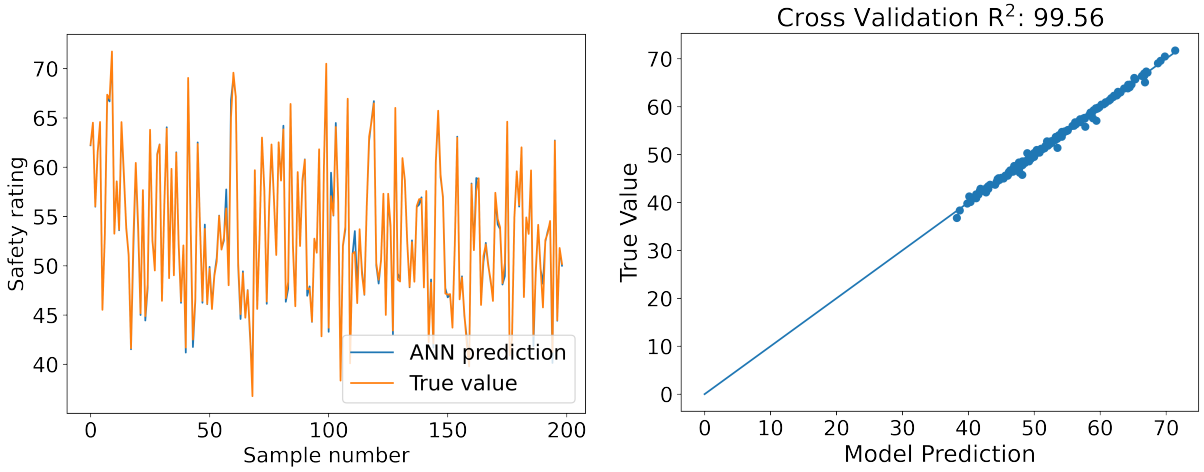

(a) Model predictions with fixed dimensions.

(b) Cross validation results for Case 1.

Figure 4.6: Case 1 results. For monitoring the safety of a single exchanger, the ANN model generated resulted in high fidelity tube rupture predictions.

In analyzing the results for case one, the optimal network size was found to contain an input

layer with 12 nodes, three hidden layers with 10 nodes each, and an output layer with a single node (representing the safety rating). The model's accuracy for the cross validation samples is greater than 99.5%. From the results, we can see that ANN was able to successfully predict the safety rating. This is impressive because the safety rating requires calculations which involve complicated thermodynamics. In particular, the safety rating requires calculating properties such as the densities, bulk modulus, and mass flow rates during the overpressure event. With ANN, these properties and calculations were able to be bypassed using widely accessible inputs.

Thus, using only composition, pressure, and temperature, one can very accurately predict the likelihood of an exchanger failure in the event of overpressure. This case study confirms the usefulness of ANN in the field of process safety. However, it should be noted that this case study had limited ranges for the composition, pressures, and temperatures. Therefore, the second case study looks more closely into a more generic safety rating prediction model.

Another point to note is in regards to the cross validation results. From the error plot, the upper portion of the curve is preferable to the lower portion of the curve. What this means is that the upper portion represents predictions that were low but ended up having high safety ratings. This is preferred since it results in a more conservative heat exchanger. Thus, while ANN can yield high accuracy predictions, it is not possible to guarantee a conservative safety rating. This lends itself to ANN serving more in a fault detection capacity, so that it is not a single point of failure.

4.6 Case study 2

From the first case study, it was clear that ANN achieved excellent results for the inputs that were fed to it and for being able to predict the safety rating. In the second case study, a more generic safety rating prediction model is developed. Here, the compositions, pressure, and temperature of both sides have much more variance. 1500 sample points are used for the training data. 200 cross validation points are used. The exchanger properties such as tube diameter, shell, volume and PSV area are left as variables as opposed to the first case study. Therefore, if successful, this model can be used throughout a plant to be able to predict the safety rating from the results. From the results, the accuracy for the ANN model was very high. It was more than 96.7%. The network size that is

proposed is 15 inputs, four hidden layers of 50 nodes each and the output node, which is the safety rating. Therefore, for both case one and case two, ANN appears to be an excellent candidate to being able to develop a fault detection program.

Table 4.2: Case 2 input bounds for training feed forward artificial neural network.

Design Parameter	Parameter Definition	Unit	Lower Bound	Upper Bound
x_{tube_comp1}	Tube side mole fraction - component 1		0	1
x_{tube_comp2}	Tube side mole fraction - component 2		0	1
x_{tube_comp3}	Tube side mole fraction - component 3		0	1
x_{tube_comp4}	Tube side mole fraction - component 4		0	1
x_{shell_comp1}	Shell side mole fraction - component 1		0	1
x_{shell_comp2}	Shell side mole fraction - component 2		0	1
x_{shell_comp3}	Shell side mole fraction - component 3		0	1
x_{shell_comp4}	Shell side mole fraction - component 4		0	1
P_{tube}	Tube side pressure	bar	5	20
T_{tube}	Tube side temperature	°C	0	100
P_{shell}	Shell side pressure	bar	5	20
T_{shell}	Shell side temperature	°C	0	100
d_{tube}	Tube diameter	cm	2	5
V_{shell}	Shell volume	m^3	2	10
A_{PSV}	Shell side pressure relief valve area	cm^2	0	100

From the previous case study shown, ANN can be used to bypass complicated process safety consequence models and calculate the potential severity of an overpressure scenario. To see how this can be implemented in a fault detection monitoring program, consider the example in Figure 4.8. This example presents what a real time safety monitoring program might look like. From the figure presented, there exists a reservoir of cooling water that is pumped through different exchangers. The hot reactor product must be cooled and is pumped through those same exchangers.

Therefore, there exists a total of four exchangers where variations in pressure are assumed for the tube side. For each of these pumps, there is an average pressure that is specified in Figure 4.8. The variation of the pressure is also given. For example, in the first pump, P-101, the average pressure is given as 11.1 bar and the pressure can vary plus or minus 0.5 bar. For each of these pumps with variations and pressure, the safety rating is calculated. Thus, one is able to see that it is possible to have a safety rating that is in real time and that can be used to monitor a plant.

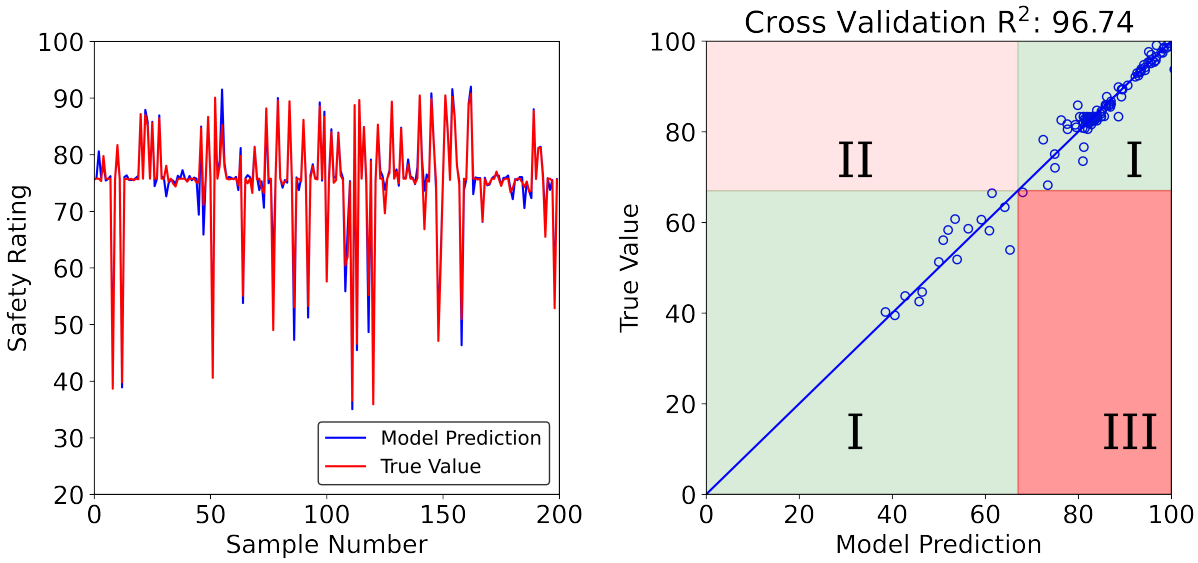

(a) Model predictions with fixed dimensions.

(b) Cross validation results for Case 2.

Figure 4.7: Case 2 cross validation results. The plot is divided on both axes along 67, the boundary defining what is considered safe. Region I highlighted in light-green represents ANN predictions that were true for both unsafe and safe regions. Region II represents ANN predictions that were too conservative. Region II represents instances where the ANN model underestimates the true safety rating. In Region II, the true safety rating is safe while the ANN model predicts unsafe. Region III represents ANN predictions that overestimated the safety rating. In Region III, while the true safety rating is less than 67, the ANN model predicts the safety rating is above 67. Clearly, ANN predictions in Region III are not protected in the event of a tube rupture.

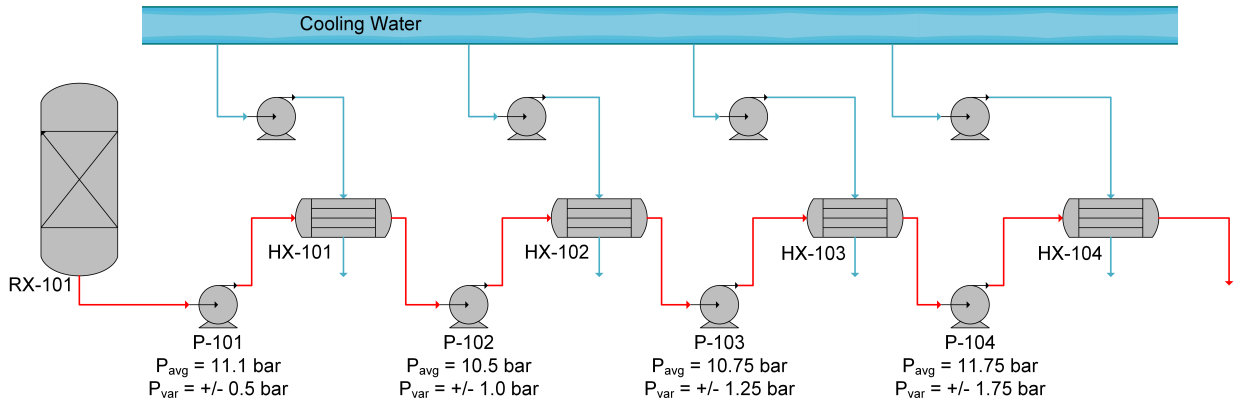

Figure 4.8: Real time monitoring of safety rating via ANN. Four exchangers in series, HX-101, HX-102, HX-103, and HX-104, are used to cool the product from reactor RX-101. Four pumps are used to transport material through the exchangers. The average output pressure of each pump, P_{avg}, is listed below its tag name. The upper and lower bounds of the pressure, P_{var}, are also listed.

4.7 Discussion

In examining the process safety and safe design of chemical plants, managing risks can be done in two common ways. The first is explained by the process safety pyramid. The process safety pyramid represents the decreasing likelihood of occurrence of more severe incidents. The main takeaway of the process safety pyramid is that high severity events such as fatalities are the cause of neglecting hundreds or even thousands of near misses. Because of this, the process safety pyramid changes the way we think of process safety since it suggests that we trace back past incidents and better control them. This is particularly important in the field of fault detection. Since a fault is equivalent/analogous to a near miss and if it is corrected, it can prevent a much more severe scenario. Another way of managing risks in a plant is through understanding the Swiss cheese model. The Swiss cheese model illustrates safeguards as a way to decrease the likelihood of a process safety incident. In particular, process safety incidents are assumed to be the result of a failure (or lack thereof) of a series of safeguards. Therefore, increasing more safeguards will decrease the likelihood of an event and increase the safety of that particular process. Artificial neural networks (ANN) have the ability to contribute to process safety on both of these fronts. Artificial neural networks can decrease the likelihood of occurrence, which would contribute to

process safety via the process safety pyramid. In addition, a fault detection system built around ANN can itself be considered a safeguard. Thus, ANN acts as an additional layer of protection in the Swiss cheese model, which ultimately results in less incidents in a plant.

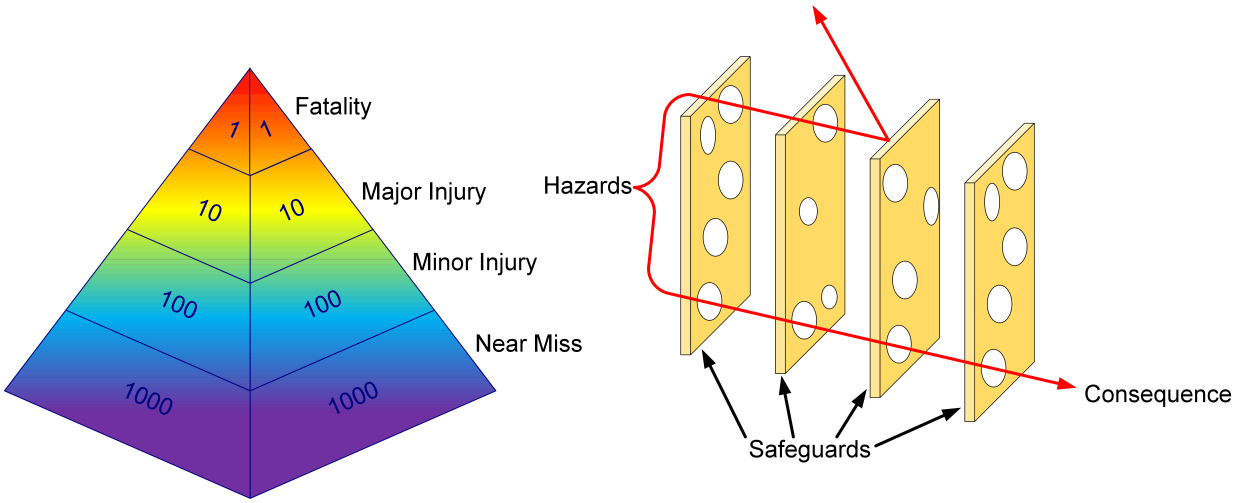

Figure 4.9: Process safety pyramid and Swiss cheese model. The process safety pyramid illustrates that most fatalities and high severity events can be traced back to ignored past incidents. With the Swiss cheese model, process safety incidents are the result of a failure (or lack thereof) of a series of safeguards.

A neural network model for predicting heat exchanger to rupture safety has been developed. The neural network model uses robust dynamic tube rupture simulations that are able to capture liquid-liquid vapor, liquid and flashing liquid scenarios. This technique offers plants the ability to perform real time process safety monitoring. The results that were obtained were highly accurate, although it should be noted that guaranteeing safety is still something that has to be developed. However, as a fault detection system, ANN offers very promising results for the future of chemical processes.

The most important variables in controlling the safety rating were the pressures. The main conclusion of this work is that artificial neural networks can be used with a great deal of accuracy to perform real-time consequence modeling. Artificial neural networks can be a significant aid to

the process safety community by predicting upsets, assessing the severity of potentially hazardous outcomes, and helping control plant operations.

It is clear that artificial neural networks are very adaptable from the results shown earlier. Furthermore, it was not necessary to have a deep understanding of the calculations done in consequence modeling to be able to predict the safety rating. All one simply needs is a set of input data and output data, after which the model can begin to train and learn patterns. Another important conclusion is that ANN was able to successfully handle noise, which is useful in a fault detection program. Thus, we can see from this example that ANN can be used in the context of process safety and also in the context of controlling operations within a plant. From this work, one can see that ANN can be used to increase the reliability of a system and make plants more economical to operate. Another important conclusion is the speed with which ANN is able to generate solutions. Since this solution would be for a monitoring program, the DCS data that is widely available is able to be used and converted to real time metrics. One can expect that in the future ANN will see an increased role in improving the safety of systems.

This ANN framework can be used and modified to predict other process safety events, including fire, toxic releases, and explosions. ANN can also be used to support decision making by assessing the risk of heat exchangers and other equipment within a process. Applying a framework like this will provide significant benefits to the process industry.

5. CONCLUSION

5.1 Tube rupture modeling

Shell and tube heat exchangers are commonly used in the oil, gas, chemical, and nuclear industries. Although rare, tube rupture overpressure events may compromise the mechanical integrity of an exchanger and can lead to the equipment's failure. This has the potential to result in catastrophic failures and should be modeled with rigorous sizing methods. This work points out the challenges in modeling tube ruptures. The importance of accurately modeling tube rupture scenarios increases with large differences in pressure between the shell and tube. In addition, low tube-to-shell density ratios increase the severity of this event. By switching from an orifice-style calculation into a more rigorous dynamic simulation, one can better predict the effects of a tube rupture. This work covered the main steps in generating a pressure profile, and a step-by-step calculation was performed for an ethylene-glycol water, methane water, and propane water system. A comparison of the PSV sizes reveals that vapor-liquid and liquid-liquid systems are the most and least severe cases, respectively. Flashing liquid-liquid tube rupture scenarios performed in between these two cases. The examples covered in this work can serve as a basis for approaching liquid-liquid, vapor-liquid, and flashing liquid-liquid systems.

5.2 HEN synthesis with overpressure protection

In the offshore industry, heat exchangers can operate at hundreds of bar. And while tube ruptures are rare events, if inadequately protected, they can result in devastating consequences. The severity of tube rupture consequences increases with large differences in pressure between the shell and tube side. The safety rating presented provides a baseline to compare the safety of different heat exchangers. This safety metric incorporates the potential effects of overpressure in network synthesis. It is also designed to only allow high pressure streams to be on the tube side, in accordance with heat exchanger design principles. The distinction between applying this metric to a single exchanger and a network has also been made. Moreover, a tight under-estimator of the

safety rating applied to different temperatures allows one to incorporate tight, yet conservative design principles in tube rupture design for HENS. With the two case studies presented, it has been shown that significant reductions to the likelihood of a tube rupture overpressure scenario can be made, while minimizing the economic burden of doing so. Ultimately, this MINLP HENS model provides a tool whereby one can specify a risk/tolerance and determine the optimum network configuration that meets their process needs.

5.3 Approximating process safety metrics using artificial neural networks

Currently, in the context of process safety, DCS data may be used to relay vessel levels and other common data for the purpose of automated or operator intervention. However, this approach is reactive and not proactive. As an extension of our prior work, we examined the possibility of artificial neural networks (ANN) in predicting the severity of a tube rupture. More specifically, we considered a system with process disturbances and wish to provide a real-time safety rating. By leveraging a plant's existing DCS data, ANN can be used to predict hypothetical process safety scenarios.

In this work, two ANN models were developed and evaluated for the prediction of the safety rating for a tube rupture. These two models were designed, the first being for a single heat exchanger and the second was for a generic heat exchanger. For each model, there were a total of 12 and 15 inputs respectively, and the single model output was the safety rating. The models that were selected were the ones that gave the best performance. The statistical values, including the mean square error, were calculated for each model to assess their performance. The first ANN model had a R squared value of 0.99 and the second model had an R squared value of 0.95. These ANN models can be used to predict the consequence. These ANN models can be used in consequence analysis of tube ruptures. The models can be further improved by adding more training data sets to cover different operating conditions.

This approach can supplement current overpressure modeling. By training an ANN model to predict process safety consequences, one can bypass the steps in modeling each specific scenario and can simply obtain the safety rating. For the case of a tube rupture, we are interested in feeding

our model with two types of inputs. The first type of inputs are exchanger design specifications. These include tube diameter, shell volume, and PSV size. The second type of inputs are operating conditions including temperature, pressure, and composition for both the shell and tube side. Whereas the first set of inputs are fixed and cannot change for each exchanger, the second set are dynamic. Note that inputs in the training data are information that is readily available from a plant's DCS data. If more complicated terms are substituted in their place, the accuracy of the ANN model may increase, but the usefulness of the model will be hampered.

One key advantage in this approach is that the effects of parameters that are not easily accounted for (temperature, phase, etc.) can be mapped and incorporated in a tube rupture prediction model. Thus, ANN may be the preferred approach for an even more complex tube rupture prediction such as one with a nonisothermal phase change.

The affordability of computing has increased the acceptance of neural networks. It's clear from the case studies performed in this work that neural networks have the ability to learn, which makes them very flexible. In addition, because artificial neural networks are able to learn, they minimize the need for developing specific programs to perform consequence modeling or other complex engineering calculations. Artificial neural networks are also suited for real time systems, allowing them to achieve rigorous results.

5.4 Methodology for inherently safe process synthesis and heat integration

An extension of this work may include incorporating safety metrics in optimally designing an inherently safe process combined with heat integration. An optimization framework that incorporates building blocks can be used to represent process synthesis and heat integration [103]. However, one challenge in incorporating process safety metrics for this application is that the heat exchanger network configuration is not initially known. As a result, the number of hot and cold streams along with their inlet and outlet temperatures are not known a priori. This is substantially different from how our HEN model is intended to perform. In our previous HEN examples, it is assumed that the stream summary information is already known. With this information, the HEN synthesis problem determines the best network configuration. For simultaneous process synthe-

sis and heat integration, the streams that will end up requiring heating and cooling have to be determined along with the network configuration and safety metrics.

In approaching this challenge, rigorous thermodynamic models would therefore need to be included in the optimization model. An alternative to this is to use an ANN-based framework to provide the safety ratings for all feasible solutions. Regardless of which approach is used to obtain the safety rating, we believe that designing inherently safe processes this way can lead to interesting results. For example, in our previous work, we have shown that liquid-liquid tube ruptures are considered the least severe compared with vapor-liquid and flashing-liquid liquid tube ruptures. Therefore, we would expect that an inherently safe process would result in streams requiring heating or cooling to be mostly liquid streams as opposed to vapor streams. In addition, as we have shown before, for processes that cannot use an alternative stream, relief devices will play an important role in improving the economics of providing a safe network.

REFERENCES

[1] C. Schroeder, "A decade of change in regulating the chemical industry," *Law & Contemp. Probs.*, vol. 46, p. 1, 1983.

[2] G. Westbrook, "Use this method to size each stage for best operation," *Hydrocarbon Process and Petroleum Refinement*, vol. 40, pp. 201–206, 1961.

[3] J. Jezowski, "Heat exchanger network grass root and retrofit design. the review of the state-of-the art: Part i. heat exchanger network targeting and insight based methods of synthesis," *Hungarian J. of Ind. Chem.*, vol. 22, pp. 279–294, 1994.

[4] J. Jezowski, "Heat exchanger network grassroot and retrofit design, the review of the state of the art: Part ii, heat exchanger network synthesis by mathematical methods and approaches for retrofit design," 1994.

[5] K. C. Furman and N. V. Sahinidis, "A critical review and annotated bibliography for heat exchanger network synthesis in the 20th century," *Industrial & Engineering Chemistry Research*, vol. 41, no. 10, pp. 2335–2370, 2002.

[6] T. Gundepsen and L. Naess, "The synthesis of cost optimal heat exchanger networks: An industrial review of the state of the art," *Computers & chemical engineering*, vol. 12, no. 6, pp. 503–530, 1988.

[7] M. Morar and P. S. Agachi, "Important contributions in development and improvement of the heat integration techniques," *Computers & Chemical Engineering*, vol. 34, no. 8, pp. 1171–1179, 2010.

[8] R. W. Serth, *Process heat transfer*. Elsevier, 2010.

[9] T. Grützner, D. Ziegenbalg, and R. Güttel, "Process intensification–an unbroken trend in chemical engineering," *Chemie Ingenieur Technik*, vol. 90, no. 11, pp. 1823–1831, 2018.

[10] J. Bielenberg and M. Bryner, "Realize the potential of process intensification," *Chemical Engineering Progress*, vol. 114, no. 3, pp. 41–45, 2018.

[11] A. I. Stankiewicz and J. A. Moulijn, "Process intensification: transforming chemical engineering," *Chemical engineering progress*, vol. 96, no. 1, pp. 22–34, 2000.

[12] J. Etchells, "Process intensification: safety pros and cons," *Process Safety and Environmental Protection*, vol. 83, no. 2, pp. 85–89, 2005.

[13] Pipeline Simulation and Integrity Ltd, "Testing and analysis of relief device opening times," tech. rep.

[14] *API 521, Pressure-Relieving and Depressurizing Systems*, 2014.

[15] M. Hellemans, *The safety relief valve handbook: design and use of process safety valves to ASME and International codes and standards*. Elsevier, 2009.

[16] J. Cassata, Z. Feng, S. Dasgupta, and R. Samways, "Prevent overpressure failures on heat exchangers," *Hydrocarbon Processing*, vol. 77, no. 11, pp. 123–128, 1998.

[17] B. Ewan and M. Moatamedi, "Design aspects of chemical plant exposed to transient pressure loads," *Chemical Engineering Research and Design*, vol. 78, no. 6, pp. 866–870, 2000.

[18] M. Ahammad, L. Hatanaka, J. Hui, K. Lapeyrouse, and E. Roche, "Learnings from mary kay o'connor process safety center (mkopsc) instrument reliability network's project on pressure transmitter maintenance data collection," in *Annual International Symposium*, vol. 19, pp. 523–532, 2016.

[19] United Kingdom's Health and Safety Executive, "Offshore hydrocarbon releases."

[20] D. Fowler, T. Herndon, and R. Wahrmund, "An analysis of potential overpressure of a heat exchanger shell due to a ruptured tube," in *ASME Petroleum Mechanical Engineering Conference, Dallas TX*, 1968.

[21] L. L. Simpson, "Dynamics of underwater gas tubing failure," Master's thesis, West Virginia University, 1971.

[22] V. Sumaria, J. Rovnak, I. Heitner, and R. Herbert, "Model to predict transient consequences of a heat exchanger tube rupture," *Proc., Am. Pet. Inst., Sect. 3;(United States)*, vol. 55, 1976.

[23] C. Ennis, K. Botros, and C. Patel, "Dynamic model for a heat exchanger tube rupture discharging a high-pressure flashing liquid into a low-pressure liquid-filled shell," *Journal of Loss Prevention in the Process Industries*, vol. 24, no. 1, pp. 111–121, 2011.

[24] K. K. Botros, "Importance of accounting for the piping system and boundary conditions in determining the maximum surge pressure following heat-exchanger tube-rupture," *Journal of Loss Prevention in the Process Industries*, vol. 37, pp. 63–73, 2015.

[25] S. Nagpal, "Evaluate heat-exchanger tube-rupture scenarios using dynamic simulation," *Chemical Engineering*, vol. 122, no. 2, p. 48, 2015.

[26] C. Acosta and N. Siu, "Dynamic event trees in accident sequence analysis: application to steam generator tube rupture," *Reliability Engineering & System Safety*, vol. 41, no. 2, pp. 135–154, 1993.

[27] A. Thyer, A. Wilday, and G. Bankes, "The experimental study and simulation of tube rupture in shell-and-tube heat exchangers," in *INSTITUTION OF CHEMICAL ENGINEERS SYMPOSIUM SERIES*, vol. 148, pp. 265–278, Institution of Chemical Engineers; 1999, 2000.

[28] R. Turton, R. C. Bailie, W. B. Whiting, and J. A. Shaeiwitz, *Analysis, synthesis and design of chemical processes*. Pearson Education, 2008.

[29] B. Linnhoff and J. R. Flower, "Synthesis of heat exchanger networks: I. systematic generation of energy optimal networks," *AIChE Journal*, vol. 24, no. 4, pp. 633–642, 1978.

[30] B. Linnhoff, "User guide on process integration for the efficient use of energy," *AIChE J.*, vol. 28, pp. 000–000, 1982.

[31] M. M. El-Halwagi and V. Manousiouthakis, "Synthesis of mass exchange networks," *AIChE Journal*, vol. 35, no. 8, pp. 1233–1244, 1989.

[32] R. R. Tan and D. C. Foo, "Pinch analysis approach to carbon-constrained energy sector planning," *Energy*, vol. 32, no. 8, pp. 1422–1429, 2007.

[33] A. Singhvi and U. Shenoy, "Aggregate planning in supply chains by pinch analysis," *Chemical Engineering Research and Design*, vol. 80, no. 6, pp. 597–605, 2002.

[34] T. F. Yee, I. E. Grossmann, and Z. Kravanja, "Simultaneous optimization models for heat integration—i. area and energy targeting and modeling of multi-stream exchangers," *Computers & chemical engineering*, vol. 14, no. 10, pp. 1151–1164, 1990.

[35] T. F. Yee and I. E. Grossmann, "Simultaneous optimization models for heat integration—ii. heat exchanger network synthesis," *Computers & Chemical Engineering*, vol. 14, no. 10, pp. 1165–1184, 1990.

[36] G. D. Corporation, "General Algebraic Modeling System (GAMS) Release 24.2.1." Washington, DC, USA, 2013.

[37] GAMS Development Corporation, Washington, DC, USA, *GAMS - A User's Guide, GAMS Release 24.2.1*, 2013.

[38] J. M. Ponce-Ortega, A. Jiménez-Gutiérrez, and I. E. Grossmann, "Optimal synthesis of heat exchanger networks involving isothermal process streams," *Computers & Chemical Engineering*, vol. 32, no. 8, pp. 1918–1942, 2008.

[39] S. Rebennack and J. Kallrath, "Continuous piecewise linear delta-approximations for univariate functions: computing minimal breakpoint systems," *Journal of Optimization Theory and Applications*, vol. 167, no. 2, pp. 617–643, 2015.

[40] American Petroleum Institute, *API Standard 521: Pressure-relieving and Depressuring Systems*.

[41] N. P. Cheremisinoff, *Handbook of chemical processing equipment*. Elsevier, 2000.

[42] A. Harhara and M. F. Hasan, "Incorporating process safety into heat exchanger network synthesis and operation," in *Computer Aided Chemical Engineering*, vol. 47, pp. 221–226, Elsevier, 2019.

[43] A. K. Saboo, M. Morari, and D. C. Woodcock, "Design of resilient processing plants—viii. a resilience index for heat exchanger networks," *Chemical Engineering Science*, vol. 40, no. 8, pp. 1553–1565, 1985.

[44] A. Saboo, M. Morari, and R. D. Colberg, "Reshex: An interactive software package for the synthesis and analysis of resilient heat-exchanger networks—i: Program description and application," *Computers & chemical engineering*, vol. 10, no. 6, pp. 577–589, 1986.

[45] A. Saboo, M. Morari, and R. Colberg, "Reshex: an interactive software package for the synthesis and analysis of resilient heat-exchanger networks—ii: Discussion of area targeting and network synthesis algorithms," *Computers & chemical engineering*, vol. 10, no. 6, pp. 591–599, 1986.

[46] D. F. Marselle, M. Morari, and D. F. Rudd, "Design of resilient processing plants—ii design and control of energy management systems," *Chemical Engineering Science*, vol. 37, no. 2, pp. 259–270, 1982.

[47] I. E. Grossmann and M. Morari, "Operability, resiliency, and flexibility: Process design objectives for a changing world," 1983.

[48] A. Nemet, J. J. Klemeš, I. Moon, and Z. Kravanja, "Safety analysis embedded in heat exchanger network synthesis," *Computers & Chemical Engineering*, vol. 107, pp. 357–380, 2017.

[49] A. M. Hafizan, S. R. W. Alwi, Z. Abd Manan, and J. J. Klemeš, "Optimal heat exchanger network synthesis with operability and safety considerations," *Clean Technologies and Environmental Policy*, vol. 18, no. 8, pp. 2381–2400, 2016.

[50] I. Chan, S. R. W. Alwi, M. H. Hassim, Z. Abd Manan, and J. J. Klemeš, "Heat exchanger network design considering inherent safety," *Energy Procedia*, vol. 61, pp. 2469–2473, 2014.

[51] S. H. A. Bakar, M. K. A. Hamid, S. R. W. Alwi, and Z. A. Manan, "Design target selection for heat exchanger network synthesis based on trade-off plot," *Energy Procedia*, vol. 61, pp. 2621–2624, 2014.

[52] Y. Huang and L. Fan, "Distributed strategy for integration of process design and control: A knowledge engineering approach to the incorporation of controllability into exchanger network synthesis," *Computers & chemical engineering*, vol. 16, no. 5, pp. 496–522, 1992.

[53] J.-j. Jiang, L. Zhang, Y.-q. Wang, Y.-y. Peng, K. Zhang, and W. He, "Markov reliability model research of monitoring process in digital main control room of nuclear power plant," *Safety science*, vol. 49, no. 6, pp. 843–851, 2011.

[54] M. Kano and Y. Nakagawa, "Data-based process monitoring, process control, and quality improvement: Recent developments and applications in steel industry," *Computers & Chemical Engineering*, vol. 32, no. 1-2, pp. 12–24, 2008.

[55] Y. Jiang, S. Yin, and O. Kaynak, "Performance supervised plant-wide process monitoring in industry 4.0: a roadmap," *IEEE Open Journal of the Industrial Electronics Society*, vol. 2, pp. 21–35, 2020.

[56] M. Sharif and R. Grosvenor, "Process plant condition monitoring and fault diagnosis," *Proceedings of the Institution of Mechanical Engineers, Part E: Journal of Process Mechanical Engineering*, vol. 212, no. 1, pp. 13–30, 1998.

[57] Z. Ge, Z. Song, and F. Gao, "Review of recent research on data-based process monitoring," *Industrial & Engineering Chemistry Research*, vol. 52, no. 10, pp. 3543–3562, 2013.

[58] R. Saada, D. Patel, and B. Saha, "Causes and consequences of thermal runaway incidents—will they ever be avoided?," *Process safety and environmental protection*, vol. 97, pp. 109–115, 2015.

[59] J. Barton and P. Nolan, "Incidents in the chemical industry due to thermal runaway chemical reactions," *Hazards X: Process Safety in Fine and Speciality Chemical Plants*, vol. 115, pp. 3–18, 1989.

[60] A. Dakkoune, L. Vernières-Hassimi, D. Lefebvre, and L. Estel, "Early detection and diagnosis of thermal runaway reactions using model-based approaches in batch reactors," *Computers & Chemical Engineering*, vol. 140, p. 106908, 2020.

[61] D. D. Slaback and J. B. Riggs, "Time to runaway in a continuous stirred tank reactor," *Industrial & engineering chemistry research*, vol. 43, no. 14, pp. 3723–3730, 2004.

[62] M. Dadashzadeh, F. Khan, K. Hawboldt, and P. Amyotte, "An integrated approach for fire and explosion consequence modelling," *Fire Safety Journal*, vol. 61, pp. 324–337, 2013.

[63] J. L. Woodward, "Improving the effect of atmospheric stability class for dispersion modeling," *Process Safety Progress*, vol. 17, no. 1, pp. 1–8, 1998.

[64] Q. Zhang and Q. Ma, "Dynamic pressure induced by a methane–air explosion in a coal mine," *Process Safety and Environmental Protection*, vol. 93, pp. 233–239, 2015.

[65] N. L. Ryder, J. A. Sutula, C. F. Schemel, A. J. Hamer, and V. Van Brunt, "Consequence modeling using the fire dynamics simulator," *Journal of hazardous materials*, vol. 115, no. 1-3, pp. 149–154, 2004.

[66] D. M. Himmelblau, "Applications of artificial neural networks in chemical engineering," *Korean journal of chemical engineering*, vol. 17, no. 4, pp. 373–392, 2000.

[67] M. S. Mannan, O. Reyes-Valdes, P. Jain, N. Tamim, and M. Ahammad, "The evolution of process safety: current status and future direction," *Annual review of chemical and biomolecular engineering*, vol. 7, pp. 135–162, 2016.

[68] Y. Maki and K. A. Loparo, "A neural-network approach to fault detection and diagnosis in industrial processes," *IEEE Transactions on Control Systems Technology*, vol. 5, no. 6, pp. 529–541, 1997.

[69] R. A. Kosiński and C. Kozłowski, "Artificial neural networks–modern systems for safety control," *International Journal of Occupational Safety and Ergonomics*, vol. 4, no. 3, pp. 317–332, 1998.

[70] M. A. Hussain, "Review of the applications of neural networks in chemical process control—simulation and online implementation," *Artificial intelligence in engineering*, vol. 13, no. 1, pp. 55–68, 1999.

[71] Z. Kurd and T. Kelly, "Establishing safety criteria for artificial neural networks," in *International Conference on Knowledge-Based and Intelligent Information and Engineering Systems*, pp. 163–169, Springer, 2003.

[72] M. T. El-Melegy, M. H. Essai, and A. A. Ali, "Robust training of artificial feedforward neural networks," in *Foundations of Computational, Intelligence Volume 1*, pp. 217–242, Springer, 2009.

[73] H. Honggui, L. Ying, and Q. Junfei, "A fuzzy neural network approach for online fault detection in waste water treatment process," *Computers & Electrical Engineering*, vol. 40, no. 7, pp. 2216–2226, 2014.

[74] S. Heo and J. H. Lee, "Fault detection and classification using artificial neural networks," *IFAC-PapersOnLine*, vol. 51, no. 18, pp. 470–475, 2018.

[75] G. Polley and M. P. Shahi, "Interfacing heat exchanger network synthesis and detailed heat exchanger design," *Trans IChemE*, vol. 69, no. Part A, 1991.

[76] M. H. Panjeshahi and N. Tahouni, "Pressure drop optimisation in debottlenecking of heat exchanger networks," *Energy*, vol. 33, no. 6, pp. 942–951, 2008.

[77] X. Nie and X. Zhu, "Heat exchanger network retrofit considering pressure drop and heat-transfer enhancement," *AIChE Journal*, vol. 45, no. 6, pp. 1239–1254, 1999.

[78] M. Ravagnani, A. Da Silva, and A. Andrade, "Detailed equipment design in heat exchanger networks synthesis and optimisation," *Applied Thermal Engineering*, vol. 23, no. 2, pp. 141–151, 2003.

[79] N. V. Sahinidis, "Baron: A general purpose global optimization software package," *Journal of global optimization*, vol. 8, no. 2, pp. 201–205, 1996.

[80] M. P. Schwartz, "Four types of heat exchanger failures," *ITT Bell & Gosset*, 1982.

[81] B. Megens, "Tube rupture study of a 300 bar heat exchanger," in *ASME 2014 Pressure Vessels and Piping Conference*, pp. V005T05A015–V005T05A015, American Society of Mechanical Engineers, 2014.

[82] S. Shahrani and S. Al-Subai, "Failure analysis of heat exchanger tubes," *Journal of Failure Analysis and Prevention*, vol. 14, no. 6, pp. 790–800, 2014.

[83] D. O. Njobuenwu and M. Fairweather, "Modelling of pipe bend erosion by dilute particle suspensions," *Computers & Chemical Engineering*, vol. 42, pp. 235–247, 2012.

[84] V. Khilnaney, "Heat exchanger vibrations-a case study (paper no. 5.12)," 1992.

[85] A. Boiler and P. V. Code, "Section viii division 1," *UG-126 Pressure Relief Valves to UG-129 Marking, ASME International, New York*, 2010.

[86] M. Stewart and O. T. Lewis, *Heat exchanger equipment field manual: common operating problems and practical solutions*. Gulf Professional Publishing, 2012.

[87] American Institute of Chemical Engineers. Center for Chemical Process Safety, *Guidelines for Initiating Events and Independent Protection Layers in Layer of Protection Analysis*. John Wiley & Sons, 2014.

[88] C. Deddis, "Shell & tube heat exchanger overpressure protection from tube rupture," tech. rep., BP Exploration Operating Co Ltd.

[89] *API Standard 520: Sizing, Selection, and Installation of Pressure-relieving Devices in Refineries, Part I — Sizing and Selection*. American Petroleum Institute.

[90] A. Singh, "An analytical study of the dynamics and stability of a spring loaded safety valve," *Nuclear Engineering and Design*, vol. 72, no. 2, pp. 197–204, 1982.

[91] MathWorks, "MATLAB 9.2," 2017.

[92] G. Krauss and D. Hudok, "Properties and selection: Iron, steel and high performance alloys," *ASM Metals Hand Book, Materials*, vol. 1, 1991.

[93] AspenTech, "Aspen HYSYS V10," 2017.

[94] E. Hagey, "The psv that did not fail—misconceptions about psvs," *Process Safety Progress*, vol. 32, no. 1, pp. 84–89, 2013.

[95] V. Golovin, N. Pechnikov, V. Shchelkov, and A. Y. Tsivadze, "Determination of the life cycle of heat-exchange tubes of vapor condensers on the basis of statistical analysis of local pitting corrosion according to data of eddy current testing," *Protection of Metals and Physical Chemistry of Surfaces*, vol. 54, no. 6, pp. 1221–1232, 2018.

[96] T. M. Ahooyi, M. Soroush, J. E. Arbogast, W. D. Seider, and U. G. Oktem, "Model-predictive safety system for proactive detection of operation hazards," *AIChE Journal*, vol. 62, no. 6, pp. 2024–2042, 2016.

[97] J. Feng, A. Aggarwal, S. Dasgupta, and H. Shariat, "Using dynamic analysis to reduce weight of offshore installations," 2009.

[98] A. Harhara and M. F. Hasan, "Dynamic modeling of heat exchanger tube rupture," *BMC Chemical Engineering*, vol. 2, no. 1, pp. 1–20, 2020.

[99] S. M. Walas, "Chemical process equipment; selection and design," tech. rep., 1988.

[100] I. Sutton, *Plant design and operations*. Gulf Professional Publishing, 2017.

[101] D. R. Moss, *Pressure vessel design manual*. Elsevier, 2004.

[102] M. Mohanraj, S. Jayaraj, and C. Muraleedharan, "Applications of artificial neural networks for thermal analysis of heat exchangers–a review," *International Journal of Thermal Sciences*, vol. 90, pp. 150–172, 2015.

[103] S. E. Demirel, J. Li, and M. F. Hasan, "Systematic process intensification using building blocks," *Computers & Chemical Engineering*, vol. 105, pp. 2–38, 2017.